The Institute of Paper Science and Technology

Atlanta, Georgia

Doctor's Dissertation

Equilibrium Adsorption of Polyallylamine from Aqueous Media

Michael A. Friese

June 25, 1993

EQUILIBRIUM ADSORPTION OF POLYALLYLAMINE FROM AQUEOUS MEDIA

A thesis submitted by

Michael A. Friese

B.S. 1986, Carroll College

Waukesha, Wisconsin

M.S. 1989, Lawrence University - The Institute of Paper Chemistry

Appleton, Wisconsin

in partial fulfillment of the requirements

for the degree of Doctor of Philosophy

from the Institute of Paper Science and Technology

Atlanta, Georgia

June 25, 1993

This work is dedicated to my wife, Chris, and my entire family. Without their constant love and support this would not have been possible. I recall my father's only advice regarding college being: survive. I survived nearly eleven years.

SUMMARY

Synthetic polyelectrolytes are commonly used as retention aids at the wet end of a paper machine. Theories in the literature describing the mechanism of retention are dependent upon the configuration of the adsorbed polyelectrolyte. The configuration of adsorbed polymers is not readily measured. However, it can be characterized by measuring the total amount of polymer adsorbed and the fraction of bound polymer segments. Measurement of the effects of common process variables on the configuration of adsorbed polyelectrolytes would contribute to a better understanding of adsorption and flocculation phenomena, ultimately leading to a more efficient use of retention aids. The development of techniques which utilize readily available instrumentation, such as fourier transform infrared attenuated internal reflection spectroscopy (FT-IR-ATR), will hopefully provide new avenues for the study of polyelectrolyte adsorption.

The adsorption of polyallylamine (PAAm) on polystyrene latex particles (PSL) was used as a model system for studying polyelectrolyte adsorption. The effects of polymer charge density (α), number average molecular weight ($M_{(n)}$), salt concentration (c_s), and particle surface charge density (σ_s) on the amount of PAAm adsorbed (Γ_m) were investigated. The dominant variable was shown to be polymer charge density. Adsorbed amounts of PAAm increased by a factor of ten or more when α decreased from 80 to 5%.

The balance of electrostatic forces also plays an important role. At low α, increasing $M_{(n)}$ or σ_s causes an increase in Γ_m due to increased looping and increased ability to neutralize charge, respectively. These effects diminish at high α due to formation of a patch configuration. At low

σ_s, increasing $M_{(n)}$ causes a small increase in Γ_m. This increase is greater at high σ_s due to increased charge neutralization which provides greater opportunity for looping.

The experimental results were compared directly with predictions made using MULPOL a version of the self-consistent-field model pioneered by Scheutjens and Fleer. In general, the trends found in the predicted amount of PAAm adsorbed (Γ_{SCF}) are similar to those found experimentally, with three exceptions. First, at low α, increasing $M_{(n)}$ causes a larger increase in Γ_{SCF} than that shown for Γ_m. Second, at high c_s and low α, Γ_{SCF} decreases slightly with increased σ_s, due to a shift to the screening-reduced adsorption regime. Third, the effects on Γ_{SCF} due to interactions between $M_{(n)}$ and σ_s are small when compared with those for Γ_m. The absolute differences in Γ_{SCF} and Γ_m range from approximately 5 to 140%. At pH 8.5, Γ_{SCF} values are higher than Γ_{SCF} at pH 10. This is opposite of the observed trend in the experimental data.

Progress has also been made in the development of an FT-IR-ATR technique for studying polyamine adsorption in aqueous media. An algorithm was developed which reproducibly subtracts water spectra from aqueous sample spectra, allowing the user to study solute peaks. The algorithm was used to analyze spectra of PAAm in solution and adsorbed to a ZnSe internal reflection element. Features of the PAAm difference spectra have been identified. Spectra of aqueous PAAm exhibit a peak near 1520 cm^{-1} due to the symmetric bending deformation of the NH_3^+ group. Adsorbed PAAm exhibits a peak near 1060 cm^{-1} due to changes in the C-N stretch on complexation.

TABLE OF CONTENTS

INTRODUCTION

Synthetic polyelectrolytes are commonly used as retention aids in the papermaking process. They adsorb to the surface of fillers, fibers, and fiber fragments in the pulp slurry. These adsorbed polyelectrolytes can, in turn, attach to other free surface area in the system. This provides a means for retaining small particles.

The process of adsorption and flocculation can be divided into three phases. In the first phase, the polymer travels from the bulk solution to a point where it meets the surface of a particle. In the second phase, the polymer adsorbs to the surface of the particle. Finally, in the third phase, the adsorbed polymer interacts with other free surface area in the system. When these interactions occur throughout the system, they cause polymer induced aggregation, or flocculation, of the particles.

The crucial step in flocculation by polymers is the adsorption step. An adsorbed polymer is typically described as being made up of tails, trains, and loops, as shown in Figure 1.

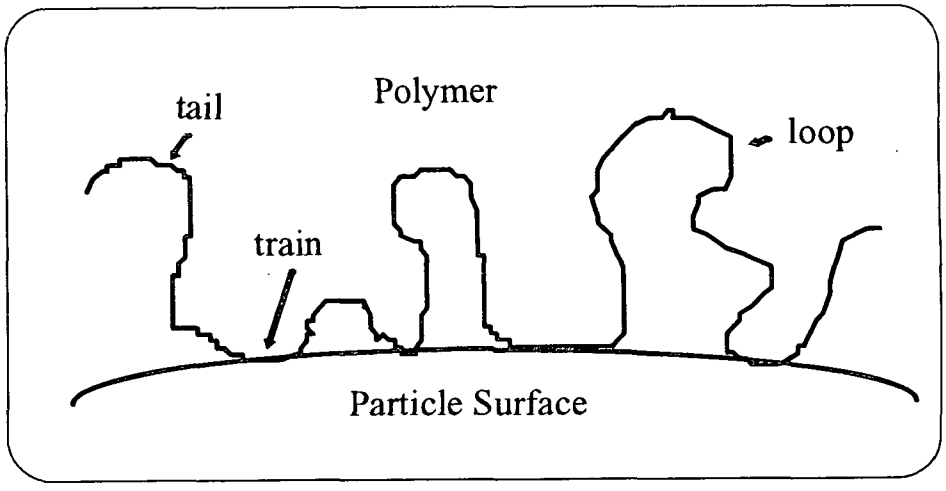

Figure 1. The tail, train, and loop sections of an adsorbed polymer.

The size and number of these tails, loops, and trains can be used to characterize the overall arrangement or configuration of an adsorbed polymer. Flocculation mechanisms proposed in the literature are based on assumptions about the configuration of the polymer at the surface.

Factors that affect the configuration of an adsorbed polymer can be categorized into two groups - chemical and mechanical. The chemical and mechanical characteristics of the polymer, the solvent, and the surface, influence interactions in the system. The chemical nature of the monomer and surface, the quality of the solvent, and the presence of small ions are important chemical characteristics to consider. Molecular weight and the degree of branching are important mechanical characteristics. The effects of these factors have been described in varying detail in the literature.

A variety of techniques have been used in the past to study polymer adsorption. Fleer and Lyklema[1] divide these techniques into three groups: those leading to the adsorbed amount, those leading to the thickness of the surface layer, and those leading to the amount at the surface (the amount bound in trains). For monolayer coverage, measurements of the adsorbed amount and the amount bound in trains can be used to characterize the adsorbed polymer configuration.

The purpose of this thesis is to further our understanding of adsorption and flocculation phenomena, including polyelectrolyte-induced retention used in the paper industry, by studying polymer adsorption in a model system. The effects of polymer charge density, molecular weight, salt concentration, and particle surface charge density on adsorption of polyallylamine (PAAm) on polystyrene latex particles have been studied. The results are compared with predictions made using the self-consistent field model pioneered by Scheutjens and Fleer. FT-IR-ATR spectroscopy has also been examined as a means for studying adsorption in-situ.

LITERATURE REVIEW

POLYMER ADSORPTION AND FLOCCULATION THEORIES

There are two basic theories which describe polymer adsorption and flocculation: the bridging mechanism and the patch mechanism.

The Bridging Mechanism

Polymer bridging was first described by Ruehrwein and Ward[2] to explain the flocculation of colloidal particles by polymers. Later, LaMer and coworkers[3,4,5,6,7,8] studied and extended the theory, suggesting that the polymer molecules adsorb onto a particle at one or more sites (trains), leaving segments (tails and loops) extending into the solution. These extended polymer segments can adsorb onto other particle surfaces with vacant sites, forming a network which flocculates as shown in Figure 2 below.

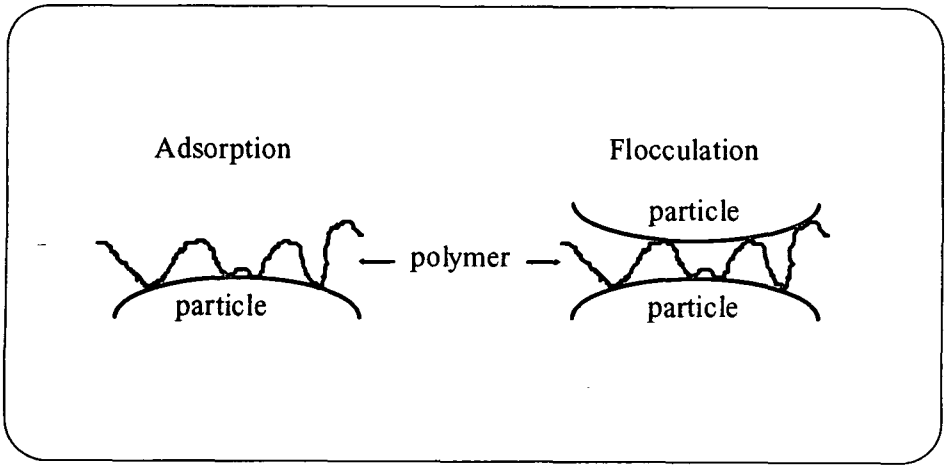

Figure 2. The bridging mechanism.

In order for flocculation to occur via the bridging mechanism, three things must be true about the adsorbed configuration. First, the extended segments must exist and remain available.[3] Then, when collisions occur, the loops and tails can adsorb to the opposite particle. Lindquist[9,10] showed that the bridging mechanism was dominant when low charge density polymers were used. These polymers should exhibit weak attraction to the oppositely charged particle, which favors the existence loops and tails.

Secondly, the extended segments must be of sufficient length (high M) and number. For bridging to occur, the extended segment must span the repulsive, electrical double layer of the two particles being flocculated. The polymer must be long enough to be able to provide such an extended segment. In addition, since the train bonding is weak, there must be a sufficient number of bridges to promote flocculation. High molecular weight polymers used at high concentrations provide the necessary length and number of loops to allow bridging to occur.

A need for sufficient free surface on the particles for bridge sites is the third criteria. If excess polymer is adsorbed, little free space will remain free to serve as bridge sites. It is clear that the potential for flocculation via the bridging mechanism is dependent upon the adsorbed polymer configuration.[11]

The Patch Mechanism

The patch mechanism was conceived by Kasper,[12] who studied it in depth and proposed the theory. Polymers having a high charge density (>10%)[13] adsorb to particles and cause flocculation via the patch mechanism[13] as shown below Figure 3.

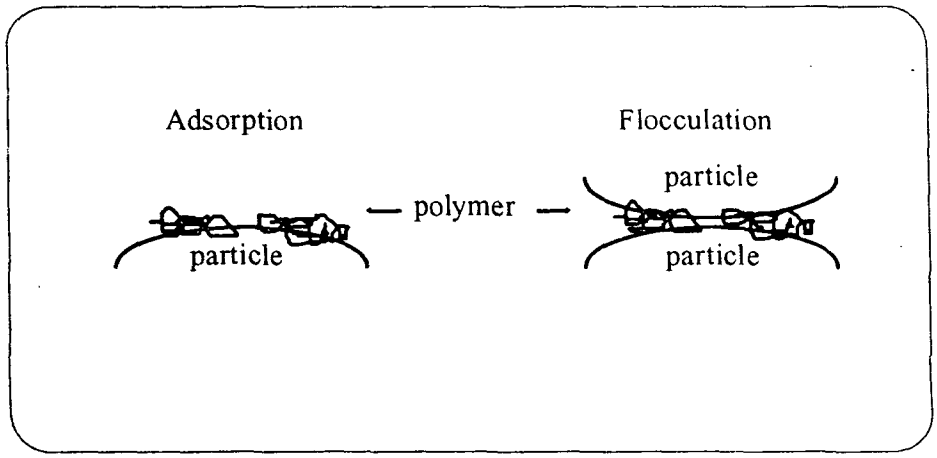

Figure 3. The patch mechanism.

The adsorbed polymer forms a very thin, flat configuration or patch for two reasons.[12] First, the particle charge is spread out in a broad pattern on the surface of the particle. Therefore, the polymer will spread out in a thin configuration, which allows the charges to interact. This allows the system to reach a minimum free energy state.

Second, since there is considerable coulombic force between charges, the polymer is bound tightly to the surface, with a large percentage of train sections and relatively few loops and tails. This coulombic force also prevents rearrangements which might lead additional loops and tails. For these reasons, the patch mechanism is applicable only to systems where the polymer has a charge opposite to that of the particle.

The polymer compensates for the particle's charge in the patch site, which compresses the repulsive, electrical double layer and promotes flocculation. Flocculation of particles by the patch mechanism is believed to occur when an adsorbed patch comes in contact with a free site on another particle.

ADSORPTION MODELS

In general, flocculation theories begin with assumptions regarding the state of the adsorbed polymer. It is either extended, for flocculation by the bridging mechanism, or lying flat, for flocculation by the patch mechanism, or somewhere in between. In any case, flocculation is affected by the configuration of the adsorbed polymer. Ideally, one would like to predict the adsorbed configuration for a given set of conditions.

A variety of models have been proposed in the literature to describe polymer adsorption. In the past two decades, two theories have come to the forefront.[14] The first, pioneered by de Gennes[15,16] involves the use of scaling theory. The second, developed by Scheutjens and Fleer,[17,18,19] uses self-consistent-field theory (SCF). Application of the SCF theory has been discussed extensively in the literature, by Scheutjens, Fleer, and their coworkers at Wageningen Agricultural University (Wageningen, The Netherlands). They have developed several computer programs for adsorption modeling, which they make available to those who are interested.[17] Many others have used, or are currently using the computer models. For these reasons, the SCF theory, and its application to the adsorption system studied in this work, will be emphasized.

A brief overview of the theory and its application is given below. The reader is referred to the articles by Scheutjens and Fleer[17,18,19] for a detailed derivation of the theory. The computer adaptation used in this thesis is described in the results and discussion section.

Adsorption Models For Uncharged Polymers

Dickinson and Lal,[20] Vincent and Whittington,[21] and Fleer and Lyklema[1] have reviewed theoretical models for polymer adsorption. The first two reviews take a more detailed approach

and discuss the adsorption of some specific molecules. The third review considers the theories of Hoeve,[22,23,24] Silberberg,[25] Roe,[26] and Scheutjens and Fleer.[17,18,19] The first theories on the subject of polymer adsorption treat the case of isolated chains on a surface.[27,28,29,30,31,32,33,34,35,36,37,38,39,40] These theories consider the segment-surface interactions and the conformational statistics of an adsorbed molecule. However, they typically neglect the interaction between polymer and solvent molecules.[1,41]

The theories of Hoeve, Silberberg, Roe, and Scheutjens and Fleer improved upon earlier theories by accounting for polymer-solvent interactions. This is accomplished by incorporation of the Flory-Huggins interaction parameter, χ, which represents the interaction energy per solvent molecule divided by kT. The theories of Roe, and Scheutjens and Fleer differ slightly from the others in their approach. Instead of modeling the adsorption of individual molecules, they model the entire adsorption system.

The adsorption system is divided into M lattice layers, each having L lattice sites. All lattice sites are occupied by either solvent molecules or polymer segments of similar size. Roe assumes that each of the segments of a chain gives the same contribution to the segment density at any distance from the surface, thereby neglecting end effects.[1] Scheutjens and Fleer, on the other hand, treat the polymer molecules as connected sequences of segments, and account for all possible chain conformations. This treatment is what sets their theory apart from that of Roe.

Scheutjens and Fleer begin by defining a partition function for the adsorption system. It is written as a product of the configurational contributions and the contributions of the internal energy of the system. The configurational contributions are derived by taking into account the

number of segments in each polymer molecule, the packing geometry, and all possible chain conformations. The expression for the internal energy contributions includes terms for polymer-surface and polymer-solvent interaction.

Application of the SCF theory by Scheutjens and Fleer provides a prediction of the polymer segment density distribution for a given system. Several overall properties of the distribution can be compared with standard experimental measurements. For an adsorption lattice with M parallel layers extending from the surface to the bulk, these properties are:

the excess surface coverage,

$$\Gamma^{exc} = \sum_{i=1}^{M} (\phi_i - \phi_*) \qquad \{1\}$$

the total surface coverage,

$$\Gamma = \sum_{i=1}^{M} \left(\phi_i - \phi_i^f \right) \qquad \{2\}$$

and the bound fraction,

$$p = \frac{\phi_1}{\Gamma} \qquad \{3\}$$

where ϕ_i is the volume fraction of polymer segments in layer i, ϕ_i^f is the volume fraction of free (i.e., belonging to unadsorbed chains) polymer segments in layer i, and ϕ_* is the volume fraction of polymer segments in the bulk solution.

Adsorption Models For Polyelectrolytes

Models for polyelectrolyte adsorption have been developed by modifying earlier theories for the adsorption of uncharged polymers. Hesselink,[42] developed the first polyelectrolyte adsorption model by modifying Hoeve's theory. Later, Van Der Schee and Lyklema[43] compared the results when the theories of Roe and Scheutjens and Fleer were extended. Papenhuijzen, et al.,[44,45] proposed a new model which was based on Roe's theory. The theory by Scheutjens and Fleer was extended by Evers,[46] et al., to model the adsorption of weak polyelectrolytes. Böhmer, et al.[47] extended the same theory to model weak polyelectrolyte adsorption between two charged surfaces.

In each treatment, the authors begin derivation of the model by adding a term to the internal energy portion of the partition function. This term accounts for electrostatic contributions. An expression for the potential energy, as a function of distance from the surface, is then defined. It is here that the theories differ. The assumptions on which the potential energy functions are based, vary. The theory developed by Böhmer, et al.,[47] is the most comprehensive.

Böhmer and coworkers define an adsorption system in which all ions have a volume equal to that of a lattice site. The fraction of charged segments in a given molecule, which for weak polyelectrolytes is a function of pH, is allowed to vary with distance from the surface. The charges due to the surface and the polymer segments are considered to be smeared out in layers parallel with the surface. They are located at the center of each plane, with the space between planes being charge free. A discrete version of the Poisson-Boltzmanm equation is used to

obtain the electrical potential in each plane. The potential difference then depends on the charge at each plane, the separation distance, and the dielectric constant.

To apply this model one must know or assume a number of system properties. For calculation of the configurational contribution these are: the number of monomer segments per molecule (r), the lattice geometry (e.g. hexagonal), the layer thickness (d), and the total segment volume fraction (ϕ_b). For calculation of the non-electrostatic contributions, the relevant system properties are: the Flory-Huggins segment-solvent interaction parameter (χ) and the Silberberg segment-surface interaction parameter (χ_s). For the calculation of electrostatic contributions the relevant system properties are: the polymer charge density (α), the surface charge (σ_s), the pH, the relative dielectric constant ($\varepsilon/\varepsilon_0$) of each component, and the salt concentration (c_s). The charge density of a polymer, α, will be defined as the fraction of charged monomer units. Strong polyelectrolytes have an α equal to one. For weak polyelectrolytes, α is dependent upon pH.

Böhmer,[47] van de Steeg,[48] and coworkers used the model to study the effects of polymer charge density, salt (c_s), surface charge (σ_s), and non-electrostatic interactions (χ_s) on the adsorption of polyelectrolytes. Böhmer, et al., modeled the adsorption of a strong polyelectrolyte and a weak polyacid onto a positively charged surface. Van de Steeg, et al., modeled adsorption of polyelectrolytes at various α on an oppositely charged surface. The trends observed are summarized below.

For strong polyelectrolytes, Böhmer and coworkers show that the amount adsorbed increases with increasing c_s. Increased c_s screens segment-segment repulsion, thereby allowing a

more looped configuration. They also show that the amount adsorbed increases linearly with increased surface charge.

For weak polyacids, they show that at high pH, where dissociation is complete, the adsorbed amount is low and increases with increased surface charge. As the pH decreases, the degree of dissociation of the polyacid decreases. Reduction in the number of charged groups reduces the total attraction for the surface, as well as the internal segment-segment repulsion. A more looped configuration forms, thereby allowing more polymer to adsorb.

The model predicts maximum adsorption at 1-1.5 pH units below the pK_a of the polyacid. Here the degree of dissociation in the first layer self adjusts to compensate for the surface charge. When the pH is further reduced, the polymer can no longer compensate the surface charge. Salt ions then adsorb, displacing polymer segments. The net effect is a reduction in the adsorbed amount at low pH. This reduction in adsorbed amount is more prominent with increasing surface charge.

Van de Steeg and coworkers[48] investigated the interplay of electrostatic and non-electrostatic segment-surface interactions. They define two distinct adsorption regimes which might occur at any given α. The first is the screening-reduced adsorption regime, where electrostatic attraction dominates and the adsorbed amount decreases with increasing salt concentration. In this region, salt can reduce the adsorbed amount by screening the electrostatic interaction between the segment and the surface. The second is the screening-enhanced regime, where non-electrostatic attraction between segment and surface dominates and the adsorbed

amount increases with increasing salt concentration. In this region salt screens repulsion between charged segments and enhances adsorption.

The strength of the electrostatic forces depends on α and σ_s. The non-electrostatic forces are taken into account by χ_s. For a system where $\chi_s = 0$, adsorption occurs in the screening-reduced regime exclusively. In general, the amount adsorbed decreases with increasing α and increases with increasing σ_s. For a system with a finite χ_s both the screening-reduced and the screening-enhanced regimes can exist. Here the adsorbed amount is a complex function of α, σ_s, c_s, and χ_s. The balance of electrostatic and non-electrostatic forces must be considered.

Böhmer,[47] van de Steeg,[48] and coworkers cite numerous articles which support, at least qualitatively, the various trends predicted by the model. A comprehensive experimental study of the variables defined by the model is lacking, for a number of reasons. First, the model incorporates a large number of variables. Performing a comprehensive study of all the variables and their effects would be an overwhelming task. Most authors limit their studies to one system and a few variables which are of particular interest.

Second, some of the variables used in the model are not readily varied. For example the Flory-Huggins segment-solvent interaction parameter (χ) and the Silberberg segment-surface interaction parameter (χ_s) are both specific to the adsorption system under consideration. To study their effects experimentally, one must change the polymer, solvent, or surface used.

EXPERIMENTAL STUDIES OF ADSORBED POLYMER CONFIGURATIONS

Overview

Tadros,[49] and Fleer and Lyklema[1] have written extensive reviews which describe many of the experimental techniques used to study adsorbed polymer. The latter divide these techniques into three groups: those leading to the adsorbed amount, those leading to the thickness of the surface layer, and those leading to the amount at the surface (trains). These quantities can be used to characterize the adsorbed polymer configuration.

Typically, the amount adsorbed, or the excess surface coverage, is determined by difference. The amount of polymer added initially is known. The amount of polymer remaining in solution at equilibrium is measured using a suitable analytical technique. The total surface coverage is then determined by difference. Colloid titration,[50] fluorescence spectroscopy,[51] total organic carbon analysis,[50] and potentiometric titration[50] are some of the analytical techniques that have been used to measure excess polymer in solution.

The thickness of an adsorbed layer is commonly measured by ellipsometry or hydrodynamics. In ellipsometric measurements, the thickness and average concentration of the adsorbed layer are derived from changes in the properties of elliptically polarized light. In hydrodynamic measurements, the thickness is deduced from the displacement of the slipping layer between the solid and liquid phase. These techniques, and the difficulties involved in using them, have been discussed elsewhere.[1]

Fleer and Lyklema[1] categorize the main techniques used to measure the amount of polymer at the surface, or the bound fraction, p, as either electrochemical or spectroscopic. Electrochemical techniques are based on measurements of electrical double-layer properties. The double layer charge, or shifts in the point of zero charge (p.z.c.), have been used to quantify the amount adsorbed at the surface.[1]

Spectroscopic techniques typically count the number of adsorbed functional groups, or the bound fraction, by quantifying changes which occur in spectra on adsorption. Some of the techniques which have been used include: diffuse reflectance spectroscopy,[52] inelastic electron tunneling spectroscopy,[53] pulsed nuclear magnetic resonance spectroscopy (NMR),[54,55,56] fluorescence spectrophotometry,[57] photon correlation spectroscopy,[58] and electron paramagnetic resonance spectroscopy (EPR).[59,60,61,62]

Small-angle neutron scattering (SANS) has also been applied to the study of adsorbed polymer layers. The spatial distribution of atoms is characterized by the intensity of the neutron scattering in an adsorption system. Variation of isotopic content allows the interfacial region to be viewed against a weakly scattering background.[1] The technique can be used to determine bound fraction, adsorbed layer thickness, and volume fraction profiles.[63]

In general, the techniques discussed above require specialized materials or instruments. On the other hand, fourier transform infrared (FT-IR) spectrometers are common analytical tools which can be used to study polymer adsorption. Their constantly decreasing size and complexity, and their progression into the industrial workplace, could provide new avenues for

the study of polymer adsorption. FT-IR spectroscopy and its application to the study of polymer adsorption is discussed in the following section.

IR Spectroscopy

Analysis of polymer adsorption by infrared spectroscopy has been reviewed by Rochester,[64] Fleer and Lyklema,[1] and Scheuing.[65] Rochester discusses experimental methods and results in detail. Fleer and Lyklyma describe how infrared techniqes are applied to the study of polymer adsorption. Scheuing[65] provides the most current and comprehensive review.

Typically, adsorption of polymer functional groups is accompanied by an observed shift in their characteristic infrared absorption peaks. These shifted peaks are then used to determine the number of adsorbed functional groups. Fontana and Thomas[66] pioneered this approach in their study of poly(alkyl methacrylate) adsorption to silica. Shifts due to H-bonding between the polar ester group of the poly(alkyl methacrylate) and the available OH groups of the silica were analyzed. The sample, which formed a gel at approximately 6 to 7% solids in CCl_4, was placed between NaCl plates and IR spectra were collected.

Others have used liquid sample cells to collect IR transmission spectra of adsorbates at the surface of silica.[67,68,69,70,71,72,73,74,75] Korn, et al.,[67,68] Sakai, et al.,[74] and Kobayashi, et al.[75] used this technique to determine the amount adsorbed, as well as the fraction of bound segments. The amount adsorbed was determined by collecting spectra of silica with adsorbate and spectra of the supernatant, and determining the amount adsorbed by difference. Kawaguchi, et al.[69,70,71,72] used UV spectroscopy to obtain an independent measure of the amount adsorbed. Kobayashi, et al.[75] describe two characteristic peaks due to free and adsorbed functional groups, obtained by

subtracting a spectrum of the adsorption system from a spectrum of free adsorbate. They use these peaks to determine the fraction of segments in loops and tails, respectively.

The authors discussed above have been successful in applying liquid cell transmission techniques to the study of adsorption in CCl_4. Part of this success is due to the non-absorbing nature of CCl_4. Water, on the other hand, adsorbs strongly in the infrared. These types of solvents make it more difficult to use infrared spectroscopy to study polymer adsorption.

There are two main problems. First, standard cuvettes, with long path lengths, become opaque to infrared energy when filled with aqueous samples. Cells with short path lengths (e.g. 25 μm) can be used to collect spectra of aqueous samples; however, these cells can be difficult to use. Care must be taken in filling and emptying the cell to prevent entrapment of air bubbles, which would give erroneous results. Rein and Wilks[76] also state that filling can change cell pressure, causing path length variations which would adversely affect accuracy and precision.

Secondly, peaks due to the solvent can overlap or completely overshadow solute peaks. In these cases the solvent must be subtracted from the sample spectra to obtain a useful spectrum of the adsorbing species.

FT-IR-ATR

Overview

The use of FT-IR-ATR spectroscopy in the study of polymer adsorption and other interfacial phenomena has grown rapidly in recent years. Although a number of different designs are available for liquid analysis, the Circle™ cell by Spectra Tech Inc. is the cell most

frequently used in studies described in the literature. In general, the principles on which these and other multiple internal reflection cells operate are the same. These principles have been described in detail by Harrick.[77]

In internal reflectance spectroscopy the sample is placed in contact with an internal reflectance element (IRE), which has a refractive index greater than that of the sample. An infrared source is then focused onto one end of the IRE. If the angle of the beam (ϕ)is less than the critical angle, the beam is only partially reflected and the remainder travels into the sample. If ϕ is greater than the critical angle, the beam is totally reflected. Only an evanescent wave travels through the sample and returns to the IRE. Spectra are recorded by analyzing the reflected beam. A diagram of internal reflectance sampling is given in Figure 4.

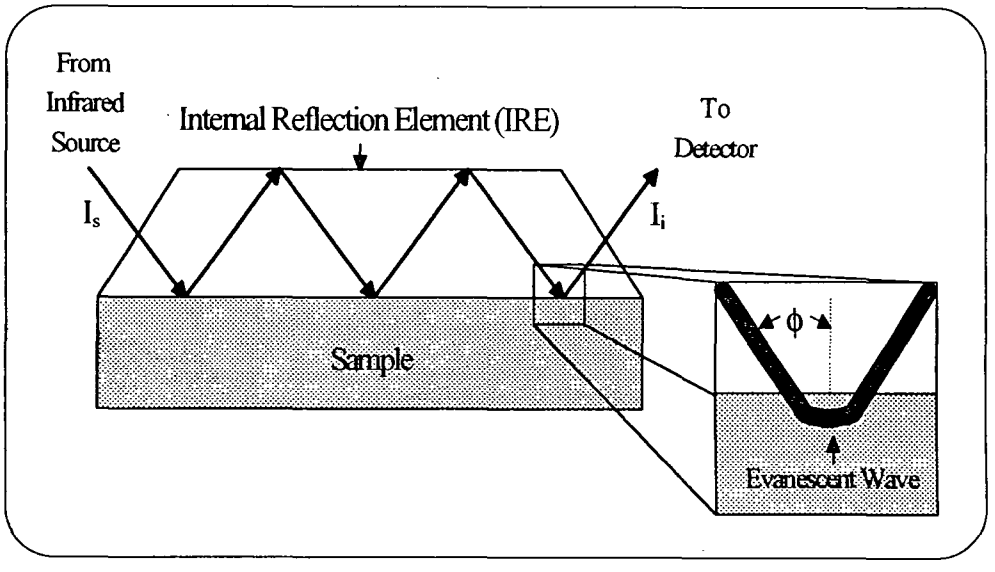

Figure 4. The beam path during internal reflectance sampling where I_s is the intensity of the source and I_i is the intensity after internal reflection.

This technique is ideal for the study of aqueous samples since the beam penetrates only a short distance, resulting in a small, effective path length. In addition, this path length is reproducible as long as the alignment and sample refractive index remain constant.

The factors which must be considered when using the Circle™ cell, and other multiple internal reflectance attachments, for quantitative analysis have been reviewed in the literature.[78,79,80,81,82] Their application to the study of macromolecules has also been discussed.[83,84] The most important factor to consider is cell alignment. The angle at which the IR beam strikes the interface of the IRE is affected by the alignment of the Circle™ cell. The depth of penetration (d_p) and the effective path length (d_e) both depend on the angle of incidence. This angle can change each time the Circle™ cell is repositioned or dismantled for cleaning. Sperline, et al.,[85] describe a spectroscopic technique for determination of the incidence angle which has been used successfully by others.[84] Solute-surface activity is another important factor to consider. Interactions at the surface can interfere with peak interpretation and quantification.

There are a variety of studies in the literature which demonstrate the utility of the Circle™ cell. They are described in the sections that follow.

Surface Studies

Scheuing,[86] and Scheuing and Hsieh[87] studied the removal of a hydrocarbon from the Circle™ cell crystal surface by the detergent action of flowing surfactant solutions. The crystal was coated with hydrocarbons and then subjected to two different flowing solutions of uncharged surfactants, by means of the flow-through Circle™ cell. Time-resolved spectra of the interface were recorded.

All spectra initially contained a distinct CH_2 scissoring peak. When the crystal was subjected to flowing water, no change was observed in the peak. Comparison of the spectra for the two flowing surfactants revealed a steady depletion of the CH_2 scissoring peak as a function of time for one surfactant and no change for the other. These results quantitatively demonstrate the applicability of the technique to the study of polymer-surface interaction phenomena.

Parry and Harris[88] used an FT-IR-ATR device similar to the Circle™ cell to study the adsorption of diphenylchlorosilane to silicon dioxide in CCl_4. A polycrystalline silicon internal reflectance element, coated with a layer of silicon dioxide, was used in the analysis. With this technique, Parry and Harris[88] were able to obtain, in situ kinetic and structural information regarding the adsorption reaction. Signal-to-noise ratio is increased by collecting a given number of scans and averaging the results. Since each FT-IR-ATR scan takes a finite amount of time (approximately 1 second), the reaction rate must be slow, so that change during the scan is negligible. Parry and Harris[88] state that the time necessary to obtain spectra with acceptable signal-to-noise ratios for their studies was approximately 5 minutes.

Sperline, et al.,[85] studied the adsorption of several surface active compounds to a ZnSe IRE. They describe the corresponding methods and equations developed for quantitative spectral analysis of the surface interaction. Surface excess values for adsorbed compounds were compared with the same values obtained by other researchers. They were able to measure the absorbance of cetylpyridinium chloride (CPC) and acetonitrile (MeCN) by integrating over the CH stretching peaks. Typical values of 0.0100 and 0.0190 absorbance units were obtained with reproducibilities of ±0.0010 and ±0.0020 absorbance units, respectively. Sperline, et al.[85] state that the calculated surface excess values compare well with those calculated by other methods.

Kuys and Roberts[89] studied the adsorption of styrene phosphonic acid (SPA) onto several surface agents using a Circle™ cell. The surface agents were coated onto the internal reflectance crystal using a vacuum evaporation method. The cell was equipped for flow-through operation and the SPA solution was pumped through. Complexation of the SPA with the surface was evident due to the replacement of the P-O vibrational peaks of the phosphoric acid group with a complex, broad peak due to the resonance stabilized phosphate group. The complexing of several surface coatings were analyzed, and the complexing mechanisms were determined.

Van der Beek, et al.[84] studied the adsorption and desorption of poly(tetrahydrofuran) (PTHF), poly(butyl methacrylate) (PBMA) and poly(methyl methacrylate) (PMMA) to an oxidized silicon IRE from CCl_4. They measured the area of characteristic infrared peaks as a function of polymer concentration. In some cases the IRE was coated with a polymer having a stronger affinity for the surface. In these experiments they found a linear relationship between peak intensity and polymer concentration. They also demonstrate the effectiveness of low molecular weight polymers and monomeric species as displacers. The relative kinetics of adsorption are also discussed when clean and coated surfaces are studied, and when narrow and polydisperse polymer samples are used.

Bulk Studies

Others have studied interfacial phenomena in the bulk of the sample using the Circle™ cell. Tejedor-Tejedor and Anderson[90] used a Circle™ cell to study the heterogeneous surface reactions which control the distribution of solute species between aqueous solutions and solid surfaces. Specifically, they studied the phosphate ion at the colloidal goethite (α-FeOOH)

interface. Spectra were measured as a function of pH (and/or pD), ionic strength, and nature of the "inert" anion. Subtracting the spectrum of the supernatant of the goethite solution from that of the solution itself left a spectrum of the goethite alone, which was comparable to those obtained by diffuse reflectance and transmission techniques. However, in addition to the normal peaks, they observed peaks resulting from the interactions of H_2O and D_2O solvents at the interface (the two were studied separately).

When ionic strength was increased, Tejedor-Tejedor and Anderson[90] observed an increase in slurry pH and changes in the relative intensities of the solvent-goethite interaction peaks discussed above. Change was dependent on the type of ion added. They made no attempt to explain these changes. The ionic species may be affecting the interaction energies between the solvent and goethite surface. They also noted the splitting of one interaction peak. This they attributed to the presence of two different types of interaction peaks, one associated with a Fe-solvent interaction and one with a H-bond interaction between the solvent and goethite. Tejedor-Tejedor and Anderson[90] discuss the effect of pH in full detail. In general, the relative intensities of the interaction peaks are again affected, and the same peak splitting discussed earlier is observed. Zeltner, et al.[91] review the work of Tejedor-Tejedor and Anderson,[90] and go into further detail regarding the technique, experimental procedure, and theoretical implications.

Urban, et al.[92] studied the structure of styrene/acrylic acid copolymer (S/AA), in an aqueous solution, using a Circle™ cell. The spectrum of the S/AA copolymer in solution by itself showed peaks at 1710 and 1733 cm^{-1} which are characteristic of non-bonded and H-bonded carbonyl groups in the acrylic acid segments. When base was added, these two peaks disappeared, and two new peaks at 1407 and 1547 cm^{-1} were observed. These new peaks were

attributed to the symmetric and asymmetric stretching modes of R-CO_2^- groups. They also note that the difference spectrum contains a new water peak at 3400 cm^{-1} due to water-polymer interactions.

Braue and Pannella[93] used the Circle™ cell to study aqueous solutions of the chemical warfare agents tabun, sarin, and soman. They used a flow-through design to obtain both qualitative and quantitative data. Concentrations in the 0.5 to 2.0 mg/ml range were analyzed with a coefficient of variation of 3.0 and 6.0 %, for intra-daily and inter-daily measurements, respectively. They state that the technique is an improvement over gas chromatographic methods used previously.

Kung and Hayes[94] have studied the spectra of cetyltrimethylammonium bromide (CTAB) and cetylpyridinium chloride (CPC) in aqueous solution and adsorbed to silica particles using a Circle™ cell. They observed a shift of the CH_2 stretching peaks to higher frequencies when spectra of aqueous surfactant were compared with solid state spectra. The authors cite a number of references to support the conclusion that the shift represents an increase in disorder of the CH_2 groups, caused by a relative change in the hydrophilic environment. A shift from high to low frequency was observed when spectra of surfactant concentrations below and above the critical micelle concentration are compared. These shifts were used to interpret the structure of the surfactants at the surface of the silica particles in suspension.

PRESENTATION OF THE PROBLEM

Synthetic polyelectrolytes are commonly used as retention aids at the wet end of the paper machine. Theories in the literature describing the mechanism of retention by polyelectrolytes are dependent upon their configuration at the surface. The configuration of an adsorbed polyelectrolyte may vary with polymer charge density, surface charge density, salt concentration, molecular weight, solubility, non-electrostatic affinity for the surface, and steric hindrance due to branching.

Solubility, non-electrostatic affinity for the surface, and steric hindrance are variables which are specific to the polymer, solvent, and surface (adsorption system) used and are, therefore, difficult to vary independently. A comprehensive study of their effects on adsorption would be impractical because of the large number of different systems which would be required. Most studies in the literature concentrate on a specific adsorption system. Various authors have studied the effects of one or several of the adsorption variables that can be varied independently. There is a need for a comprehensive study of these variables.

Böhmer, et al.[47] have extended the self-consistent field model for polymer adsorption, developed by Scheutjens and Fleer,[17,18] to allow modeling of polyelectrolyte adsorption. The model is applicable to straight chain polyacids or polybases, with repeating monomer segments. The system variables described above are taken as input. The authors and their coworkers have made comparisons with experimental data which support the model predictions, at least qualitatively, if not quantitatively. Direct comparisons by researchers outside of this group are

frequently limited to general qualitative statements. An independent evaluation of the model, using data from a well defined system, would be valuable.

The configuration of adsorbed polymers is not readily measured. However, it can be characterized with knowledge of measurable quantities which include: the total amount adsorbed, the fraction of bound segments, the adsorbed layer thickness, and the segment density distribution near the surface. A variety of techniques have been used to measure these quantities. However, many require specialized materials or instruments. The development of simplified techniques for the study of polymer adsorption in aqueous systems would be beneficial to the paper industry.

THESIS OBJECTIVES

1. Determine the effects of pH, molecular weight, salt concentration, and particle surface charge density on the adsorption of a weak polyelectrolyte onto a well characterized, oppositely-charged, surface.

2. Compare the experimental results with predictions obtained by applying the self-consistent field model for polyelectrolyte adsorption proposed by Böhmer, et al.[47]

3. Develop a FT-IR-ATR technique for studying polyelectrolyte adsorption in aqueous media.

GENERAL APPROACH

The first step was to select an appropriate adsorption system. It was necessary to choose the system carefully to allow study of the broadest range of each adsorption variable, to provide data for direct comparison with predictions made via the Böhmer model, and to allow corollaries to be drawn with papermaking systems. In this case the clear choice for solvent is water. The proper choices for polymer and surface are less obvious.

Highly branched, quaternary polyamines are frequently used as retention aids in the paper industry. However, these types of polyamines would not be suitable since branching is not considered in the Böhmer model and since polymer charge density can not be varied without changing the structure of the polymer. Polyallylamine (PAAm) was chosen as the best compromise for several reasons. First, PAAm is available commercially, which eliminated the need for synthesis work. Secondly, since PAAm has a linear backbone, it can be modeled adequately by the Böhmer model. Thirdly, the charge density can be varied by changing pH, due to ionization behavior of the primary amine functional group.

The ideal surface to study would be pulp fibers. However, because of the porous nature of pulp, it can be difficult to characterize the accessible surface area and net surface charge. The need for a well defined system led to the selection of a model colloid. Well characterized polystyrene latex particles were purchased for this purpose.

The system described above has been used to study the effects of pH, molecular weight, salt concentration, and particle surface charge density (Objective 1). The adsorption experiments were planned using a statistical response surface design. Batch adsorptions were

prepared at the various levels of the experimental design. In each case, the adsorption samples were shaken for 24 hours and filtered. A colloid titration technique was used to determine the quantity of PAAm in the filtrate. The amount adsorbed was determined by difference. Adsorption isotherms were plotted showing the amount of PAAm adsorbed versus equilibrium concentration in the bulk.

MULPOL, a version of the program described by Böhmer, et al,[47] was generously provided by the late Dr. Jan M. H. M. Scheutjens of Wageningen Agricultural University, The Netherlands. The program was loaded on a VAXstation 3100 (Digital Equipment Corporation) with a VMS (Virtual Memory System) operating system. MULPOL was used to model equilibrium adsorption of PAAm. The predictions were compared with the adsorption levels found in the plateau region of the experimental adsorption isotherms (Objective 2).

The application of FT-IR-ATR techniques to the study of polyamine adsorption is hindered by two obstacles. First, it is difficult to separate moderate and weak intensity amine peaks from strong water peaks in sample spectra. Interactive subtraction techniques are commonly used for removing the peaks of one component from a multicomponent spectrum. However, these techniques typically lack objectivity. To overcome this obstacle, an algorithm has been developed to objectively subtract reference spectra from sample spectra (Objective 3).

Secondly, there is limited information regarding changes in polyamine spectra as a result of adsorption. To effectively isolate and study PAAm adsorption to colloidal PSL particles in the bulk via FT-IR-ATR spectroscopy, adsorption of PAAm to the IRE must be prevented, or fully characterized. The latter approach was taken here. Adsorption of PAAm to the ZnSe IRE was

studied at various pH and concentration levels. Experiments were also performed to study PAAm adsorption as a function of time. Several trends have been identified for adsorption of PAAm to a ZnSe internal reflectance element. A spectrum of PAAm adsorbed to colloidal PSL was obtained (Objective 3).

MATERIALS

POLYSTYRENE LATEX (PSL) PARTICLES

Polystyrene latex particles, with sulfate surface groups, were used as the model colloid in this study. PSL particles have been used as model particles by a number of IPST researchers, both past [4,11,95,96,97] and present (Matthew H. Lang). PSL particles are well suited for model colloidal studies for the following reasons: 1) the particle size and particle size distribution can be accurately controlled within a narrow range, 2) the particles are spherical, 3) the particles are non-porous, and 4) the particles are stable over a wide pH range.[4]

The surfactant-free PSL used in this thesis was purchased from Interfacial Dynamics Corporation (IDC). The samples and their relevant characteristics are listed in Table 1 below.

Table 1. The PSL samples used and their characteristics.

Lot No.	10-52-90	10-118-34	7-108-7
Mean Diameter (μm)	0.086 ± 11.6%	0.081 ± 12.1%	0.098 ± 10.9%
Percent Solids	10.600 ± 0.1	10.67 ± 0.1	9.180 ± 0.1
Surface Charge Density	0.0062 C/m^2	0.0081C/m^2	0.0116 C/m^2

Certificates of analysis are shipped with each PSL sample sold by IDC. These certificates provide a detailed description of all relevant PSL characteristics. The protocols used by IDC [98] to acquire this data are similar to, if not more advanced than, those in the literature and those used at IPST in the past. Particle size is determined by electron microscopy, percent solids by

gravimetric means, and surface charge density by conductimetric titration. The data provided in the certificates of analysis were used without additional testing.

The samples described above have only sulfate groups at the surface. The sulfate groups provide a constant negative surface charge over a pH range of 3-10.[11] The samples were chosen to cover the broadest surface charge density range possible. The samples were stored in a refrigerator during the duration of this thesis.

POLYALLYLAMINE HYDROCHLORIDE (PAAm)

In 1984, Harada and Hasegawa[99] developed the first practical methods for the preparation of PAAm.[100] In these methods an aqueous solution of monoallylamine hydrochloride is refluxed with gentle heating in the presence of one of two radical initiators containing an azo group and ammonium groups. In addition, some of the solutions contained; water, $ZnCl_2$, phosphoric acid, and sulfuric acid. Polysciences Incorporated and Aldrich Chemical Company are two commercial sources for PAAm. The chemical structure of PAAm is shown in Figure 5 below.

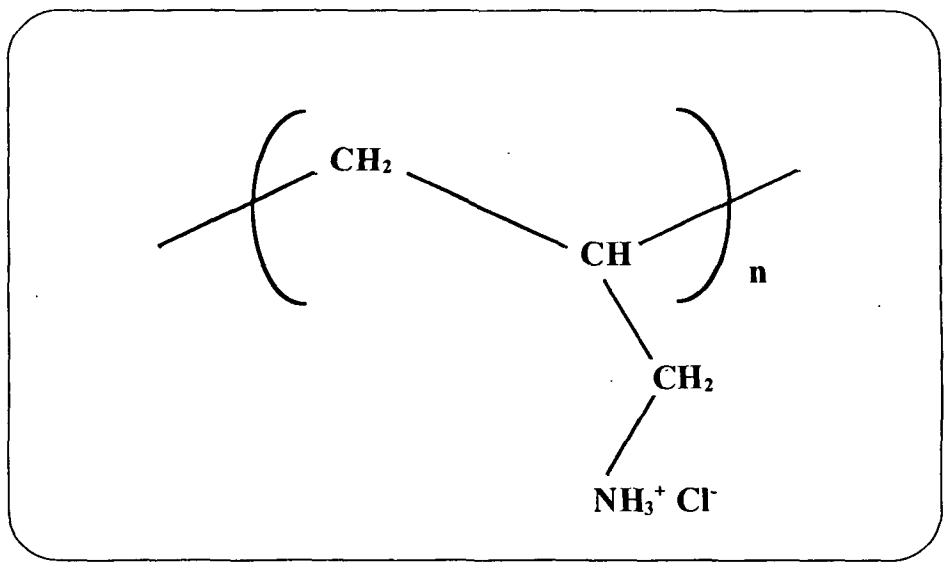

Figure 5. The chemical structure of polyallylamine hydrochloride (PAAm).

A sample of the Aldrich PAAm was shipped to Galbraith Laboratories, Inc. for elemental analysis. The sample was dried after shipment and the quantity of C, H, N, Cl, and O in the sample was determined. The results are as follows: C (37.22%), H (8.63%), N (14.32%), Cl (36.88%), and O (3.47%). C, N, and Cl are present in the proper proportions. H and O are present in excess, which may indicate the presence of water. This would not be surprising, since PAAm is extremely hygroscopic.

Two PAAm samples were purchased from Aldrich Chemical Company for experimental purposes. The samples are described by Aldrich as being high and low MW (approximately 50,000 - 60,000 and 8500 - 11,000, respectively). These polydisperse samples were fractionated using size exclusion chromatography to obtain samples with narrow MW distributions.

Size exclusion chromatography and capillary viscometry were used to determine M_n and M_w for the PAAm fractions. The degree of PAAm protonation as a function of pH was determined by potentiometric titration. These characterization techniques and the results are discussed in detail in the methods section below.

After weeks of storage in a dark cabinet, the fractionated PAAm solutions developed a slight yellow tint. Analysis of the samples via FT-IR showed that no significant changes occurred in the PAAm spectrum. The samples were then stored in a refrigerator at 5°C. After this step was taken no noticeable discoloration occurred. Periodic analysis of the samples via FT-IR showed no changes in the PAAm spectrum.

EQUIPMENT

SIZE EXCLUSION CHROMATOGRAPHY SYSTEM

Size exclusion chromatography (SEC) was used to fractionate PAAm into different molecular weight (MW) samples with narrow MW distributions. The following is a detailed description of this system.

A Vista Series 5000 HPLC with a Varian Universal column heater and a Valco injection system was linked to a Hewlett Packard HP1047A refractive index detector with analog output. A tube directed sample flow from the detector outlet to a Gilson FC-100K Fractionator. A Dell computer with a Princeton EGA monitor and a Metrabyte® analog to digital converter board was used to receive the detector signal. CODAS software provided a real time display of the signal, in addition to data storage capabilities. LABCALC® software was used to convert and process the stored data.

The Varian Universal column heater was used to control the temperature of the analytical scale columns. This heater was too small to be used for the semi-preparative column. A water jacket was built, using 2" I.D. plexiglass tubing, to heat the semi-preparative column and guard. A Thermomix 1460 heat pump, by B. Braun, was used to maintain water temperature in a reservoir and to pump this water to the water jacket.

A 100 x 4.6 mm, 5.6 μm Hypersil® ODS column was used to verify that the detector and the data acquisition system were functioning properly (the test procedure is described in the HP1047A manual). A 250 x 4.6 mm I.D. SynChropak® CATSEC 1000 analytical column with

a 50 x 4.6 mm I.D. guard column was used for some of the preliminary method development work and for analysis of the fractions after they had been collected. A 250 x 21.2 mm I.D. SynChropak® CATSEC 1000 semi-preparative column with a 65 x 21.2 mm I.D. guard column was used for preliminary method development work and for the actual PAAm fractionation.

The applicability of SynChropak® CATSEC columns to SEC fractionation of polyamines, and in particular the fractionation of the Aldrich PAAm, has been demonstrated in the literature.[101,102] Gooding et al.[101] briefly review earlier techniques for SEC analysis of cationic polymers. They also describe the characterization and use of the CATSEC column. Their results demonstrate that when acidic eluents containing salt are used, polyamines are effectively fractionated via size exclusion chromatography. The salt was added to eliminate ion-exclusion effects. Different concentrations of acid and various salts were tested.

Nagy and Terwilliger[102] used a series of CATSEC columns to demonstrate the use of a differential viscometry detector. In their study, they fractionated the high and low MW Aldrich PAAm described earlier using a solution containing 0.1% trifluoroacetic acid (TFA) and 0.2 M $NaNO_3$ for eluent. Due to its demonstrated applicability, the same eluent was used in this study.

TITRATION EQUIPMENT

Titrations were automated through the use of a Metrohm Potentiograph Recording Titrator, model 536. The titrator came equipped with a Dosimat 665 titrant dispensing unit. This particular unit has a buret volume of 20 ml and a one liter titrant reservoir. Results were recorded on chart paper.

A Metrohm combination electrode was used to measure pH for all potentiometric titrations. Figure 6 below shows the flask used for potentiometric titrations. The flask was constantly stirred and blanketed with N_2 throughout the titration process.

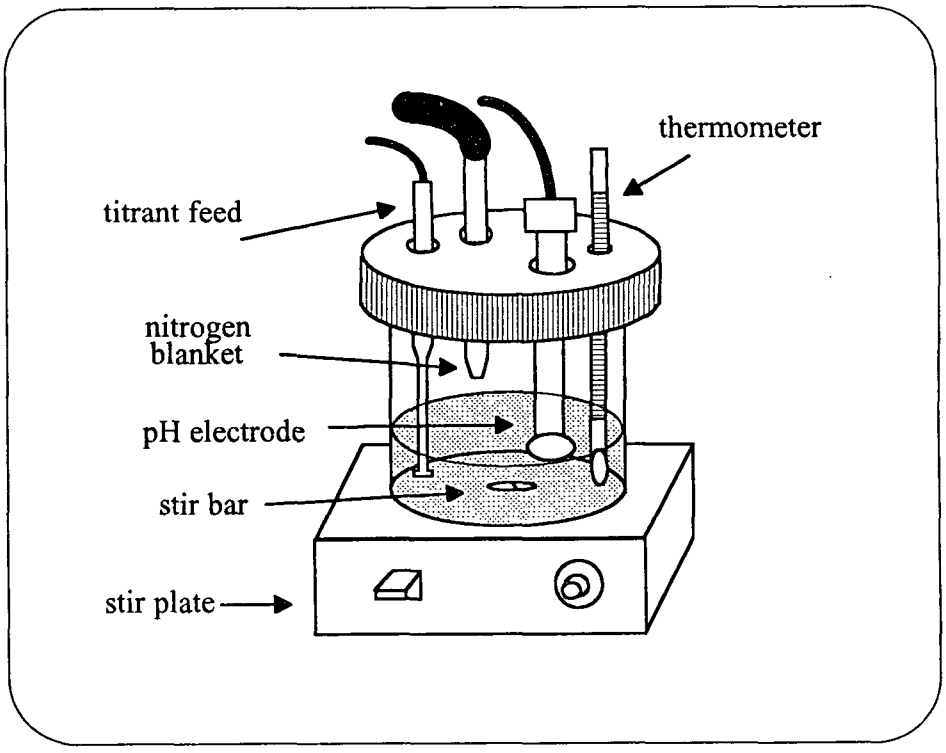

Figure 6. The flask used for potentiometric titrations of PAAm.

The Metrohm Potentiograph Recording Titrator was also used to perform the colloid titrations for PAAm quantification. A Brinkmann Probe colorimeter, model PC801, was used to detect the colorimetric end point. The colorimeter is equipped with an analytical filter wheel which holds 450, 470, 520, 570, 620, and 670 nm filters. Colloid titrations were performed in a polyethylene beaker.

FT-IR SPECTROMETER WITH ATR SAMPLING

Spectra were collected at 4 cm^{-1} resolution on a Nicolet 60SXR FT-IR spectrometer equipped with a liquid nitrogen cooled MCT-B detector and a KBr beam splitter. A total of 1000 and 500 single beam scans were collected and averaged for static and kinetic measurements, respectively. The aperture was set to medium and the gain to 1 for all scans.

The sample holder was a Spectra Tech Inc. flow-through, micro Circle™ cell. The sealed, flow-through Circle™ cell prevented evaporation which would contaminate the FT-IR bench purge. Teflon tubing connected to the Circle™ cell inlets was extended through seals in the sample compartment doors. Use of these tubes allowed samples to be injected and the cell to be flushed without breaking the bench purge. Figure 7 below show a simplified diagram of the Circle™ cell.

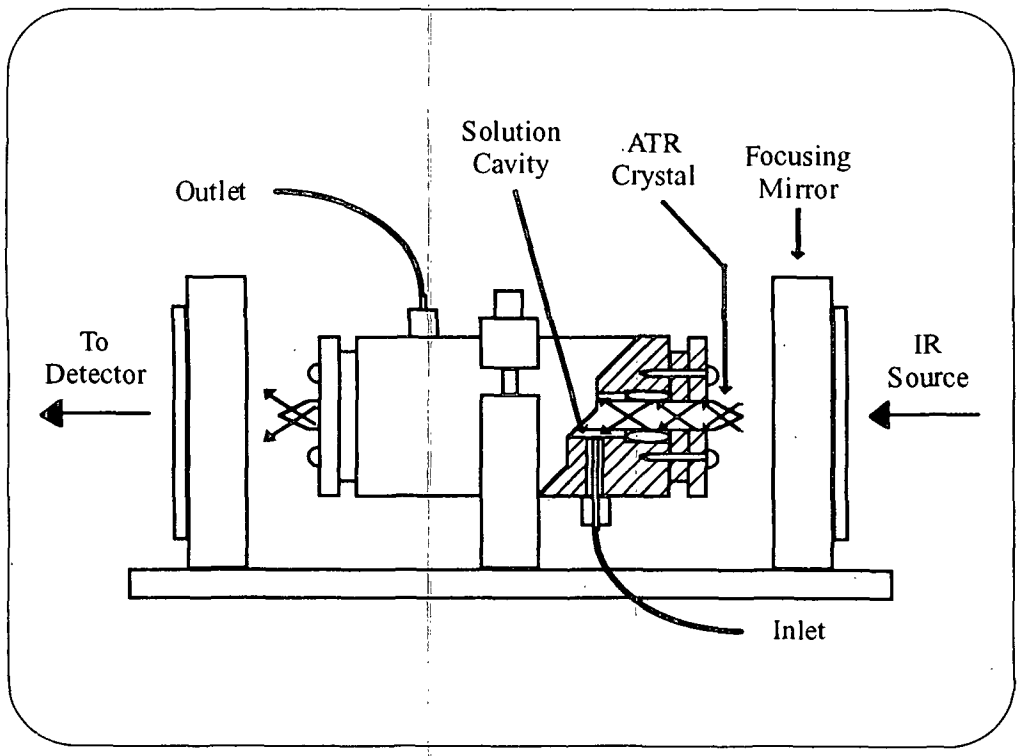

Figure 7. A simplified diagram of the Circle™ cell.

The Circle™ cell was mounted in a removable sample compartment designed by Nicolet for the 60SXR FT-IR. The sample compartment is designed to provide a way to load and unload the sample cell reproducibly. The intensity of the positive spike in the interferogram was recorded in volts per scan, before and after loading the sample compartment. On this particular instrument, the best results were obtained when this intensity was 0.13 volts/scan (± 0.02). Normally, it was necessary to reduce the total amount of infrared beam reaching the detector to obtain measurements of the appropriate intensity. This was accomplished by inserting $\frac{1}{8}$ inch screening, painted flat black, into the path between the cell and the detector.

METHODS

PAAM FRACTIONATION

Two polyallylamine hydrochloride (PAAm) samples (high and low MW, respectively), with broad MW distributions, were purchased from Aldrich Chemical Company, Inc. These samples were fractionated using SEC and the resulting fractions had narrow MW distributions. The fractionation method used is described in general terms below. A detailed, step by step description of the fractionation technique is given in Appendix I.

To determine whether the SynChropak® CATSEC 1000 analytical column was an effective means for fractionating polymer by molecular weight, a series of poly(2-vinyl pyridine) (PVP) molecular weight standards were injected. Table 2 lists the molecular weights used and their supplier.

Table 2. Poly(2-vinyl pyridine) standards used to determine effectiveness of the SynChropak® CATSEC 1000 analytical column.

MW	Source
460,000	Reilly Industries, Inc.*
240,000	Polysciences, Inc.
110,000	Polysciences, Inc.
70,000	Polysciences, Inc.
30,000	Polysciences, Inc.
13,200	Scientific Polymer Products, Inc.

* Sample donated by Ms. Susan Vorhies of Reilly Industries, Inc.

Ten microliters of each PVP standard at 1 mg/ml were injected onto the column. The HPLC was set to run at 0.4 ml/min and at 35°C. Figure 8 below is an overlay of the chromatograms for each standard.

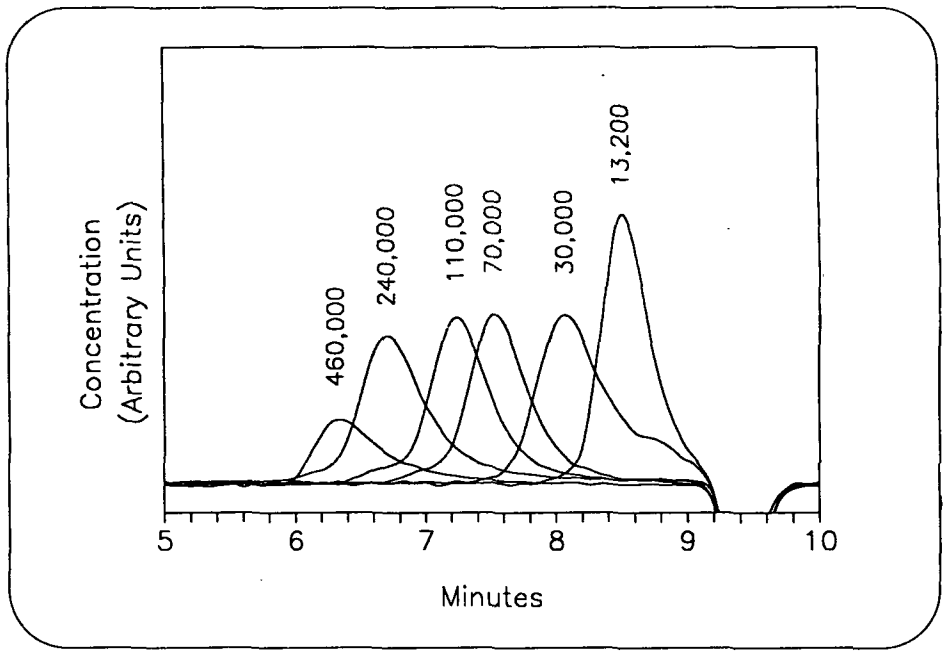

Figure 8. Chromatograms of PVP MW standards run at 35°C and 0.4 ml/min.

Figure 8 shows that under the conditions described above the CATSEC analytical column is effective at separating PVP in the 13,000 to 460,000 MW range. Typically, for a given polymer-solvent system, the natural log of MW plotted vs. retention time gives a straight line. This was done for the peaks shown in Figure 8. The retention time at the maximum was determined by using the automatic peak picking function in LABCALC®. The results are shown in Table 3.

Table 3. Retention time values obtained for PVP standards.

MW	Elution Time
460,000	6.341
240,000	6.709
110,000	7.24
70,000	7.533
30,000	8.069
13,200	8.510

Figure 9 below shows the plotted data points with the fitted line. The good linear fit supports the conclusion that fractionation is both effective and consistent.

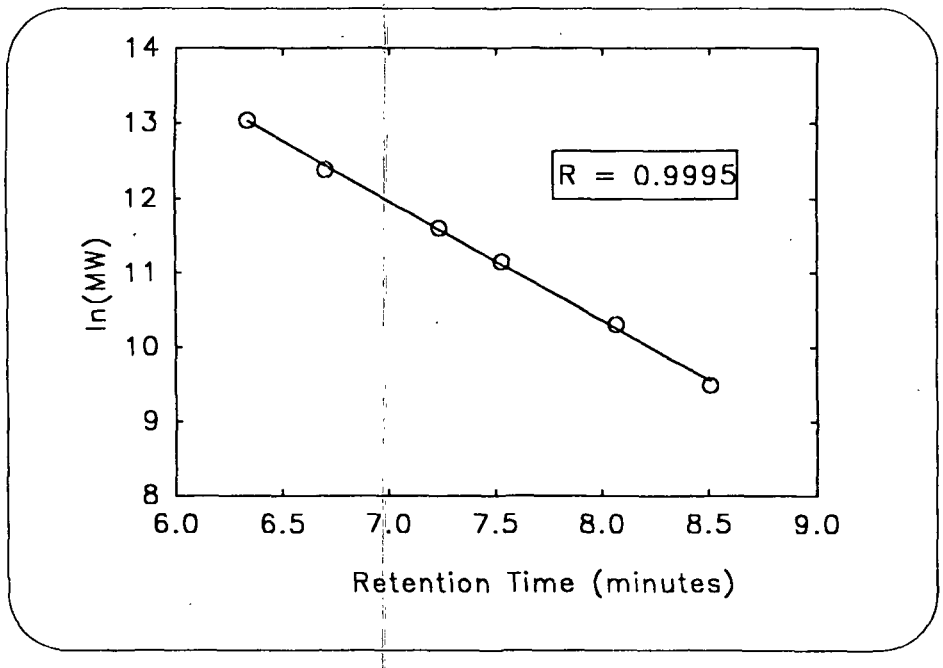

Figure 9. A plot of ln(MW) vs. retention time for the PVP standards with the linear regression fit.

The CATSEC analytical column was used to characterize the MW fractions after collection. The 250 x 21.2 mm I.D. CATSEC semi-preparative column was used to fractionate large quantities of the PAAm. To minimize the time required to collect sufficient quantities, the limits of the CATSEC semi-preparative column were tested.

Synchrom Inc. provides general guidelines for maximum flow rate, sample volume, and sample mass for their gel permeation chromatography columns but none specifically for their CATSEC columns. The stated limits for the 21.2 mm I.D. CATSEC semi-preparative columns are as follows: 204 atm of pressure, a 8.0 ml/min. flow rate, a 200 µl sample volume, and a 8-16 mg sample mass.

The HPLC pump has a maximum flow rate of 15 ml/min. Starting with 1 ml/min, we steadily increased flow rate and took note of the column pressure. The pressure reached 84 atm at a flow rate of 10 ml/min. Since this value was near the recommended maximum flow rate we chose to stop there and run a test injection. The resulting peaks were symmetric, which indicates that the column had not been overloaded. Subsequent injections were run at 10 ml/min.

To study the effects of sample volume, two injections were made, one near the recommended maximum (250 µl) and one at a considerably lower volume (100 µl). Figures 10 and 11 show the resulting chromatograms of the high and low MW Aldrich PAAm samples.

The chromatograms in Figures 10 and 11 are reasonably symmetric. No appreciable change in symmetry occurs in going from 100 to 250 µl injections. To study the effects of concentration, several injections at various concentrations were made. Figures 12 and 13 below show the resulting chromatograms. Again, no significant changes in symmetry occurred in going from 10 to 100 mg/ml.

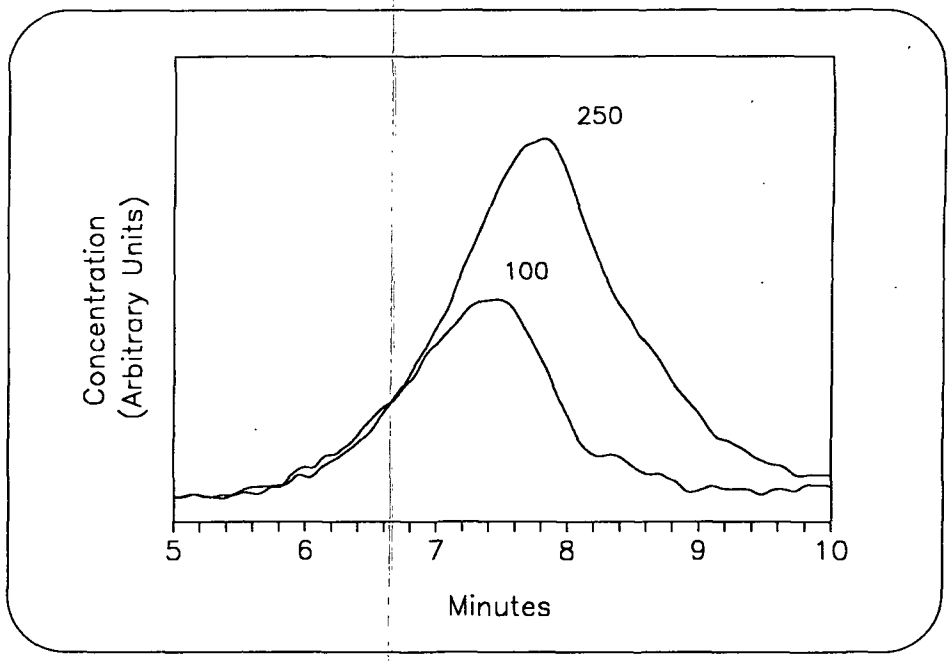

Figure 10. Chromatograms of 100 and 250 µl injections of high MW Aldrich PAAm (100 mg/ml, 10 ml/min).

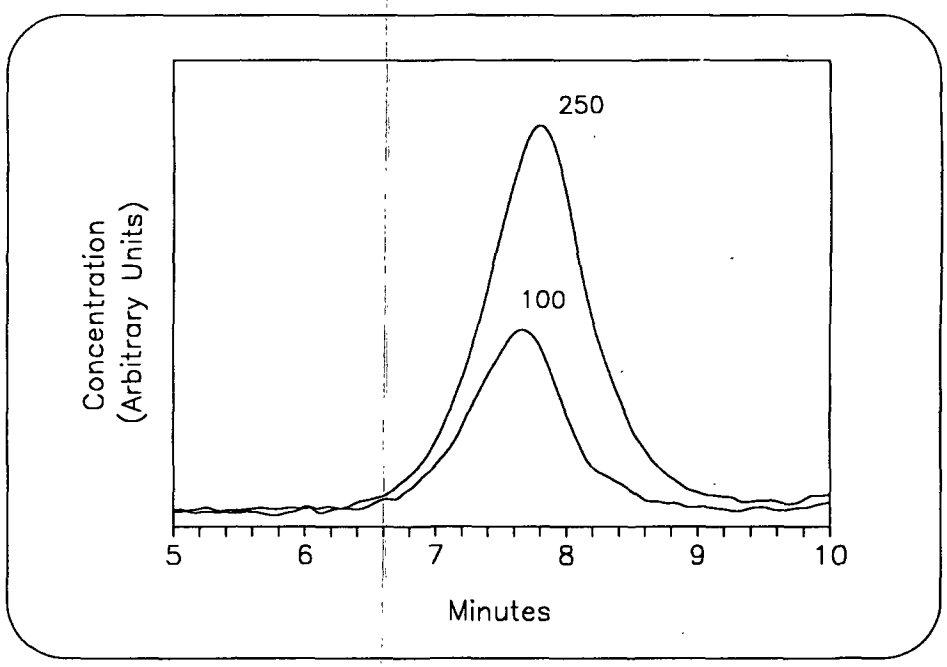

Figure 11. Chromatograms of 100 and 250 µl injections of low MW Aldrich PAAm (100 mg/ml, 10 ml/min).

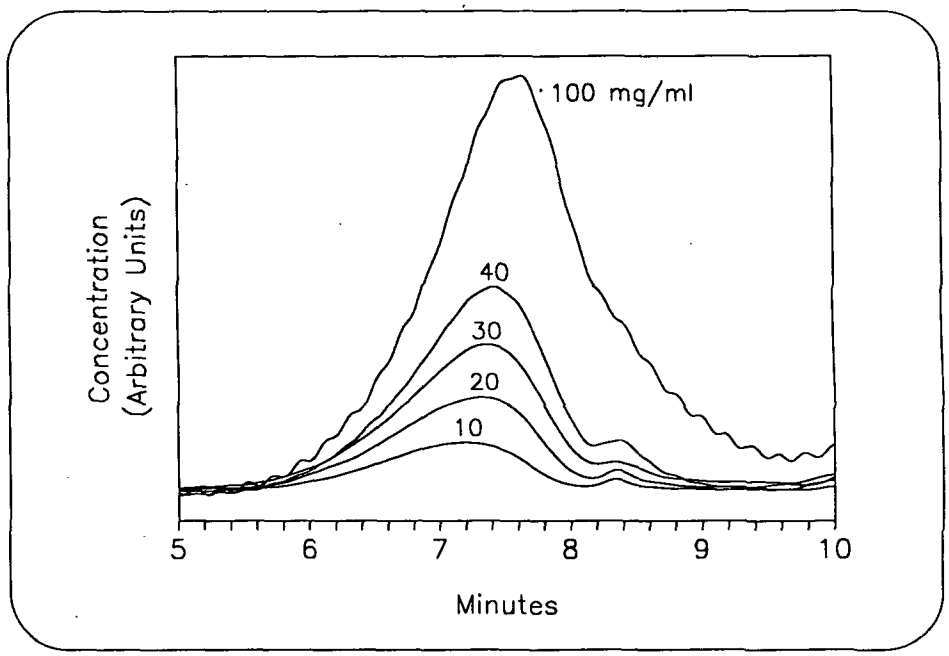

Figure 12. Chromatograms of injections of the high MW PAAm at various concentrations (250 µl, 10 ml/min).

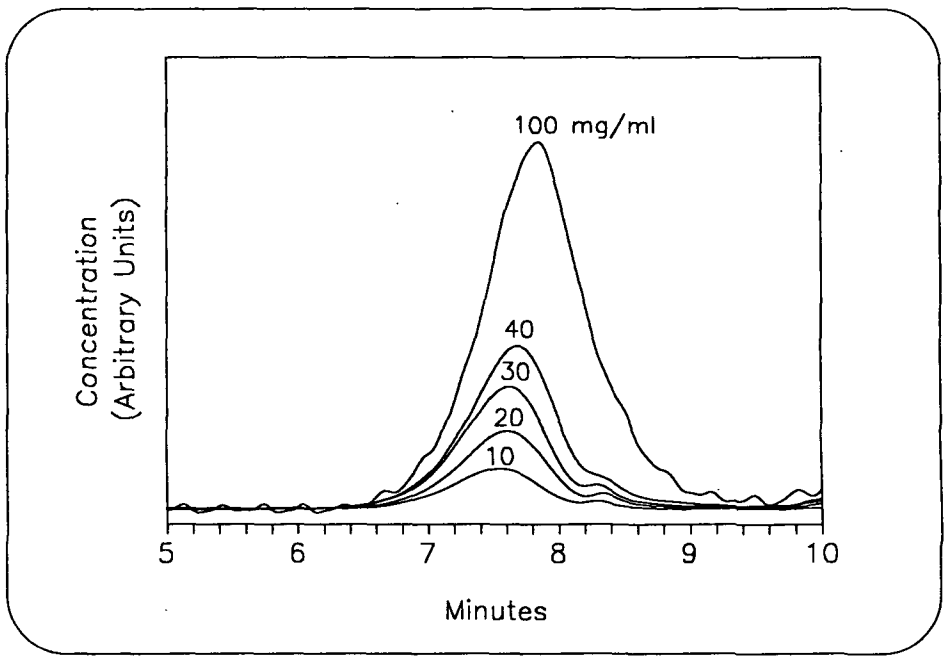

Figure 13. Chromatograms of injections of the low MW PAAm at various concentrations (250 µl, 10 ml/min).

Based on the finding described above, the PAAm fractions were collected using 250 µl injections, at 100 mg/ml and a flow rate of 10 ml/min. A total of 19 fractions were collected from both the high and low MW samples between 6.1 and 9.9 minutes. Figure 14 below shows an overlay of the chromatograms of the high and low MW Aldrich PAAm samples under these conditions.

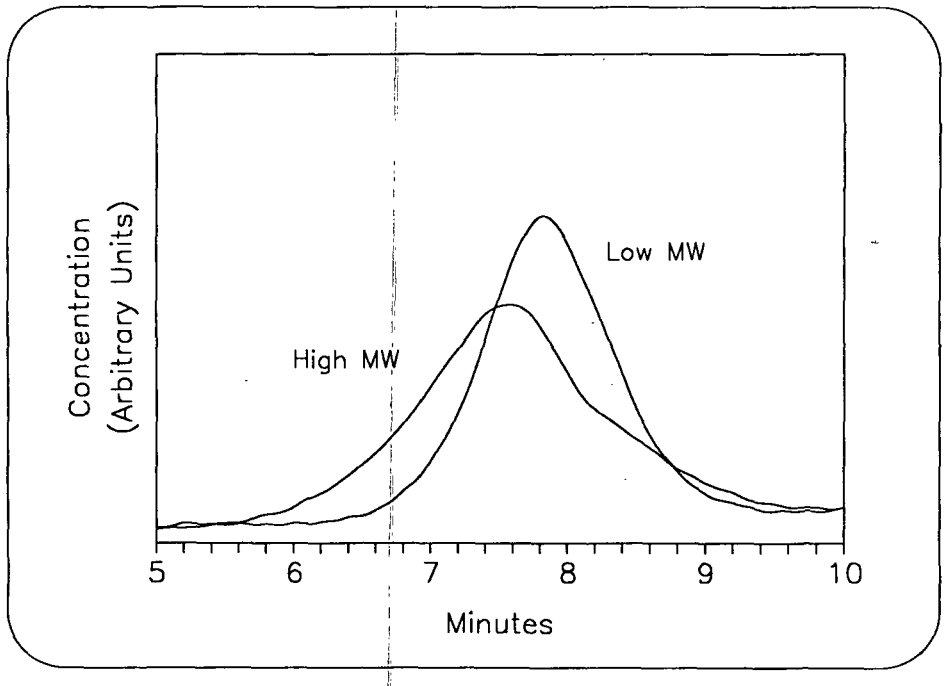

Figure 14. Chromatograms of the high and low MW PAAm samples (250 µl, 100 mg/ml, 10 ml/min).

PAAm CHARACTERIZATION

Determination Of Fraction Molecular Weight

Size exclusion chromatography can be used for molecular weight characterization if the system is calibrated. For a given polymer-solvent system, and a properly sized column, a linear relationship exists between the natural log of molecular weight and the retention time (t_r) of the

polymer sample. A calibration curve can be developed if molecular weight standards of the polymer being tested are available. Since standards are not available for PAAm, additional steps are required.

It follows from the Flory-Fox theory of solution viscosity that the size of a polymer in solution will be related to the product of its molecular weight (MW) and intrinsic viscosity ([η]).[103] A plot of ln([η]MW) versus (t_r) should give a straight line for many different linear and branched polymers. The resulting curve is referred to as the universal calibration curve. By measuring [η] and (t_r), it is possible to calculate the MW of the PAAm fractions.

Nagy and Terwilliger[102] developed a universal calibration curve for a SEC system with three Synchropak® CATSEC columns in series, with 100, 300, and 1000 Å pore size, respectively. Since only the latter column was used in this work, a new universal calibration curve was developed.

A plot of ln(MW) versus ln([η]) for the PVP standards was generated from data presented by Nagy and Terwillinger.[102] Linear regression analysis was used to obtain the Mark-Houwink relationship as follows:

$$\ln([\eta]) = 0.726(\ln(MW)) - 8.5 \qquad \{1\}$$

This relationship was then used to obtain [η] values for the PVP standards used in our work. The data are given in Table 4 below. Figure 15 shows the corresponding plot.

Table 4. Data for PVP standards from Nagy and Terwillinger.[102]

PVP MW	[η]	ln(MW)	ln([η])
1,000,000	4.46	13.82	1.5
451,000	2.72	13.02	1
240,000	1.72	12.39	0.54
110,000	1.03	11.61	0.03
70,000	0.7	11.16	-0.36
28,000	0.29	10.24	-1.24
10,500	0.15	9.26	-1.9
7,000	0.12	8.85	-2.12
2,900	0.08	7.97	-2.53

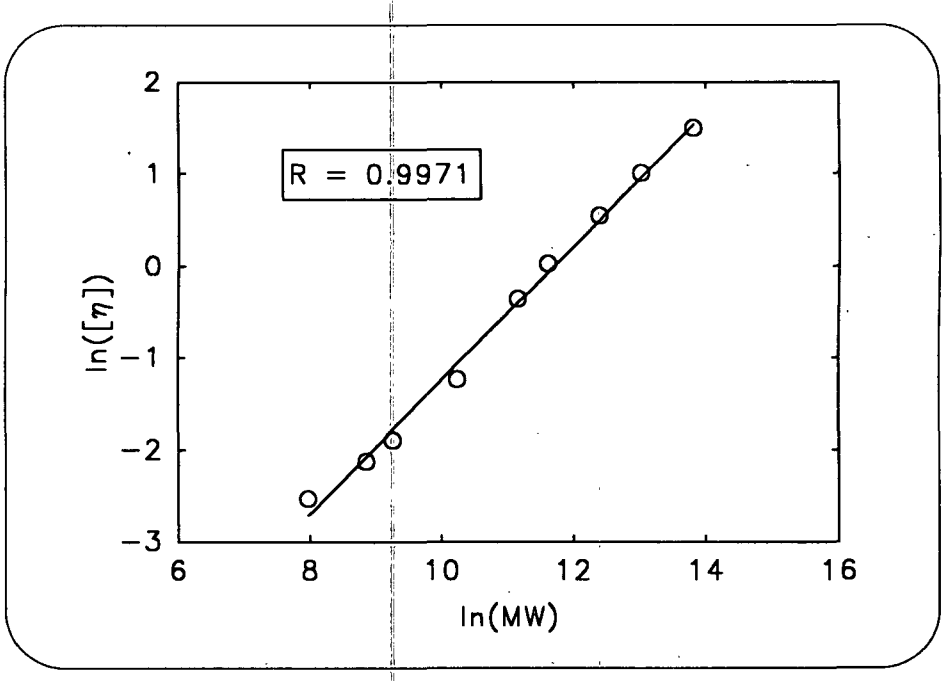

Figure 15. A plot of ln([η]) versus ln(MW) for data in Table 4.

Equation 1 was used to calculate intrinsic viscosities for the PVP standards analyzed in our experiments. The peak retention times were determined by using the automatic peak picking function in LABCALC®, a data analysis software package by Galactic Industries Corporation. This data, along with the corresponding molecular weights, appears in Table 5 below. Figure 16 shows the plot of ln([η]MW) versus retention time.

Table 5. PVP data for the universal calibration curve.

PVP MW	retention time (t_r)	calculated [η]	ln([η]MW)
460,000	6.341	2.6474	14.0126
240,000	6.709	1.6502	12.8893
110,000	7.24	0.9362	11.5423
70,000	7.533	0.6741	10.7619
30,000	8.069	0.3642	9.299
13,200	8.51	0.2006	7.8815

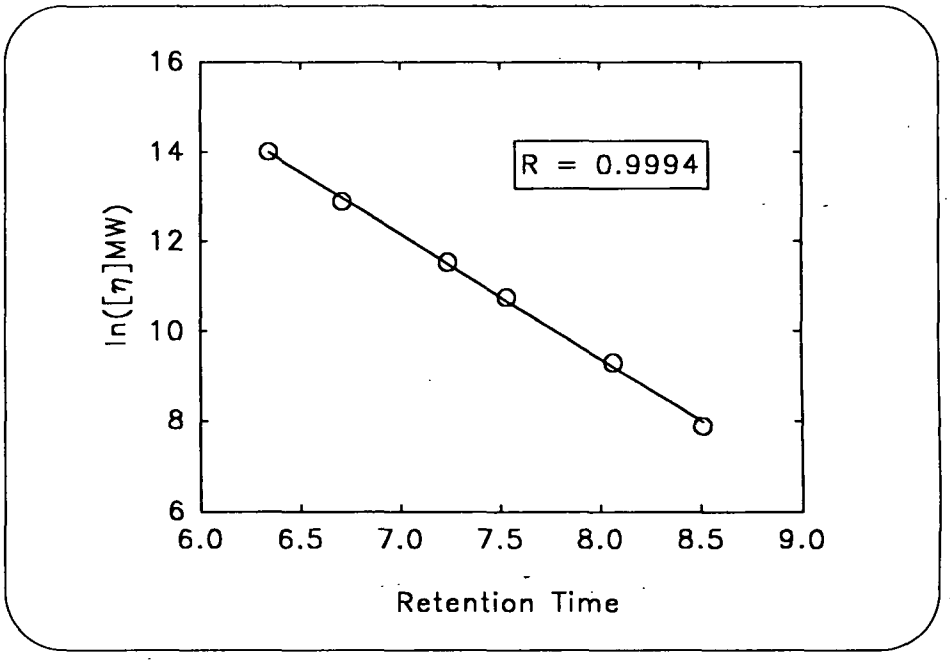

Figure 16. The PVP universal calibration curve.

Linear regression analysis was used to obtain the universal calibration curve equation below.

$$\ln([\eta]MW) = 31.6 - 2.77(t_r) \qquad \{2\}$$

The intrinsic viscosity of six primary PAAm fractions, covering a broad MW range, were determined using a CANNON 75 M150 suspended-level viscometer. The analysis began with 1 ml being pipetted into the viscometer. The solution was drawn into the bulb several times and then allowed to equilibrate to bath temperature (35°C). Then the sample was drawn into the bulb and the flow time between markings was measured with a stopwatch. This procedure was repeated five times to obtain an average. Then 0.25 ml of eluent was added and the steps above were repeated. After five consecutive dilutions, the viscometer was rinsed and dried, and a new fraction was tested. The data are given in Appendix II.

In some cases the fraction concentrations were too low to obtain good viscosity measurements. In these instances, the fractions were concentrated using an Amicon 400 ml ultrafiltration cell with Amicon Diaflo YM3 (76 mm dia.) membranes. Concentration was determined by measuring the refractive index (R.I.) on the HP 1047A detector and comparing the measurements with a standard curve. The R.I. standard curve was found to be linear in the 0.0126- 0.1754 % PAAm (w/w) range. The PAAm concentrations upon dilution during viscosity measurements were calculated.

The intrinsic viscosity is the y-intercept of the line obtained when the reduced specific viscosity ($\eta_{sp/c}$) is plotted against sample concentration. For dilute solutions, $\eta_{sp/c} = \frac{(t - t_0)}{(t_0 c)}$, where t and t_0 represent the time it takes for the sample and solvent to pass between the viscometer markings, respectively, and c is the fraction concentration.

The molecular weights of the six PAAm fractions tested were determined by inserting the measured values for [η] and t_r into the equation for the universal calibration curve (Equation 2). The data are summarized in Table 6 below.

Table 6. Data for the six primary PAAm fractions.

PAAm fractions	retention time (t_r)	measured [η]	calculated MW
H4	7.09	0.989	152,000
H5	7.28	0.833	106,000
H7	7.6	0.609	60,600
L6	7.66	0.557	55,800
L9	8.13	0.298	28,400
H14	8.14	0.327	24,900

The data in Table 6 were used to find the Mark-Houwink relationship for PAAm fractionation. Figure 17 below shows the plot of ln([η]) versus ln(MW).

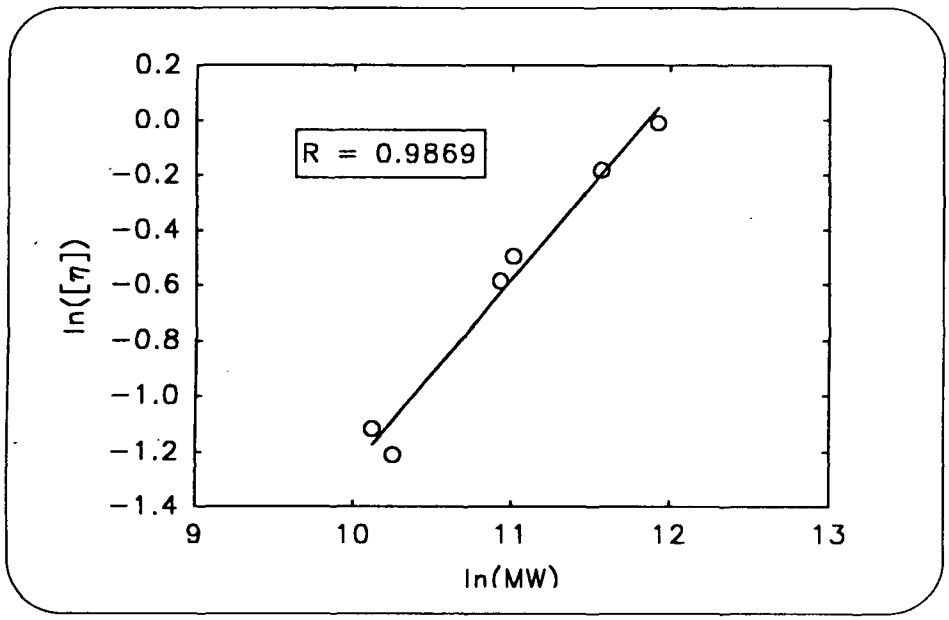

Figure 17. A plot of ln([η]) versus ln(MW) for the six primary PAAm fractions.

Linear regression analysis of the data in Figure 17 gives equation 3 below.

$$\ln([\eta]) = 0.674(\ln(MW))-8.0 \qquad \{3\}$$

Substituting equation 3 into equation 2 and solving for MW gives Equation 4 below.

$$MW = e^{(23.6-1.66t_r)} \qquad \{4\}$$

In theory, the molecular weight calculated in this manner should be between the weight average ($M_{(w)}$) and number average ($M_{(n)}$) molecular weight of the sample. To obtain a better estimate for $M_{(w)}$ and $M_{(n)}$, and the polydispersity ($M_{(w)}/M_{(n)}$) for each sample, the chromatograms for each fraction were analyzed further. Each fraction chromatogram was divided into 50 parallel time bins. The median retention time for each bin was used to calculate its molecular weight by means of equation 4. The ratio of the bin area to the total area under the curve was used to estimate the mass fraction of the molecules in each bin. These values were then used to estimate $M_{(w)}$ and $M_{(n)}$ for each fraction. The procedure is described in Appendix III. The data for all the fractions are given in Appendix IV. Only the fractions used will be discussed here.

Three PAAm fractions were used in the adsorption and FT-IR experiments discussed below. Table 7 below summarizes the results of MW characterization for the three fractions. Figure 18 shows the corresponding chromatograms.

Table 7. MW characterization data for the PAAm fractions used.

PAAm	t_r	MW[a]	$M_{(w)}$	$M_{(n)}$	$M_{(w)}/M_{(n)}$
H4	7.09	152,000	154,000	109,000	1.4
H7	7.60	60,600	82,400	50,400	1.64
L11	8.37	17,600	18,200	12,600	1.45

a - calculated using Equation 4.

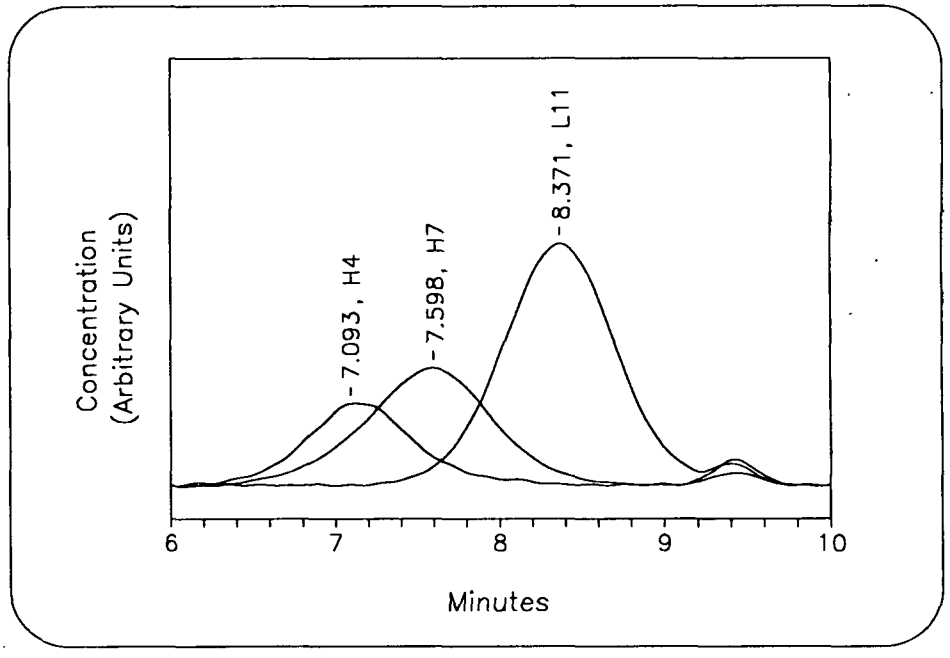

Figure 18. Chromatograms for the three PAAm fractions used.

Analysis Of PAAm Protonation Behavior

Polyallylamine is a polybase which can accept hydrogen ions to form a positively charged polyelectrolyte. The reaction is depicted below:

$$R-(CH_2NH_2)_a + bH^+ \Leftrightarrow R-(CH_2NH_3^+)_c + R-(CH_2NH_2)_{a-c} + (b-c)H^+$$

The degree of protonation (α) is the fraction of amine functional groups that are protonated, or ($\frac{c}{a}$) as shown in the reaction above. In general, the equilibrium for reactions of this type will depend upon the hydrogen ion concentration (pH), the characteristics of the individual ionic groups, and the influence of the electrostatic field of all charge groups on a given molecule.[11,104] Potentiometric titrations can be used to study α as a function of pH.

Previous studies have shown that the titration curves of polyelectrolytes extend over a wide pH range and that, in general, they do not resemble those of the monomeric species.[105,106] That is, the relationship between the fraction of charged species and pH is not strictly linear. For instance, the fraction of protonated monomers in a weak polybase typically increases rapidly with decreasing pH and then levels out at low pH. This non-linear behavior is attributed to the increasing difficulty in protonating internal monomer units due to repulsion from adjacent charges. Often, even at low pH, the degree of ionization of these weak polybases is far from complete. Bloys van Treslong and Staverman[105] suggest that fully protonated polyethylenimine (PEI) behaves as a strong acid with the degree of dissociation of approx. 30%, depending on concentration and ionic strength. They have also shown that, at any given pH, α increases with increasing ionic strength. Katchalsky, et al.[107] and Nagasawa, et al.[108,109] have shown that titration behavior is independent of both molecular weight and polymer concentration.

The potentiometric titration of proteins has been covered extensively by Kenchington, Tanford, and others.[110,111,112,113,114,115] Other studies have been published on the titration behavior of polyethylenimine,[10,105,106,] polyvinylamine,[11,104] and polyallylamine.[116,117,118,119] Kenchington[110] gives a particularly good review of potentiometric titrations, including equipment descriptions and precautions to follow. In general, it is important to eliminate CO_2 from all reagents and

from the reaction vessel itself. It is also important to carefully control temperature and salt concentration. In these types of titrations, one typically assumes that the activity coefficients depend only upon the amount of acid or base present and that the total salt concentration is held constant.

An equation for the degree of ionization, α, of charged polymers has been given by Bloys van Treslong, et al.[105] and Sikora.[11] No reference to its derivation appears in the literature. However, it can be derived if one starts with the electroneutrality condition (see Appendix V). The equation for any pH is given as follows:

$$\alpha = \frac{(C_H)_{added} - (C_H)_{free} + (C_{OH})_{free}}{C_M} \qquad \{2\}$$

where $(C_H)_{added}$ is the proton concentration after addition of HCl; $(C_H)_{free}$ and $(C_{OH})_{free}$ are the concentrations of free proton and hydroxyl ions as determined from titration of strong acid or base, respectively, and C_M is the polymer concentration in monomeric units.

Applying equation 2 to polyelectrolyte (R) and blank titrations, gives α^R and $\alpha,^{blank}$ respectively. Subtracting the two at any pH gives the expression for α^R shown below:

$$\alpha^R = \frac{(C_H)^R_{added} - (C_H)^{blank}_{added}}{C_M} \qquad \{3\}$$

since the $[H^+]_{free}$ and $[OH^-]_{free}$ terms cancel at equal pH and since $\alpha_{blank} = 0$. Since both the terms in the numerator are relative quantities, that is, they are measured in terms of the hydrogen ions present in addition to the starting concentration, both titrations must begin at the same pH. An alternate method, which was used in this work, is to titrate the polyelectrolyte and the blank, and then apply a numerical correction.

Samples of aqueous PAAm and NaOH, at various NaCl levels, were titrated with 0.1 M HCl. The low molecular weight Aldrich PAAm sample described in the materials section was used in each case. The concentration used was approximately 0.1% by weight. A detailed description of the procedure used is given in Appendix VI. The curves were then digitized using UnPlotIt®. Examples of these curves are given in Figure 19 below, which shows the pH of PAAm and NaOH as a function of ml of 0.1M HCl added.

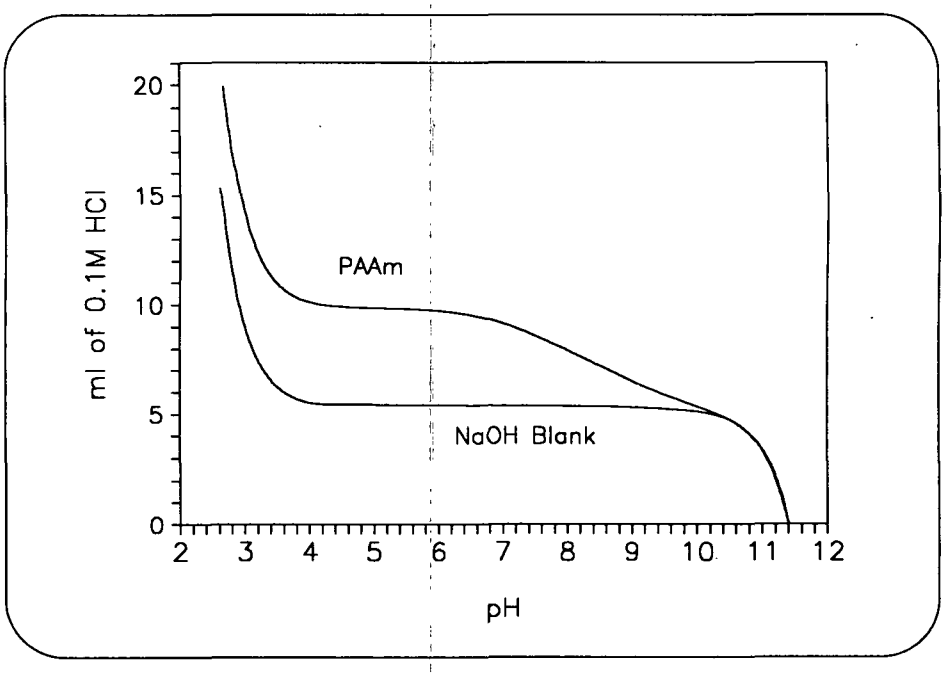

Figure 19. Curves for the titration of PAAm and NaOH with 0.1M HCl.

Duplicate curves were averaged and the number of milliliters of titrant was converted to moles of H^+. The strong base curve was then subtracted from the PAAm curve and the result was divided by the number of monomer moles of PAAm. This gives a plot of α as a function of pH as shown in Figure 20. The data are given in Appendix VII.

In general, the degree of protonation increases with increasing NaCl concentration. The increased salt concentration provides more efficient shielding of adjacent charges, thereby reducing the resistance to protonation. This effect then diminishes as the degree of protonation reaches a maximum.

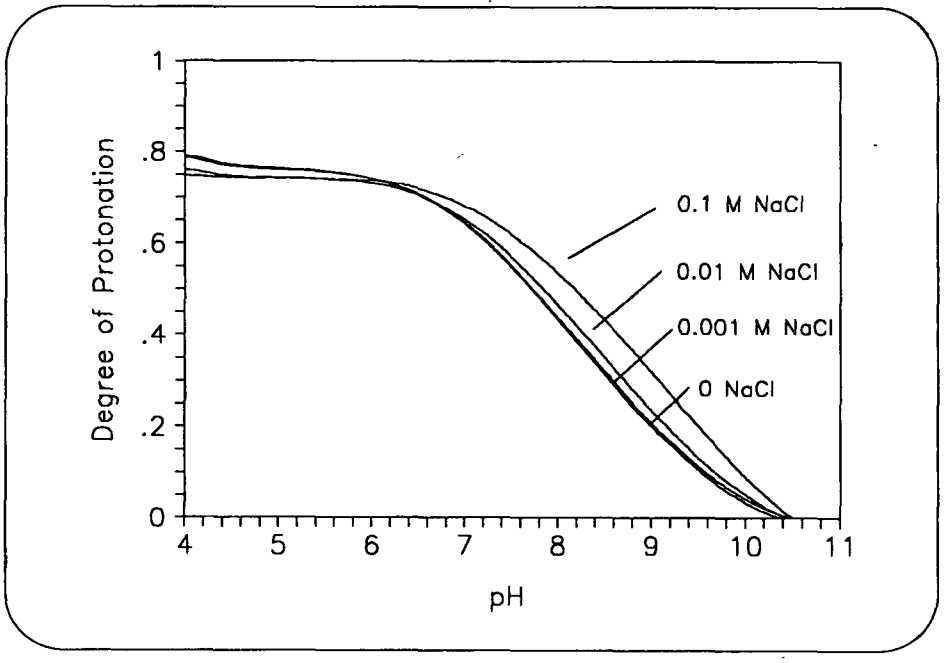

Figure 20. The degree of protonation, α, of PAAm as a function of pH at various NaCl concentrations.

Conductimetric titrations were performed to determine the pH at which PAAm is completely deprotonated and the protonation curves were zeroed accordingly. The titration

vessel, pictured in Figure 6 in the equipment section, was used for all conductimetric titrations. Just prior to analysis, the temperature was noted, and the thermometer was replaced with a Cole-Palmer conductivity probe. Conductivity measurements were taken from the digital readout of the Markson ElectroMark pH/conductivity analyzer. The Metrohm Potentiograph Recording Titrator (model 536) was used to record pH. Details of the conductimetric titration technique are given in Appendix VIII. The conductimetric titration data are given in Appendix IX. Figures 21 - 24 below show pH and conductivity plotted versus ml of 0.1M HCl for titration of PAAm.

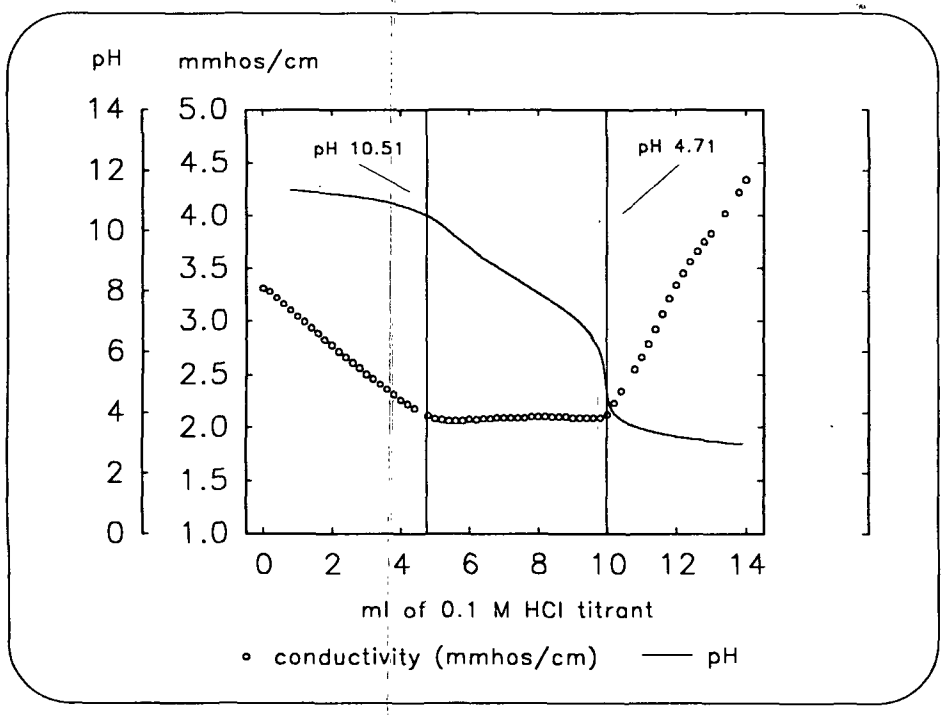

Figure 21. A plot of conductivity and pH versus ml. of 0.1M HCl added for the titration of PAAm with no added NaCl.

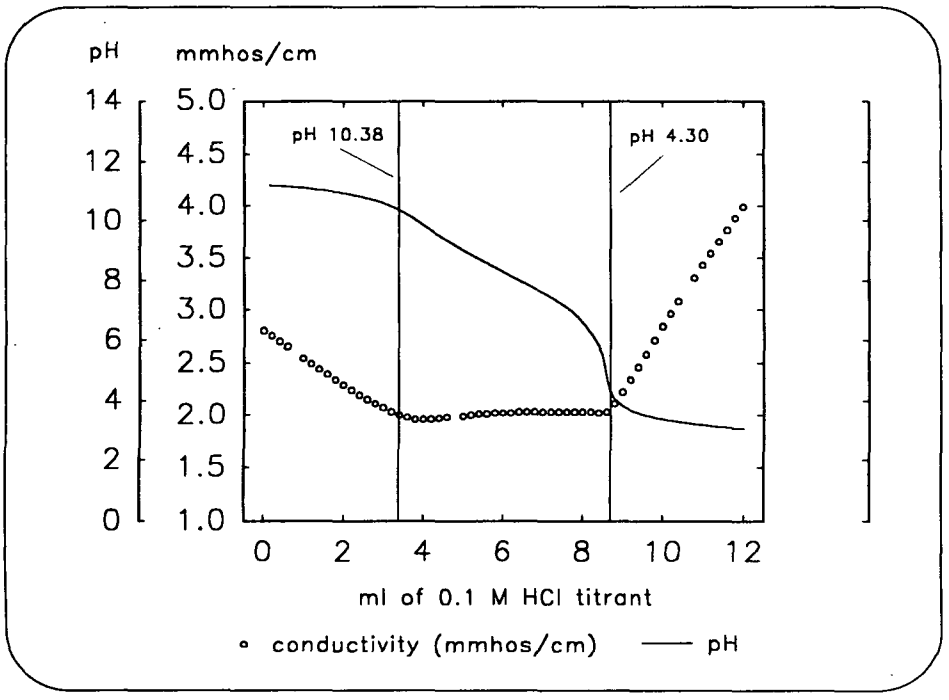

Figure 22. A plot of conductivity and pH versus ml. of 0.1M HCl added for the titration of PAAm in 0.001 M NaCl.

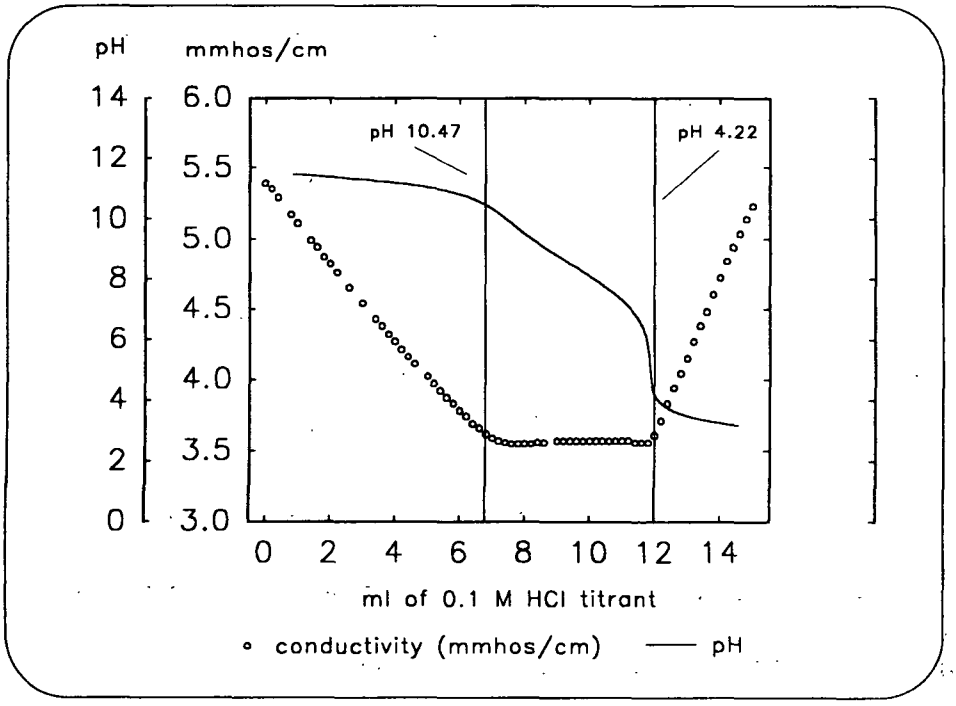

Figure 23. A plot of conductivity and pH versus ml. of 0.1M HCl added for the titration of PAAm in 0.01 M NaCl.

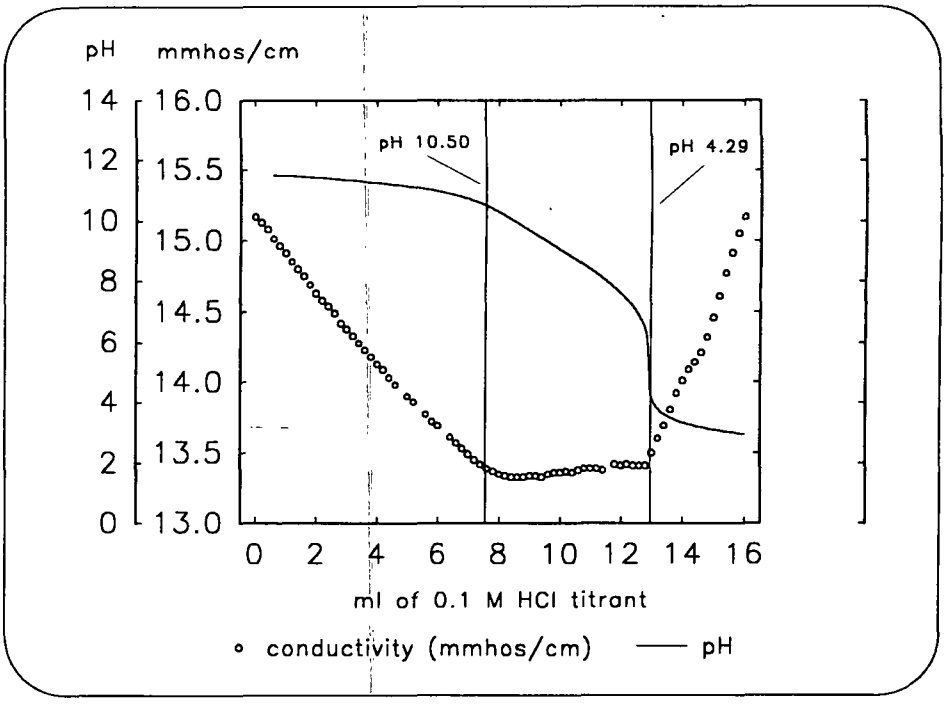

Figure 24. A plot of conductivity and pH versus ml. of 0.1M HCl added for the titration of PAAm in 0.1 M NaCl.

The conductivity curves exhibit a different slope in three distinct regions. In the first region, excess OH^- in solution is neutralized. The conductivity decreases because Cl^- is replacing OH^-, which has a larger mobility. In the second region PAAm begins to protonate and the reaction below is driven to the right by increasing H^+ concentration.

$$R-(CH_2NH_2)_a + bH^+ \Leftrightarrow R-(CH_2NH_3^+)_c + R-(CH_2NH_2)_{a-c} + (b-c)H^+$$

The conductivity increases slowly with addition of HCl. The contribution of charged PAAm to conductivity is negligible, due to its small diffusion coefficient. In the third region, the protonation of PAAm has reached a maximum and conductivity increases rapidly with HCl addition.

Linear regression analysis was used to find the equation for a line through the data in each region. The intersection of these lines was used to mark the inflection points. The first and second inflection points coincide with the point at which PAAm in completely deprotonated, where α equals zero, and the point where the protonation of PAAm reaches a maximum, respectively. Table 8 below lists the corresponding pH at each inflection point, for all NaCl conditions.

Table 8. Summary of conductimetric and potentiometric titration data.

NaCl concentration	pH inflection[1]	pH inflection[2]	$pK_{½}$
0	10.51	4.71	7.73
0.001 M	10.38	4.3	7.72
0.010 M	10.47	4.22	7.84
0.100 M	10.5	4.29	8.19

The dissociation expression for polyallylamine hydrochloride is shown in Equation 4 below.

$$K = \frac{[R-CH_2-NH_2][H^+]}{[R-CH_2-NH_3^+]} \qquad \{4\}$$

Equation 5 gives an expression for the dissociation constant in terms of pH and α.

$$pK = pH - \log\left(\frac{1-\alpha}{\alpha}\right) \qquad \{5\}$$

Since α does not vary linearly with pH, pK is not constant. The pK must then be calculated using Equation 5 and experimental values of α and pH. The resulting pK will be referred to here as the apparent dissociation constant.

The apparent dissociation constant at $\alpha = ½$ ($pK_{½}$) is frequently used for making comparisons, due to the relative ease with which it is calculated. According to Equation 5, pK is equal to pH when α equals ½. Table 8 also lists the values of $pK_{½}$ for each condition studied.

Ochiai, et al.[118] found the $pK_{½}$ for PAAm in 0.1 M NaCl to be 8.78, here it is given as 8.19 in Table 8. The difference may be attributable to differences in the purity of the product or the level of dryness. The PAAm used here was purchased from Aldrich Chemical Co. Ochiai, et al. used PAAm obtained from Nitto Boeski Co. Ltd. In addition, two different drying techniques were used. The PAAm used here was dried at 105°C to a constant weight. Ochiai, et al. dried the PAAm in vacuo at room temperature for one week. They reported that the PAAm they used formed insoluble material when dried at higher temperatures. This was not observed in any of the solutions prepared in this work.

ADSORPTION PROCESS

The first objective of this thesis was to study the effects of pH, molecular weight (MW), salt concentration (c_s), and particle surface charge density (σ_s) on PAAm adsorption. A central composite design in a cube (CCC) was used to determine the significance of these variables and their interactions. Table 9 below summarizes the conditions studied.

Table 9. The conditions for the CCC experiment.

Treatment	pH	NaCl Conc. M	Surface Charge C/m^2	Molecular Weight M_n
#1	4.00	0.0000	0.0062	12,600
#2	10.00	0.0000	0.0062	12,600
#3	4.00	0.0100	0.0062	109,000
#4	10.00	0.0100	0.0062	109,000
#5	4.00	0.0000	0.0116	12,600
#6	10.00	0.0000	0.0116	12,600
#7	4.00	0.0100	0.0116	12,600
#8	10.00	0.0100	0.0116	12,600
#9	4.00	0.0000	0.0062	109,000
#10	10.00	0.0000	0.0062	109,000
#11	4.00	0.0100	0.0062	12,600
#12	10.00	0.0100	0.0062	12,600
#13	4.00	0.0000	0.0100	109,000

Treatment	pH	NaCl Conc. M	Surface Charge C/m^2	Molecular Weight M_n
#14	10.00	0.0000	0.0116	109,000
#15	4.00	0.0100	0.0116	109,000
#16	10.00	0.0100	0.0116	109,000
#17	8.50	0.0010	0.0081	50,400
#18	4.00	0.0010	0.0081	50,400
#19	10.00	0.0010	0.0081	50,400
#20	8.50	0.0000	0.0081	50,400
#21	8.50	0.0100	0.0081	50,400
#22	8.50	0.0010	0.0062	50,400
#23	8.50	0.0010	0.0116	50,400
#24	8.50	0.0010	0.0081	12,600
#25	8.50	0.0010	0.0081	109,000
#26-31	8.50	0.0010	0.0081	50,400

The PSL samples and PAAm fractions used have already been described above. The PAAm fractions were concentrated and washed (to remove the eluent) prior to use. A 200 ml Amicon ultrafiltration cell equipped with an Amicon YC05 membrane, with a molecular weight cut-off of 500, was used in each case. The fractions were first concentrated to 100 ml. Each concentrate was then washed with ten volumes of 0.1 M NaCl to remove the eluent and exchange any associated NO_3^- with Cl^-. In the final step, the fractions were washed with ten volumes of Nanopure® water to remove excess NaCl.

The same adsorption technique was used in all cases. PSL suspensions and PAAm solutions were prepared using dilution water with identical characteristics. Samples of each

were drawn into syringes and mixed by directing the syringe streams into one another as the samples were injected into Teflon vials. The syringes were weighed before and after mixing to determine the amount of PAAm solution and PSL suspension added. After mixing, the vials were shaken for 24 hours to allow the adsorption to reach equilibrium.

Polycarbonate membranes with 0.08 μm diameter pores made by Poretics Corporation were used to filter the PSL from the adsorption samples. The colloid titration technique described earlier was used to determine the amount of PAAm in solution prior to adsorption and the amount of PAAm remaining in the filtrate. The amount of PAAm adsorbed to the surface of the PSL was determined by difference. Adsorption isotherms were obtained for each treatment by performing adsorptions over a series of PAAm concentrations. The data in each case were fit with a linearized form of the Langmuir equation. The fit provided a value for the maximum adsorbed amount. This value was used as the response variable when determining the statistical significance of the controlled variables.

PAAm QUANTIFICATION BY COLLOID TITRATION

Overview

Research concerning reactions of polycations and polyanions dates back to the early 30's and 40's. The colloid titration technique, a product of this research, is an analytical test method for the quantification of polyelectrolytes. Terayama[120] was one of the first to recognize its analytical applications and study the technique in depth. Since its development, it has been used

to study coagulant dosage requirements in waste water treatment,[121,122] polyelectrolyte adsorption,[50,95] and the charge state of papermaking systems.[123,124,125,126]

The colloid titration technique is based on the observation that oppositely charged polyelectrolytes will react in near stoichiometric proportions to form polyelectrolyte complexes. Typically, o-toluidine blue indicator (TB) is used to detect the end point of the titration. The conjugated aromatic rings of TB tint solutions of the compound blue. This color remains when polycations are added. When the solution is titrated, the polyanions complex with the TB, changing the nature of the conjugation and the color from blue to pink The chemical structure of TB is shown in Figure 25 below.

Polycations can be quantified by direct titration with polyanions. Polyanions can be quantified by treating them with a known excess of polycations and back titrating with polyanions. A similar approach can be used to quantify the amount of polyelectrolyte adsorbed to a surface. The surface is treated with a known amount of polyelectrolyte and the excess is determined by colloid titration. The amount of polymer adsorbed is then calculated by difference. This approach was used to determine the amount of PAAm adsorbed in experiments for this thesis. The equipment and reagents used are those recommended by Dr. Charles Potter.[127] A detailed description of the technique appears in Appendix X. A brief description is given below.

PAAm samples were analyzed using the Metrohm Potentiograph Recording Titrator discussed in the equipment section. Potassium polyvinylsulfate (PVSK) was used as the polyanionic titrant. All PVSK solutions were standardized on a daily basis with benzethonium

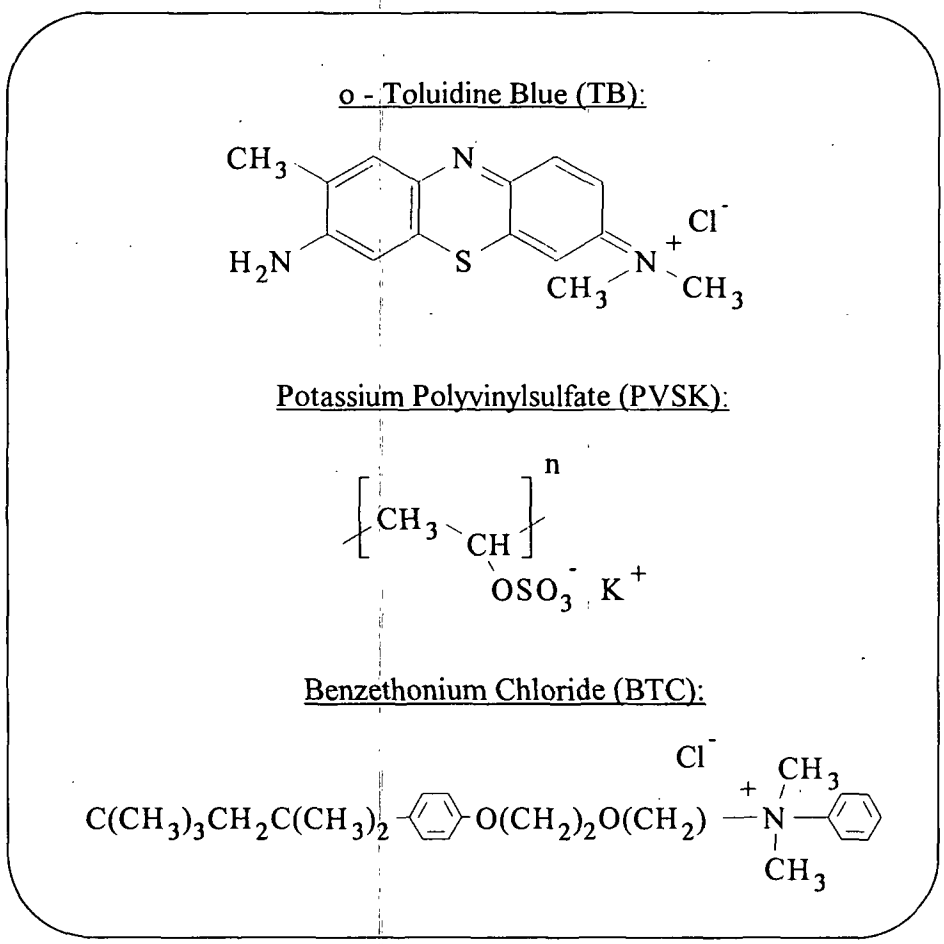

Figure 25. Chemical structures for o-toluidine blue (TB), potassium polyvinylsulfate (PVSK), and benzethonium chloride (BTC).

chloride (BTC). The chemical structures of PVSK and BTC are also shown in Figure 25. The analysis proceeded as follows. An aliquot of the sample, between 0.1 and 10.0 gm, was weighed in a polypropylene beaker. Then, 0.1 ml of 0.005% (w/w) toluidine blue indicator (TB) was added and the solution was diluted to 50 ml with Nanopure® water, adjusted to pH 4. The solution was titrated with standardized PVSK at approximately 10 mg/L. The metachromatic color change was monitored at 620 nm, using the Brinkmann Probe colorimeter, model PC801. The titrator recorded the titration curve on graph paper. All titration values were corrected using the calibration curve discussed below.

Accuracy and Precision

Experiments were performed to determine the accuracy and precision of the colloid titration technique. PAAm samples were prepared at known concentrations. Five replicates were run at each concentration. The results are shown below in Table 10.

Table 10. Comparison of calculated and titrated concentrations for PAAm samples.

sample	calculated, C_c ppm	ave. titrated, C_t ppm	titrated, C_t (% std. dev.)	interaction ratio (calc.:titr.)
#A1	78.985	90.376	0.568	0.874
#B1	70.189	80.552	0.429	0.871
#C1	44.655	51.417	0.513	0.869
#D1	27.233	31.296	0.359	0.870
#E1	18.448	21.206	0.457	0.870
#F1	7.915	8.972	0.823	0.882
#G1	7.155	8.248	1.938	0.867
#H1	4.452	5.104	0.400	0.872
#I1	2.769	3.176	0.929	0.872
#J1	1.910	2.192	0.446	0.871
#K1	0.810	0.885	2.951	0.915
#L1	0.715	0.776	8.671	0.921
#M1	0.455	0.517	0.829	0.879
#N1	0.278	0.314	1.503	0.882
#O1	0.188	0.214	2.217	0.879
#P1	0.082	0.089	2.417	0.926
#Q1	0.074	0.080	2.968	0.920
#R1	0.046	0.054	10.732	0.855
#S1	0.028	0.031	6.904	0.918

The titrated values are found by assuming a 1:1 stoichiometry. The interaction ratio, defined here as the calculated value divided by the titrated value, is a measure of the equivalents of PAAm which interact with each PVSK equivalent. The interaction ratios in Table 11 show that the stoichiometry of the reaction between PVSK and PAAm is not one to one. Onabe[128] showed that for the titration of 1,1-dimethyl piperidium-3,5 dimethyl methylene chloride (poly-DMDAAC) the colorimetric end point occurred at a titration ratio equal to, or slightly above unity. Presently, there is no explanation for the relatively large deviation from stoichiometry shown for the titration of PAAm.

To obtain an accurate measurement the technique was calibrated. Regression analysis of the calculated (C_c) and titrated concentrations (C_t) showed that a linear relationship exists in the concentration range studied. The regression results are shown in Equation 6 below, where the concentration terms have units of equivalents/gm of solution.

$$C_c = 0.872(C_t) - 1.29 \times 10^{-11} \qquad \{6\}$$

All colloid titrations were corrected using Equation 6. The percent standard deviation of the titration measurement is less than 1% for all but one of the concentrations studied in the 80 to 1 ppm range. Below 1 ppm, the precision of the colloid titration technique begins to decrease.

The Effects of pH, Molecular Weight, Salt, and Titrant Addition Rate

The colloid titration technique was used to quantify PAAm under all the conditions studied. Therefore, it is important to discuss the effect of each variable on its accuracy. The effects of

pH, molecular weight, and salt are described below. The effect of titration addition rate was also studied. Since only the filtrate was analyzed, the presence of PSL was not a factor.

Since the colloid titration is based on charge neutralization, it is important to consider PAAm charge density. Samples varied in size between 0.1 and 10 gm of PAAm solution at pH 4, 8.5, and 10. Each sample was diluted to 50 ml with pH 4, Nanopure® water. The final pH was calculated to be in the 4.0 to 4.2 range. Since the degree of protonation remains relatively constant between pH 4 and 5, the dilution with pH 4 water was sufficient to compensate for variation in the initial pH.

The effect of molecular weight on the colloid titration technique has not been discussed in the literature. Onabe[125] showed that 50,000 M_n, poly-DMDAAC reacts in near stoichiometric proportions with 324,000 M_n, PVSK. When these values are used, the calculated ratio of poly-DMDAAC molecules to PVSK molecules is 6.5 to 1. Since the complexation does not involve the interaction of an even number of poly-DMDAAC molecules with one PVSK molecule, the reaction must proceed in a different manner. It is possible that multiple polymer molecules or polydisperse polymer molecules interact resulting in a near stoichiometric reaction between the respective charge groups. It is also possible that non-stoichiometric reactions occur and average out over the entire titration sample. If complexation proceeds in either manner, molecular weight should have a limited effect on the accuracy of the titration. This hypothesis was not tested due to the limited supply of fractionated PAAm. The remaining variables, salt concentration and titrant addition rate, were examined experimentally.

The effect of salt on the colloid titration has been studied in depth by Tanaka.[129] He showed that for titration of cationic polymers, salt can increase the amount of PVSK required for

neutralization by as much as a factor of two. The extent of the deviation was dependent upon the polymer being titrated and the concentration of salt.

Titration rate is also an important variable to consider. When performing titrations manually, by adding aliquots of titrant in a stepwise fashion, ample time is taken between additions to allow the system to reach equilibrium. When performing automatic titrations, as was done here, the titrant is added continuously. Therefore, the titrant addition rate must be reduced to a point where the time to equilibrium is negligible.

A 2^2 factorial experiment was used to study the significance of salt concentration and titrant addition rate on the accuracy of the colloid titration. PAAm samples were prepared at known concentrations and titrated according to the technique described above. Each experimental case was run in duplicate. In all cases, approximately 10 gm of sample was used. The results are shown in Table 11 below.

Table 11. Conditions and results for the study of the effects of salt concentration and titrant addition rate.

Cases	NaCl concentration	titrant addition rate (ml/min.)	calculated, C_c ppm	ave. titrated, C_t ppm	interaction ratio (calc.:titr.)
#23-1	0.000	1.333	1.081	1.155	0.936
#23-2	0.000	1.333	1.081	1.135	0.952
#23-3	0.000	4.000	1.081	1.168	0.926
#23-4	0.000	4.000	1.081	1.170	0.924
#24-1	0.01 M	1.333	1.112	1.155	0.962
#24-2	0.01 M	1.333	1.112	1.173	0.948
#24-3	0.01 M	4.000	1.112	1.177	0.944
#24-4	0.01 M	4.000	1.112	1.168	0.952

An analysis of variance performed on the data showed that salt concentration and titrant addition rate had no significant effect on the titration ratio at the 99% confidence level in the ranges studied. In addition, no interactions between variables were significant.

FT-IR-ATR STUDIES

Sample Preparation and Loading

Two experiments were performed to study the spectrum of PAAm in solution and at the ATR crystal surface. In the first experiment FT-IR spectra were collected from a set of PAAm samples at pH 4.0, 8.5, and 10.0. Each set consisted of seven samples of increasing concentration prepared from stock solutions at each pH. In the second experiment a single sample was prepared at each pH and spectra were collected as a function of time. The stock solutions were prepared by diluting 0.5 gm of Aldrich high molecular weight PAAm to 50 ml in a 200 ml Amicon ultrafiltration cell equipped with an Amicon YC05 membrane (MW cutoff: 500). Each solution was then washed with approximately ten volumes of Nanopure® water at the appropriate pH.

Three PSL samples with PAAm adsorbed at pH 4.0, 8.5, and 10 were also analyzed. The samples were prepared in a manner similar to that described in the adsorption section above. A 200 ml PSL suspension and a PAAm solution were prepared at the desired pH in polyethylene squeeze bottles. Each bottle was weighed and the two were mixed into a 500 ml jar. The bottles were again weighed and the amount added was determined by difference. The adsorption sample was shaken for 24 hours by means of a shaker table. A 5 ml sample of the suspension

was taken for quantification of residual PAAm in the filtrate (see the PAAm quantification section above). The adsorption sample was then concentrated to approximately 8 ml in a 200 ml Amicon ultrafiltration cell equipped with a Poretics Inc. membrane with 0.08 μm dia. pores. The suspension was then transferred to a 10 ml Amicon ultrafiltration cell with a similar membrane and washed with ten volumes of Nanopure® water at the appropriate pH. This final step washed away any excess PAAm.

All samples were loaded into the Circle™ cell by injection into a luer-lock fitting at the end of the teflon tubing (see Figure 7). Samples were removed by forcing air through the Circle™ cell. The ATR crystal was removed for cleaning between each set of experiments. The cleaning procedure varied, depending upon the relative level of contamination. However, in most cases the ATR crystal was polished with toothpaste[130] and then treated in a plasma cleaner (Harrick Scientific Corporation) for twenty minutes. The Circle™ cell was recalibrated according to the technique of Sperline, et al.,[85] each time the ATR crystal was removed.

Reduction and Analysis Of Spectra

General Preparation of Spectra

All spectra were collected and saved as single beam interferograms. The interferograms were then transferred to a DOS based PC via a RS232 connection. NICOS Kermit software was used to send the files from the Nicolet system. PC-Kermit software was used in the server mode to receive the files. All spectra were analyzed using LABCALC® software, a product of Galactic Industries Corporation. (LABCALC® is a versatile program developed for analysis of a wide

variety of spectra and chromatograms. It includes many useful tools for data analysis and report preparation. However, its most valuable function may be that it provides a structure which allows the user to develop his or her own subprograms. In addition, the user has access to the source code (Array Basic) for most existing functions and subprograms, which can be modified to fit the user's needs.)

After the interferograms were transferred, they were Fourier processed using triangular apodization. Sample spectra were then converted to absorbance. A modified LABCALC® subprogram called BASELN2 was used to baseline correct the sample spectra. The subprogram allows the user to type in wavenumber values for linear multi-point baseline corrections as opposed to selecting them with the computer mouse. The program then selects the actual data point closest to the typed value for correction. This provides greater reproducibility in baseline correction from sample to sample when compared with selection via computer mouse. In all cases, three points were used to baseline correct aqueous spectra; 4000, 2630, and 1890 cm^{-1}. Another modified subprogram, OFFSET2, was used to zero the baseline. This subprogram allows the user to type in the data point used for zeroing. All spectra were zeroed at 4000 cm^{-1}.

Subtraction of Spectra

Once the spectra have been baseline corrected, a water reference spectrum must be subtracted from the aqueous sample spectra to give a spectrum of the solute. In FT-IR spectroscopy, interactive subtraction techniques are commonly used for removing the peaks of one component from a multicomponent spectrum. They are suitable for most qualitative work.

However, when performing quantitative analyses, individual bias and uncertainties may result in artificial absorbance peaks and variation in peak absorbance levels. Where reproducibility is important, an objective subtraction technique is needed.

Mathematical algorithms have been used in the past to study multicomponent spectra. Techniques described in the literature include methods based on component ratios,[131] factor analysis,[132] and least square fits.[133,134,135,136] Each of these make assumptions which limit their applicability. The component ratio method assumes that band overlap is negligible and that differences in component absorbance levels are small. Water peaks frequently overlap or completely swamp solute bands or band shifts due to component interactions. The least square and factor analysis methods assume that some or all of the multicomponent spectrum can be described as a linear combination of known component spectra. For many aqueous systems, the spectra of all components are not known and peak shifts due to component interaction cannot be measured independently.

A technique that would reproducibly subtract a water spectrum from aqueous sample spectra would be very useful. Powell[137], et al., and Dousseu[138], et al., have documented techniques for the subtraction of water spectra from spectra of aqueous protein solutions. In both cases, an iterative subtraction technique is used in the 2650-1750 cm^{-1} region. In their systems, this region contains a combination peak due to rotation and deformation of the water molecule, but is devoid of protein peaks. The iterative techniques subtract a reference spectrum of water until a flat baseline is achieved in the region. Their methods differ in the approach used

to evaluate the flat baseline. Powell,[137] et al., monitor the slope in two areas in the region. When the slope equals zero, the subtraction is stopped. Dousseau,[138] et al., use a second order polynomial fit and least squares analysis to detect a flat baseline.

These methods work well when the difference spectrum (subtraction result) has a high signal to noise ratio. If the ratio is low, small errors in the subtraction can cause distortion in the difference spectrum due to under or over subtraction. When using either method, a shift in the water peak due to component interactions could also produce erroneous results.

The subtraction technique described in this thesis was first proposed by Banerjee and Li.[139] Friese and Banerjee,[140] used the technique to study diffuse reflectance spectra of wood pulp. The method is based on the observation that the complexity of a multicomponent spectrum should decrease if a constituent is completely removed. One measure of complexity is the integrated area (positive and negative) of the first derivative. Thus, if a scaling factor is applied to the reference spectrum and the resulting spectrum is subtracted from the sample spectrum, the reference spectrum will be factored out when the area under the derivative curve is minimized (the optimum scaling factor). Dewiggling has been proposed as a simple, descriptive moniker for this technique. An interactive subprogram has been written in LABCALC® for this purpose.

The subprogram, DEWIGGLE, prompts the user for the sample spectrum, the reference spectrum, the scaling factor tolerance, and the limits for the wavenumber region to be monitored during analysis. The minimum and maximum scaling factors are determined within the subprogram. The minimum scaling factor is simply zero. The maximum scaling factor is

defined as 1.5 times the maximum sample spectrum intensity divided by the maximum reference spectrum intensity. DEWIGGLE then locates the optimum scaling factor.

To find the optimum scaling factor, DEWIGGLE takes advantage of the shape of the plot of integrated area of the derivative curve versus scaling factor. If the reference is a significant component of the sample spectrum, this plot will resemble a parabola. When a small scaling factor is used, the reference spectrum is under subtracted, resulting in a large integrated area. As the scaling factor is increased, the integrated area decreases, until the optimum scaling factor is reached. Increasing the scaling factor further then over subtracts the reference, resulting in negative peaks and increased integrated area.

DEWIGGLE uses a semi-numeric approach to find the minimum in the parabola. The integrated area is evaluated at the minimum and maximum scaling factor, and at the value midway between the two factors. A parabola is then fit to the three points and the resulting function is used to estimate the minimum in the curve. Three new points are then selected using the scaling factor at the estimated minimum, and two scaling factor values at ±20% of the previous scaling factor interval. The process is then repeated until the net change in the scaling factor at the estimated minimum is less than a user-defined scaling factor tolerance. At this point, the estimated minimum is equal to the optimum scaling factor to within the tolerance limit. The program then stops and displays the subtraction result at the optimum scaling factor.

The subtraction technique is demonstrated below. A spectrum of Nanopure® water (A), and a spectrum of D_2O (1.054% w/w) in Nanopure® water (B), appear in Figure 26 below.

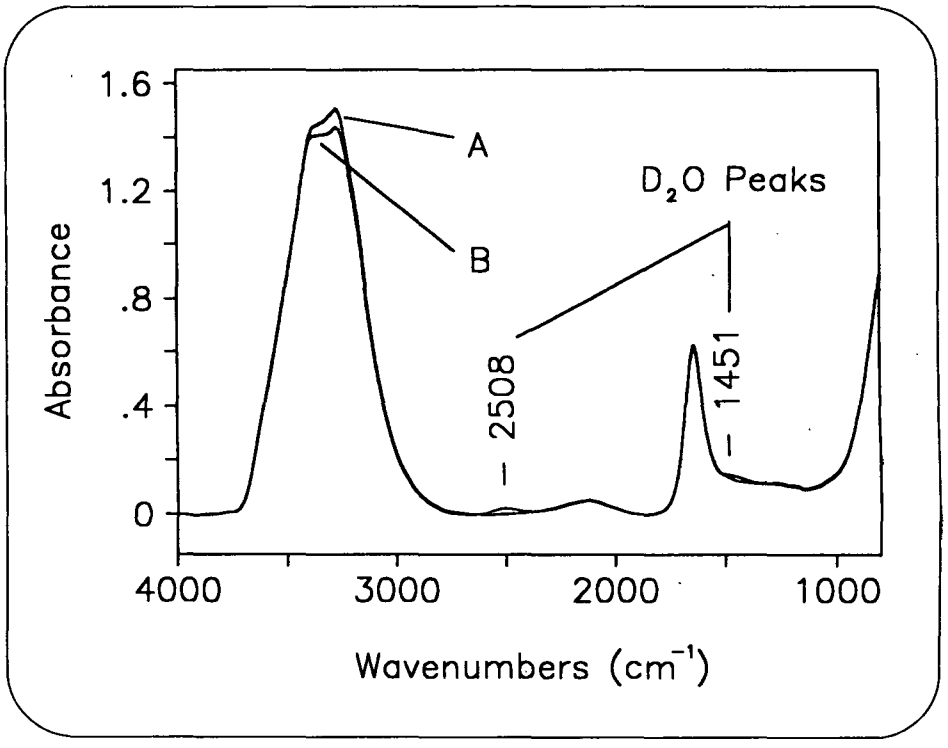

Figure 26. Spectra of Nanopure® water (A) and 1.054% (w/w) D_2O prepared with Nanopure® water (B).

Both spectra contain the three characteristic water peaks in the 3800 - 2800, 2400 - 1900, and 1800 - 1500 cm^{-1} regions (see the results and discussion section for peak assignments). The latter also contains two charateristic D_2O peaks at approximately 2508 and 1451 cm^{-1}.

Figure 27 shows the integrated area of the derivative curve plotted versus the applied scaling factor, when DEWIGGLE is used to subtract the spectra. The minimum and maximum scaling factors are 0 and 1.430, respectively. The plot contains data points in 0.001 scaling factor increments. The inset provides an expanded view of the minimum in the curve.The 2630 - 950 cm^{-1} region of the difference spectrum was monitored during dewiggling. The optimum scaling factor for this subtraction was 0.9743. It is calculated from the equation for the parabola found in the last iteration. The calculated value is indeed close to the low data point shown in the inset in Figure 27. The resulting difference spectrum is shown in Figure 28 below.

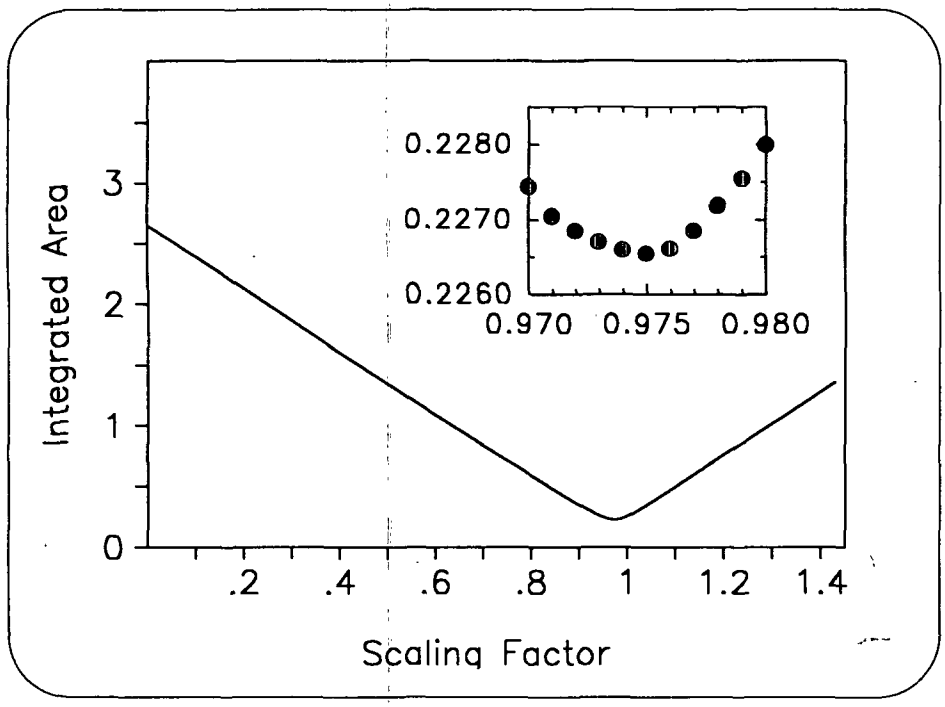

Figure 27. A plot of integrated area versus the applied scaling factor with the minimum expanded in the inset.

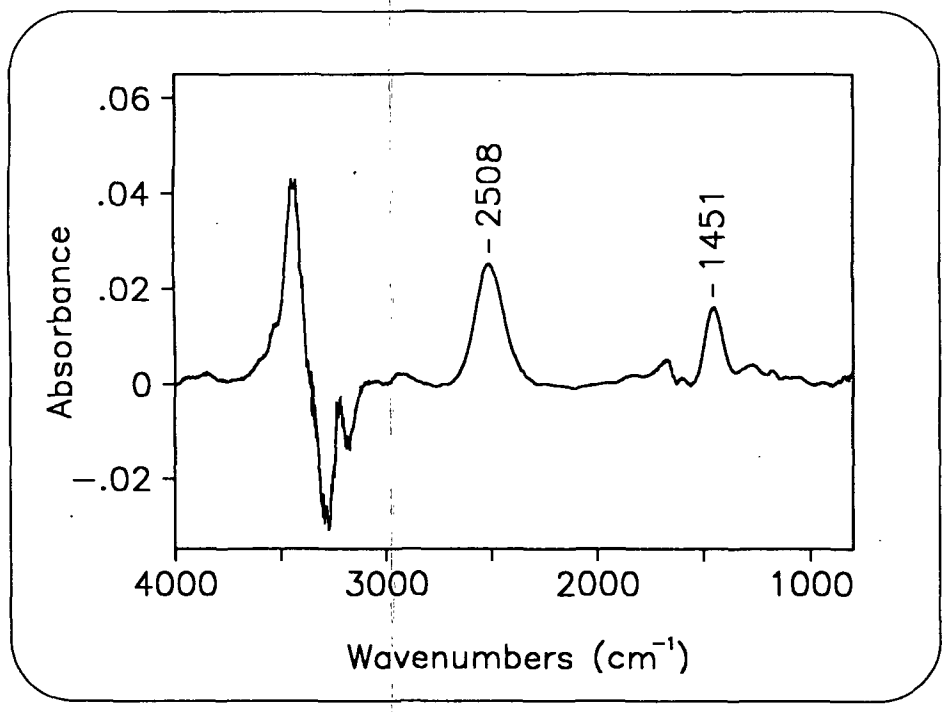

Figure 28. The difference spectrum produced by DEWIGGLE when the spectra in Figure 25 are subtracted (D_2O solution minus water).

The characteristic D_2O peaks at 2508 and 1451 cm^{-1} are now clearly visible. Positive and negative peaks are also present in the 3800 - 2800 cm^{-1} region. These peaks reflect shifts in the intensity and frequency of the peaks associated with O-H stretching vibrations. The shifts are caused by differences in the hydrogen bonding patterns in the water and aqueous D_2O samples.[141,142,143] Noise and subtraction artifacts may also be present due to the intense absorbance of the water peak in this region. Subtle detector overloading can cause small irregularities in the water spectra which become apparent when the two are subtracted.

To test its ability to measure differences, DEWIGGLE was used to subtract two independently measured spectra of Nanopure® water. Figure 29 below shows the resulting difference spectrum.

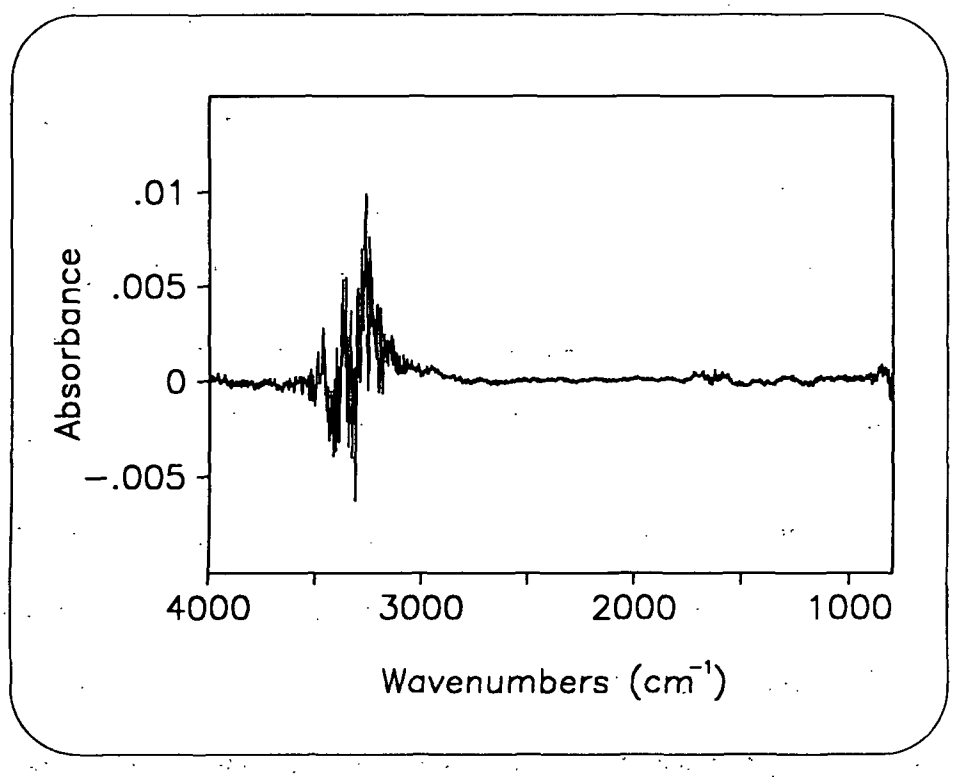

Figure 29. The difference spectrum produced by DEWIGGLE when two Nanopure® water spectra are subtracted.

The 2800 - 900 cm^{-1} region of the difference spectrum is devoid of peaks. The water peaks in this region are completely subtracted out. However, this is not the case for the 3800 - 2800 cm^{-1} region. This region contains increased noise with underlying subtraction artifacts. They are a result of subtle detector overloading due to the intense absorbance of the water peak in this region.

DEWIGGLE was used to analyze all spectra collected for this thesis. In all cases, including those subtractions shown above, the 2630 - 950 cm^{-1} region was monitored during analysis. The 4000 - 2630 cm^{-1} region, with the intense water peak, was excluded. This was done to prevent artifacts, due to detector overload, from interfering with the subtraction. Reduction of the throughput to the detector would also prevent these interferences. However, it was necessary to maximize throughput, to allow detection of weak PAAm peaks in the 1600 - 900 cm^{-1} region.

All difference spectra were baseline corrected using BASELN2, the linear multi-point baseline correction technique described previously. D_2O difference spectra were baseline corrected at six points: 4000, 2732, 2286, 1625, 1000, and 900 cm^{-1}. Six points were also used to baseline correct PAAm difference spectra: 4000, 2630, 1890, 1450, 950, and 900 cm^{-1}. All baseline corrected spectra were zeroed at 4000 cm^{-1} using OFFSET2.

Integrated peak areas were used for quantitative comparisons. A LABCALC® subprogram, INTEGRAT, which uses the trapezoid technique, was run to calculate the area of the D_2O peak at 2508 cm^{-1}. The area (A) and D_2O (C) concentration values were used to calculate the internal reflection incidence angle (θ) and the number of internal reflections (N) according to the

technique of Sperline, et al.[85] The depth of penetration (d_p) at 2508 cm^{-1} was estimated using the equation defined by Harrick.[77]

The presence of overlapping peaks in the PAAm difference spectra made the use of INTEGRAT impractical for measuring peak area. Instead, the peaks of interest were fit with a combination Gaussian-Lorentzian curve using CURVEFIT. The area of the fitted curve was then taken as the area of the corresponding PAAm curve.

RESULTS AND DISCUSSION

PAAm ADSORPTION

The first objective of this thesis was to study the effects of pH, molecular weight (M), salt concentration (c_s), and particle surface charge density (σ_s) on PAAm adsorption to PSL particles. Batch adsorptions were prepared for each treatment condition studied. Figure 30 below shows three typical adsorption isotherms at pH 4.0, 8.5, and 10.0.

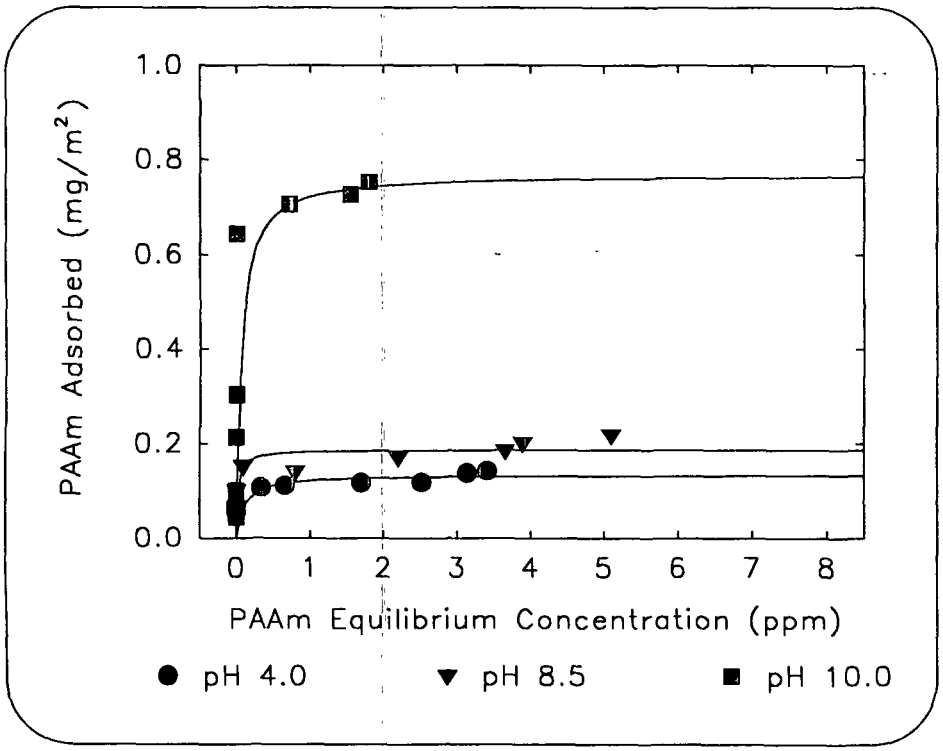

Figure 30. The amount of PAAm adsorbed (Γ_m, mg/m^2) plotted versus PAAm equilibrium concentration for adsorptions at pH 4.0, 8.5, and 10.0 (M_n = 50,400; c_s = 0.001 M; σ_s = 0.0081 C/m^2).

The solid lines represent curves fitted to the data using Langmuir's relationship for monolayer adsorption from solution. The equation can be stated as follows:

$$\frac{Ce}{\Gamma} = \frac{1}{k\Gamma_m} + \frac{Ce}{\Gamma_m} \quad \{13\}$$

where Ce is the PAAm concentration at equilibrium in the bulk, Γ is the amount of polymer adsorbed, Γ_m is the maximum monolayer coverage, and k is a constant.

Plots for all the conditions studied appear in Appendix XI. The adsorption data are given in Appendix XII. A total of 25 different treatment conditions were studied. Six replicates of treatment 17 were performed. The treatment conditions and results are summarized in Table 12 below. The pK values were calculated using Equation 5 and experimental values for pH and α. The pK of points which fell between experimental data points were interpolated.

The adsorption data in Figure 30 and Appendix X are plotted with error bars in Appendix XI. The error in the amount adsorbed for each data point was estimated using a knowledge of the error associated with the colloid titration technique and error propagation calculations. The size of the error bars ranged from 2 to 79%. The large errors are a result of the difference technique used to determine the amount of polymer adsorbed. When large initial and equilibrium concentration values are subtracted, the error associated with each value is added to give the error in the adsorbed amount. If the adsorbed amount is small, the percent error can be very large. In spite of the error, the trends in adsorption are clear. The percent standard deviation in Γ_m for treatment 17 replicates (26-31) is 8.8%.

The adsorption experiments were planned using a central composite design in a cube (CCC). This response surface design provides the data needed to test the statistical significance of the controlled variables and their interactions. The resulting regression equation is used below as a context to discuss the significant effects. The physical interpretation of these effects

Table 12. Conditions and adsorbed amounts for all treatments studied.

Treatment No.	pH	α	pK	c_s (M)	σs (C/m^2)	$M_{(n)}$	Γ_m (mg/m^2) exp.
1	4.00	0.790	4.58	0.0000	0.0062	12,600	0.056
2	10.00	0.043	8.66	0.0000	0.0062	12,600	0.813
3	4.00	0.761	4.50	0.0100	0.0062	109,000	0.111
4	10.00	0.052	8.74	0.0100	0.0062	109,000	0.915
5	4.00	0.790	4.58	0.0000	0.0116	12,600	0.075
6	10.00	0.043	8.66	0.0000	0.0116	12,600	0.888
7	4.00	0.761	4.50	0.0100	0.0116	12,600	0.092
8	10.00	0.052	8.74	0.0100	0.0116	12,600	0.779
9	4.00	0.790	4.58	0.0000	0.0062	109,000	0.143
10	10.00	0.043	8.66	0.0000	0.0062	109,000	0.889
11	4.00	0.761	4.50	0.0100	0.0062	12,600	0.109
12	10.00	0.052	8.74	0.0100	0.0062	12,600	0.751
13	4.00	0.790	4.58	0.0000	0.0116	109,000	0.173
14	10.00	0.043	8.66	0.0000	0.0116	109,000	1.102
15	4.00	0.761	4.50	0.0100	0.0116	109,000	0.121
16	10.00	0.052	8.74	0.0100	0.0116	109,000	1.128
17	8.50	0.314	8.16	0.0010	0.0081	50,400	0.210
18	4.00	0.790	4.58	0.0010	0.0081	50,400	0.138
19	10.00	0.034	8.55	0.0010	0.0081	50,400	0.740
20	8.50	0.322	8.18	0.0000	0.0081	50,400	0.182
21	8.50	0.352	8.23	0.0100	0.0081	50,400	0.145
22	8.50	0.314	8.16	0.0010	0.0062	50,400	0.129
23	8.50	0.314	8.16	0.0010	0.0116	50,400	0.133
24	8.50	0.314	8.16	0.0010	0.0081	12,600	0.108
25	8.50	0.314	8.16	0.0010	0.0081	109,000	0.219
26	8.50	0.314	8.16	0.0010	0.0081	50,400	0.214
27	8.50	0.314	8.16	0.0010	0.0081	50,400	0.191
28	8.50	0.314	8.16	0.0010	0.0081	50,400	0.193
29	8.50	0.314	8.16	0.0010	0.0081	50,400	0.167
30	8.50	0.314	8.16	0.0010	0.0081	50,400	0.179
31	8.50	0.314	8.16	0.0010	0.0081	50,400	0.183

is discussed later in this section. It is important to note that the value of the regression equation as a predictive tool is limited, since it can only be applied to the adsorption system studied here.

The results from the analysis using SAS statistical software are shown in detail in Appendix XII; they will be summarized here. The regression equation for the CCC design contains all first order terms, second order terms, and all terms for first order interactions. The regression equation is shown below (Equation 14). Figure 31 shows experimental Γ_m plotted versus Γ_m calculated using the regression equation.

$$\Gamma_m = b_0 + b_1\alpha + b_2 c_s + b_3\sigma_s + b_4 M_{(n)} + b_5 c_s\alpha + b_6\sigma_s\alpha + b_7\sigma_s c_s + b_8 M\alpha + b_9 M c_s + b_{10} M\sigma_s + b_{11}\alpha^2 + b_{12} c_s^2 + b_{13}\sigma_s^2 + b_{14} M^2 \quad \{14\}$$

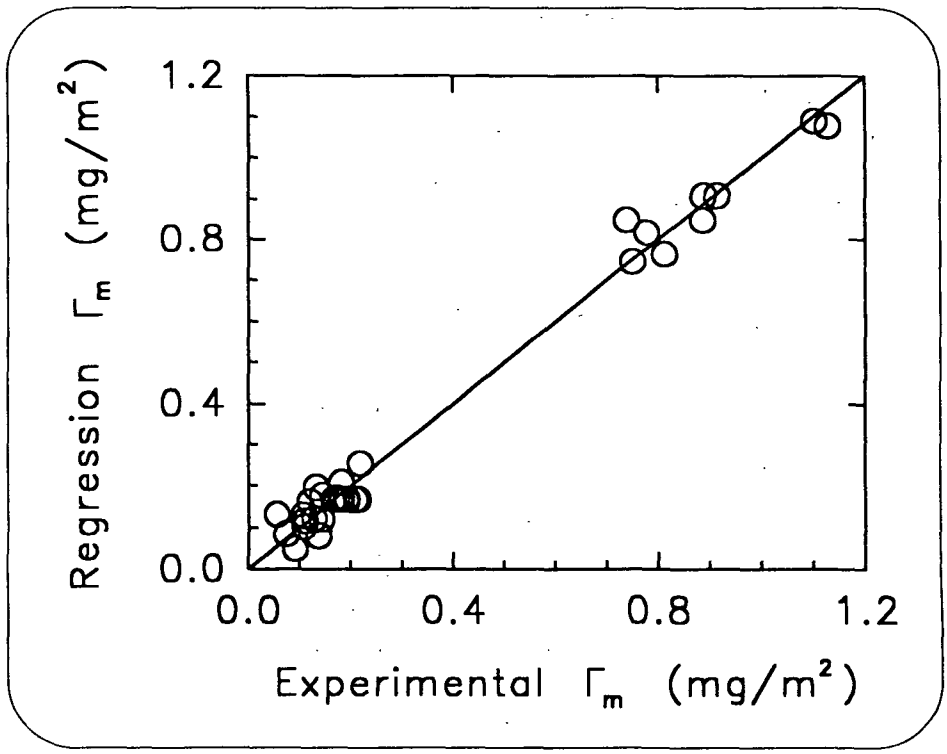

Figure 31. A plot of experimental Γ_m versus Γ_m calculated using Equation 14.

The statistical analysis shows that the R^2 for the regression is 0.988. However, SAS reports that the regression equation shows a significant lack of fit. Typically, this is caused by systematic variation brought about by higher order terms. Attempts to improve the fit by transforming the variables or dropping terms were unsuccessful.

Tests for significance are not effected by the lack of fit. Several terms were significant. The first and second order effects of α were significant at the 99% confidence level. The following first order interactions were significant: $\sigma_s \cdot \alpha$, $M_{(n)} \cdot \alpha$, and $M_{(n)} \cdot \sigma_s$ (95%, 95%, and 90% confidence level, respectively). The effects of salt, and salt interactions, were not significant. The corresponding regression equation, with the significant terms, is shown below.

$$\Gamma_m = b_0 - b_1\alpha - b_6\sigma_s\alpha - b_8 M_{(n)}\alpha + b_{10} M_{(n)}\sigma_s + b_{11}\alpha^2 \qquad \{15\}$$

The regression coefficients for equation 15 are provided in Table 13 below, to give meaning to the relative weight of each term.

Table 13. The coefficients for Equation 15.

Regression	Coefficients
b_0	0.59
b_1	3.1
b_6	32.7
b_8	2.16E-6
b_{10}	1.84E-4
b_{11}	2.98

The data and the statistical analysis clearly show that α is the dominant variable in terms of its effect on Γ_m. When α decreases from 0.8 (pH 4.0) to 0.3 (pH 8.5), Γ_m doubles. Decreasing α

from 0.3 (pH 8.5) to 0.05 (pH 10) results in a fourfold increase in Γ_m.

Interpretation of the effect of the first order interaction terms is more complicated. It is useful to rewrite the Equation 15, grouping the variables of interest. This is shown in Equation 16, where the α terms have been grouped in parentheses.

$$\Gamma_m = b_0 + (b_{11}\alpha - b_1 - b_6\sigma_s - b_8 M)\alpha + b_{10} M\sigma_s \qquad \{16\}$$

At low α, the last term in Equation 16 dominates, giving higher Γ_m at high $M_{(n)}$. As α increases, Γ_m decreases at both high and low $M_{(n)}$. The slope of the decrease is greater at high $M_{(n)}$. At high α, the terms in the regression equation offset one another, resulting in only a small increase with increasing $M_{(n)}$. The same can be said for the interaction between σ_s and α. Figure 32 below is a sketch of the effects due to first order interactions involving α (i.e., $M_{(n)}\cdot\alpha$, and $\sigma_s\cdot\alpha$).

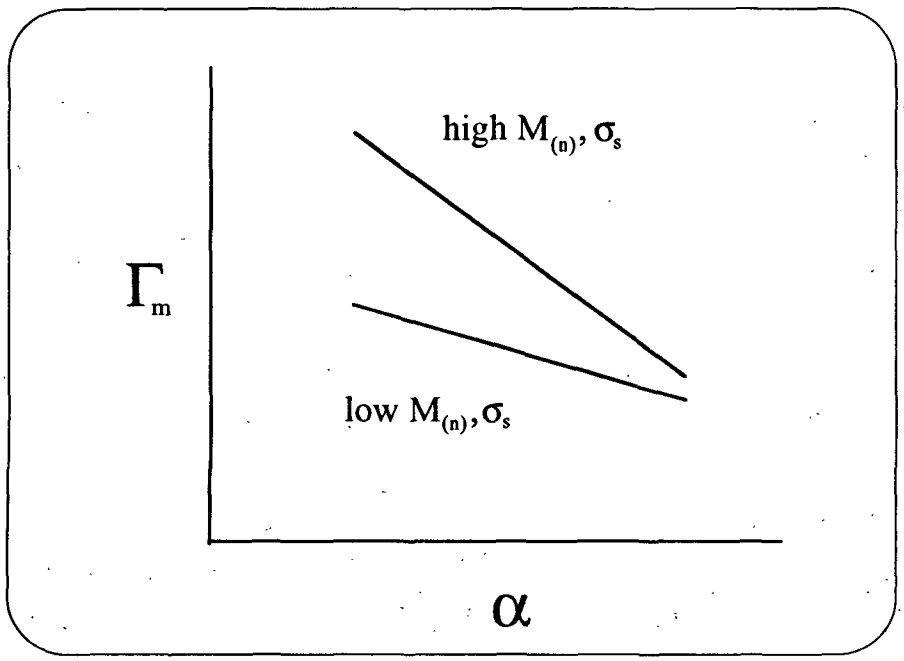

Figure 32. A sketch representing the effect of first order interactions involving α ($M_{(n)}\cdot\alpha$, and $\sigma_s\cdot\alpha$).

Tables 14 and 15 below contain examples from the adsorption data which illustrate the interaction between $M_{(n)}$ and α, at high and low σ_s, respectively. The data in Tables 16 and 17 illustrate the interaction between σ_s and α, at high and low $M_{(n)}$, respectively.

Table 14. Adsorption data which illustrate the interaction between $M_{(n)}$ and α, at high σ_s (with treatment numbers in parentheses).

Γ_m (mg/m^2)	low α:		high α:	
(high σ_s)	low salt	high salt	low salt	high salt
high $M_{(n)}$	1.102 (14)	1.128 (16)	0.173 (13)	0.121 (15)
low $M_{(n)}$	0.888 (6)	0.779 (8)	0.075 (5)	0.092 (7)
net change	0.214	0.349	0.098	0.029

Table 15. Adsorption data which illustrate the interaction between $M_{(n)}$ and α, at low σ_s (with treatment numbers in parentheses).

Γ_m (mg/m^2)	low α:		high α:	
(low σ_s)	low salt	high salt	low salt	high salt
high $M_{(n)}$	0.889 (10)	0.915 (4)	0.143 (9)	0.111 (3)
low $M_{(n)}$	0.813 (2)	0.751 (12)	0.056 (1)	0.109 (11)
net change	0.076	0.164	0.087	0.002

Table 16. Adsorption data which illustrate the interaction between σ_s and α, at high $M_{(n)}$ (with treatment numbers in parentheses).

Γ_m (mg/m^2)	low α:		high α:	
(high $M_{(n)}$)	low salt	high salt	low salt	high salt
high σ_s	1.102 (14)	1.128 (16)	0.173 (13)	0.121 (15)
low σ_s	0.889 (10)	0.915 (4)	0.143 (9)	0.111 (3)
net change	0.213	0.213	0.030	0.010

Table 17. Adsorption data which illustrate the interaction between σ_s and α, at low $M_{(n)}$ (with treatment numbers in parentheses).

Γ_m (mg/m^2)	low α:		high α:	
(low $M_{(n)}$)	low salt	high salt	low salt	high salt
high σ_s	0.888 (6)	0.779 (8)	0.075 (5)	0.092 (7)
low σ_s	0.813 (2)	0.751 (12)	0.056 (1)	0.109 (11)
net change	0.075	0.048	0.019	-0.017

A similar approach can be used to interpret the effect of the interaction between $M_{(n)}$ and σ_s on Γ_m, while holding α constant. Equation 17 shows Equation 15 rewritten with the σ_s terms grouped together.

$$\Gamma_m = b_0 - b_1\alpha - b_8 M\alpha + b_{11}\alpha^2 + (b_{10}M - b_6\alpha)\sigma_s \qquad \{17\}$$

Since b_{10} is considerably larger than b_8, the last term in Equation 17 dominates when changes in $M_{(n)}$ and σ_s are considered. For the variable ranges studied, this term is always positive. At low σ_s, the regression terms offset one another, resulting in only a moderate increase in Γ_m, with increasing $M_{(n)}$. Increasing σ_s causes an increase in Γ_m at both high and low $M_{(n)}$. The greatest increases in Γ_m with increasing $M_{(n)}$ occur at high σ_s. Figure 33 below is a sketch representing the effect of $M_{(n)}$ and σ_s on Γ_m. Tables 18 and 19 below contain examples from the adsorption data which illustrate the interaction between $M_{(n)}$ and α, at high and low σ_s, respectively.

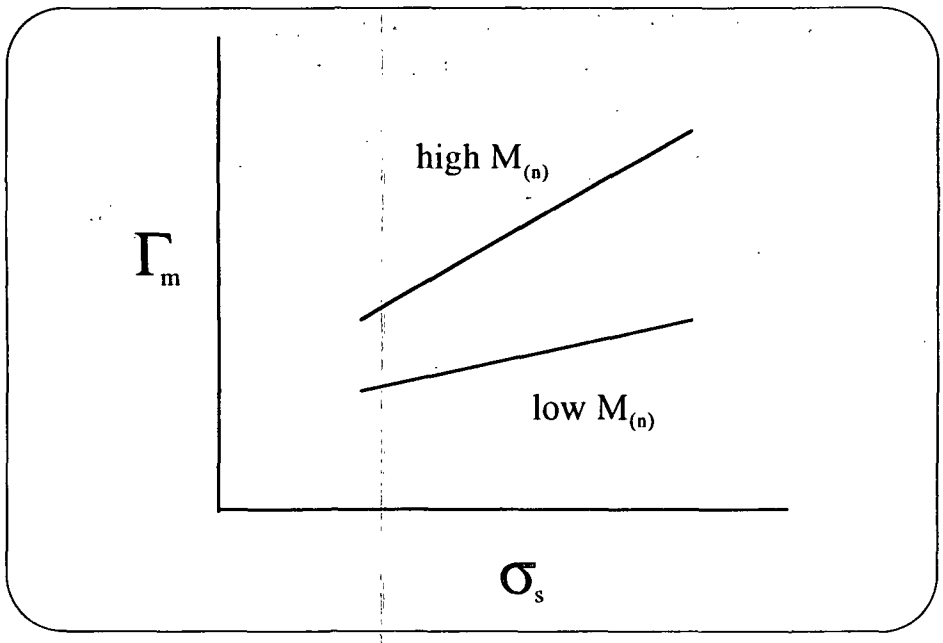

Figure 33. A sketch representing the effect of the interaction between $M_{(n)}$ and σ_s at constant α.

Table 18. Adsorption data which illustrate the interaction between $M_{(n)}$ and σ_s, at high α (with treatment numbers in parentheses).

Γ_m (mg/m^2)	low σ_s:		high σ_s:	
(high α)	low salt	high salt	low salt	high salt
high $M_{(n)}$	0.143 (9)	0.111 (3)	0.173 (13)	0.121 (15)
low $M_{(n)}$	0.056 (1)	0.109 (11)	0.075 (5)	0.092 (7)
net change	0.087	0.002	0.098	0.029

Table 19. Adsorption data which illustrate the interaction between $M_{(n)}$ and σ_s, at low α (with treatment numbers in parentheses).

Γ_m (mg/m^2)	low σ_s:		high σ_s:	
(low α)	low salt	high salt	low salt	high salt
high $M_{(n)}$	0.889 (10)	0.915 (4)	1.102 (14)	1.128 (16)
low $M_{(n)}$	0.813 (2)	0.751 (12)	0.888 (6)	0.779 (8)
net change	0.076	0.164	0.214	0.349

The observed trends can be interpreted by considering the balance of electrostatic forces. The dramatic increase in Γ_m with decreasing α can be attributed to the development of a looped configuration at the surface. As α decreases, the reduction in repulsion between adjacent charges, and the overall reduction in the net attraction for the surface, gives the polymer segments the freedom to approach one another, promoting the formation of extended loops and tails. In all cases studied, positive charges were in excess. The charge ratio, defined here as the ratio of the total number of positive charges on the adsorbed polymer to the number of negative charges at the surface, ranged from 2:1 to 19:1. The importance of repulsion between adjacent charge groups is magnified by the presence of excess of positive charges.

At low α, where PAAm adsorbs in a looped configuration, increasing $M_{(n)}$ or σ_s caused a significant rise in Γ_m. Increasing $M_{(n)}$ extends the total polymer length, which in turn extends the length of loops and tails. The result is an increase in the amount of PAAm adsorbed. Increasing σ_s changes the balance of electrostatic forces. More positive charges are adsorbed and neutralized at high σ_s. This causes a decrease in repulsion between adjacent positive charges and an increase in the packing density of the polymer. The net result is an increase in Γ_m.

At high α, PAAm adsorbs in a flat configuration. Therefore, an increase in $M_{(n)}$ results in only a small increase in Γ_m. The repulsion between charged segments and the increased attraction for the surface dominates. Therefore, increasing σ_s causes only a small increase in Γ_m.

At low σ_s, the ability of the surface to offset polymer charge repulsion is diminished. Increasing $M_{(n)}$ under these conditions results in only a small rise in Γ_m. At high σ_s, this trend is reversed and an increase in $M_{(n)}$ results in a significant increase in Γ_m.

While collecting adsorption data for the pH 10 treatments cases, an interesting trend was observed. In preliminary experiments, PSL samples with adsorbed PAAm were filtered to near dryness using the technique described in the methods section. The amount of PAAm in the filtrate was determined by colloid titration, and the amount adsorbed calculated by difference. In each of these pH 10 adsorptions, Γ increased rapidly with increasing Ce to a maximum, and then decreased with increasing Ce. In subsequent experiments, PSL samples with adsorbed PAAm were only partially filtered to minimize particle interaction. In each case, the adsorption isotherms exhibited behavior more typical of monolayer adsorption. Examples of the adsorption isotherms for the two filtering techniques are shown in Figure 34 below.

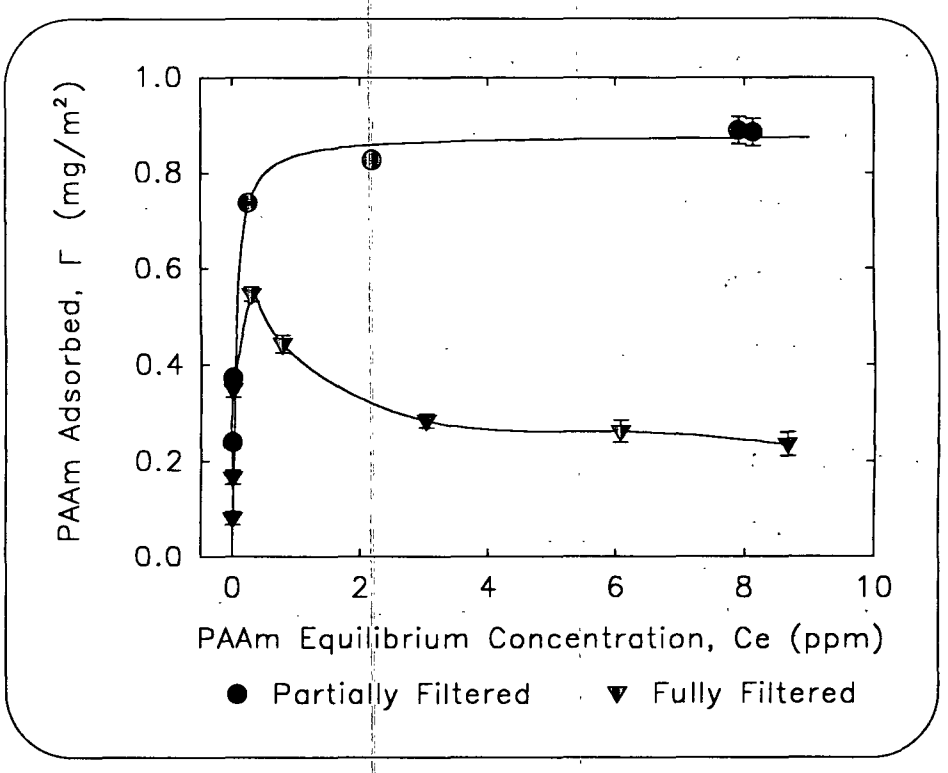

Figure 34. A plot of PAAm adsorbed, Γ (mg/m^2) versus PAAm equilibrium concentration, Ce (ppm) for partially filtered and fully filtered samples (pH = 10, M_n = 12,600, c_s = 0, σ_s = 0.0116 C/m^2).

The decrease in Γ occurred only when pH 10 adsorptions were fully filtered. The degree of protonation at pH 10 is low, allowing the polymer to adopt an extended configuration at the surface. It is possible that the adsorbed polymer molecules on adjacent particles interact as the solvent in the bulk is depleted, resulting in desorption. The desorbed polymer then passes through the filter and into the filtrate. The concentration in the filtrate would then be artificially high causing a reduction in the amount of adsorbed PAAm determined by difference.

Israelachvili, et al.[144] have studied the forces between two mica plates with adsorbed polyethylene oxide (PEO). In general, they showed that the repulsive force increased rapidly and then slowed as the mica surfaces were brought together. During the approach, the force measurements showed sudden yields and inward drifts, reminiscent of a gel under compression. This, they observe, is consistent with intermittent rupture of the bonds that form the adsorbed network. The strain is reduced when some of the adsorbed layer of PEO is desorbed and the remainder forms a flatter layer. Ultimately, the mica comes into molecular contact, effectively extruding the PEO from the surface. Presumably, the amount of polymer forced from the surface would depend upon the strength of the network bonds and the thickness of the adsorbed layer. The effects should be most apparent in the plateau region of the adsorption isotherms.

Others have published adsorption isotherms containing maxima in the literature.[145,146] Joppien[145] showed that isotherms for adsorption of 20,000 MW PEO on silica contained maxima, whereas those for 400 MW PEO did not. With the combination of weak attractive forces and high MW one might expect the adsorbed polymer layer to assume an extended configuration. On centrifugation, interaction of adsorbed polymer on adjacent particles may have resulted in depletion-desorption. Lowering the MW would reduce the amount of PEO adsorbed and the thickness of the adsorbed layer, thereby reducing the potential for depletion desorption.

Pefferkorn, et al.,[146] showed that maxima occurred in isotherms for adsorption of partially hydrolyzed polyacrylamide (PAA) to modified glass beads with a small positive charge (pH 4.7). The shape of these curves was explained in terms of the kinetics of the adsorption process. Pefferkorn, et al.,[146] state that the strong level of attraction and high polymer concentration forces the polymer to adsorb quickly, in a configuration similar to that adopted by the polymer in solution. Once the surface is covered, segments must desorb before additional polymer molecules can adsorb. Since the electrostatic attraction is strong, this process is exceedingly slow. This theory is supported by data which show the adsorbed amount increasing with time to give an isotherm which more closely resembles those for equilibrium monolayer coverage. The isotherm for adsorption of uncharged PAA (pH 3.3) exhibited behavior more typical of monolayer adsorption. In this case, the net attraction for the surface is reduced. This adsorbed layer is likely to be more accommodating to continued adsorption due to the relatively weak segment attachments formed via hydrogen bonding.

It is doubtful that depletion-desorption played a significant role in the adsorptions performed by Pefferkorn, et al.[146] They separated the suspended particles by allowing the large beads to settle. With this technique the force on interacting layers is reduced considerably.

Likewise, it is doubtful that nonthermodynamic equilibrium adsorption played a role in the experiments performed here. All adsorptions were allowed to equilibrate for 24 hours. In all pH 10 cases, complete filtering of the sample caused maxima to appear in the adsorption isotherms, whereas partial filtering did not, so the effect was reproducible. In addition, adsorptions which shook for 168 hours showed no increase in the amount of polymer adsorbed.

SELF-CONSISTENT-FIELD THEORY (SCF) PREDICTIONS

A VMS version of MULPOL was graciously supplied by the late Dr. Jan Scheutjens of Wageningen Agricultural University, Wageningen, The Netherlands. MULPOL is a program for modeling polyelectrolyte adsorption. Details regarding the program can be found in the article by Böhmer, et al.[47] The theory on which the model is based was discussed in the literature review section of this thesis. In this section, comparisons will be made between the experimental data and model predictions made using MULPOL. The input required by MULPOL is listed in Table 20 below.

The values for pK were calculated using Equation 5, and the experimental values for pH and α at each treatment condition. The pK of points which fell between experimental data points were interpolated. The number of segments per molecule, r, was calculated by dividing $M_{(n)}$ by the monomer molecular weight with the associated Cl^- counter ion. The monomer structure is shown in Figure 5 in the materials section.

All other variables are fixed by experimental conditions, except χ, χ_s, and the number of layers in the adsorption space. The layer thickness and the total number of layers specified determines the distance between two parallel plates on which the polymer adsorption is modeled. Input and output concentrations are expressed in volume fractions, so the absolute volume of the adsorption space is not important. The choice of the number of adsorption layers does not affect the predicted values so long as the separation is great enough to prevent interaction of the adsorbed layers.

The Flory-Huggins interaction parameter, χ, accounts for the interaction energy between the polymer segments and the solvent molecules. For cases where the polymer is soluble the

Table 20. Input for modeling the PAAm adsorption isotherm using MULPOL.

1. Type of system?	Type 4 [a]
2. Number of layers,d?	150
3. Distance between middles of layers?	0.6 nm
4. Fixed surface potential?	No
5. Surface charge, σ_s?	Varied [b]
6. Name of solvent?	Water
7. Name of polymer?	PAAm
8. Name of negative salt ion?	Cl
9. Name of positive salt ion?	Na
10. Polymer - solvent interaction parameter, χ?	0
11. Polymer - surface interaction parameter, χ_s?	0.55
12. Number of polymer segments, r?	Varied [b]
13. Restricted polymer chain?	No
14. Initial segment volume fraction in the bulk, ϕ_b?	Varied [c]
15. Polymer valence?	1^+
16. Weak polyelectrolyte?	Yes
17. Polyelectrolyte pK?	Varied [b]
18. Relative polymer dielectric constant, $\varepsilon/\varepsilon_0$?	20
19. System pH?	Varied [b]
20. Salt concentration, c_s?	Varied [b]

[a] Solvent, salt, and charged or uncharged polymer, including pH effects.
[b] These values varied from treatment to treatment (see Table 15).
[c] Sufficiently high initial concentrations were chosen for each pH case (pH 4.0: 2.5E-7, pH 8.5: 7.5E-7, pH 10: 2.5E-6) to ensure that the equilibrium amount of PAAm adsorbed would be in the plateau region.

limits of χ are 0 and 0.5, where $\chi = 0$ is a very good solvent and $\chi = 0.5$ is a theta solvent. The Silberberg interaction parameter, χ_s, accounts for the non-electrostatic interaction energy between the polymer segments and the surface. Values for χ_s found in the literature range from 0.5 to 2.

Trial and error was used to find χ and χ_s values which provided the best possible fit between experimental and predicted data. Six treatment conditions were used as test cases (No. 1, 2, 6, 10, 14, and 16). These cases spanned the range in each variable studied. The values obtained for χ and χ_s using this method were 0 and 0.55, respectively. These values were then used for modeling all treatment conditions studied experimentally.

MULPOL predicts the adsorbed amount in terms of the volume fraction of adsorbed polymer segments (Γ^{exc} or θ^{exc}). To allow for direct comparisons with experimental results, the adsorbed amount was converted to mg/m^2 (Γ^{SCF}) using Equation 18 below:

$$\Gamma^{SCF} = \frac{\Gamma^{exc} MW_{(monomer)}}{\pi r^2 N} \qquad \{18\}$$

where r is the radius of the monomer segment and N is Avagodro's number. The monomer segement was assumed to have a radius of 0.15 nm. Table 21 below summarizes the results of the modeling work. Treatments 26 through 31 are replicates and are not shown here.

MULPOL was unable to model the conditions for treatment number 20. Dr. Frans Leermakers of Wageningen Agricultural University, Wageningen, The Netherlands, proposed an explanation for this problem.[147] For treatment 20, the residual ion concentration is very low. The Debye screening length is therefore very large, giving coupling of electrostatic interactions over large distances in the adsorption space. To model this case, the number of layers must be

set high. In these instances, thousands of iterations may be necessary to reach convergence. It is not possible to model this case, since our version of MULPOL is limited to 500 iterations.

Table 21. Results for modeling of PAAm adsorption using MULPOL.

Treatment No.	pH	α	pK	c_s (M)	σ_s (C/m^2)	$M_{(n)}$	Γ_m (mg/m^2)	Γ^{SCF} (mg/m^2)	p model
1	4.00	0.790	4.58	0.0000	0.0062	12,600	0.056	0.060	0.647
2	10.00	0.043	8.66	0.0000	0.0062	12,600	0.813	0.391	0.521
3	4.00	0.761	4.50	0.0100	0.0062	109,000	0.111	0.071	0.626
4	10.00	0.052	8.74	0.0100	0.0062	109,000	0.915	1.187	0.404
5	4.00	0.790	4.58	0.0000	0.0116	12,600	0.075	0.115	0.683
6	10.00	0.043	8.66	0.0000	0.0116	12,600	0.888	0.558	0.515
7	4.00	0.761	4.50	0.0100	0.0116	12,600	0.092	0.121	0.666
8	10.00	0.052	8.74	0.0100	0.0116	12,600	0.779	0.303	0.525
9	4.00	0.790	4.58	0.0000	0.0062	109,000	0.143	0.061	0.654
10	10.00	0.043	8.66	0.0000	0.0062	109,000	0.889	1.321	0.392
11	4.00	0.761	4.50	0.0100	0.0062	12,600	0.109	0.066	0.630
12	10.00	0.052	8.74	0.0100	0.0062	12,600	0.751	0.323	0.525
13	4.00	0.790	4.58	0.0000	0.0116	109,000	0.173	0.115	0.688
14	10.00	0.043	8.66	0.0000	0.0116	109,000	1.102	1.585	0.381
15	4.00	0.761	4.50	0.0100	0.0116	109,000	0.121	0.126	0.663
16	10.00	0.052	8.74	0.0100	0.0116	109,000	1.128	1.156	0.404
17	8.50	0.314	8.16	0.0010	0.0081	50,400	0.210	1.587	0.397
18	4.00	0.790	4.58	0.0010	0.0081	50,400	0.138	0.083	0.659
19	10.00	0.034	8.55	0.0010	0.0081	50,400	0.740	0.980	0.438
20	8.50	0.322	8.18	0.0000	0.0081	50,400	0.182	*	*
21	8.50	0.352	8.23	0.0100	0.0081	50,400	0.145	0.993	0.443
22	8.50	0.314	8.16	0.0010	0.0062	50,400	0.129	1.363	0.409
23	8.50	0.314	8.16	0.0010	0.0116	50,400	0.133	2.013	0.383
24	8.50	0.314	8.16	0.0010	0.0081	12,600	0.108	0.780	0.505
25	8.50	0.314	8.16	0.0010	0.0081	109,000	0.219	1.888	0.356

* MULPOL was unable to model this case. See the discussion below.

The changes in Γ^{SCF} caused by interactions between $M_{(n)}$ and α are similar to those found in the experimental data, with the exception that the magnitude of the change differs. At low α,

increasing $M_{(n)}$ causes a larger increase in Γ^{SCF} than that shown for Γ_m. As α is increased, Γ^{SCF} decreases at both high and low $M_{(n)}$. The absolute difference at high α is small. Figure 35 shows a sketch of the trends for both Γ_m and Γ^{SCF}. Direct comparisons of the data are given in Tables 22 and 23.

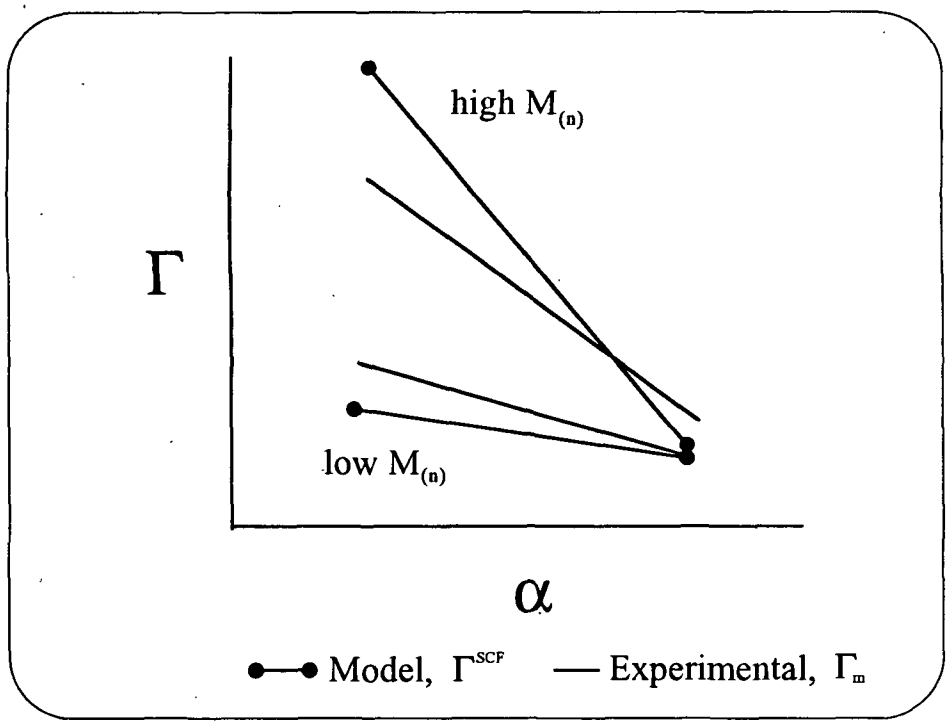

Figure 35. A sketch representing the effect of first order interactions involving $M_{(n)}$ and α for both model and experimental data.

Table 22. MULPOL Γ^{SCF} values which illustrate the interaction between $M_{(n)}$ and α, at high σ_s (with treatment numbers in parentheses).

Γ^{SCF} (mg/m^2)	low α:		high α:	
(high σ_s)	low salt	high salt	low salt	high salt
high $M_{(n)}$	1.585 (14)	1.160 (16)	0.114 (13)	0.126 (15)
low $M_{(n)}$	0.558 (6)	0.303 (8)	0.114 (5)	0.121 (7)
net change	1.027	0.857	0.000	0.005

Table 23. MULPOL Γ^{SCF} values which illustrate the interaction between $M_{(n)}$ and α, at low σ_s (with treatment numbers in parentheses).

Γ^{SCF} (mg/m^2)	low α:		high α:	
(low σ_s)	low salt	high salt	low salt	high salt
high $M_{(n)}$	1.320 (10)	1.187 (4)	0.061 (9)	0.071 (3)
low $M_{(n)}$	0.391 (2)	0.323 (12)	0.060 (1)	0.066 (11)
net change	0.929	0.864	0.001	0.005

Interactions between σ_s and α caused changes in Γ^{SCF} similar to those found experimentally at low salt concentration. However, at high salt concentration and low α, Γ^{SCF} decreases slightly with increased σ_s. In their modeling work, van de Steeg and coworkers[48] show that for a system where $\chi = 0$ and $\chi_s = 0.6$, the screening-enhanced adsorption regime dominates. However, when charge density is low and surface charge is high, the system moves into the screening-reduced adsorption regime. The result is a reduction in Γ^{SCF} at high c_s. This trend is not observed in the experimental data. MULPOL Γ^{SCF} values are compared in Tables 24 and 25. Figure 36 shows a sketch of the trends which result from interactions between σ_s and α, in the experimental and model data.

Table 24. MULPOL Γ^{SCF} values which illustrate the interaction between σ_s and α, at high $M_{(n)}$ (with treatment numbers in parentheses).

Γ^{SCF} (mg/m^2)	low α:		high α:	
(high $M_{(n)}$)	low salt	high salt	low salt	high salt
high σ_s	1.585 (14)	1.160 (16)	0.114 (13)	0.126 (15)
low σ_s	1.320 (10)	1.187 (4)	0.061 (9)	0.071 (3)
net change	0.265	-0.027	0.053	0.055

Table 25. MULPOL Γ^{SCF} values which illustrate the interaction between σ_s and α, at low $M_{(n)}$ (with treatment numbers in parentheses).

Γ^{SCF} (mg/m^2)	low α:		high α:	
(low $M_{(n)}$)	low salt	high salt	low salt	high salt
high σ_s	0.558 (6)	0.303 (8)	0.114 (5)	0.121 (7)
low σ_s	0.391 (2)	0.323 (12)	0.060 (1)	0.066 (11)
net change	0.167	-0.020	0.054	0.055

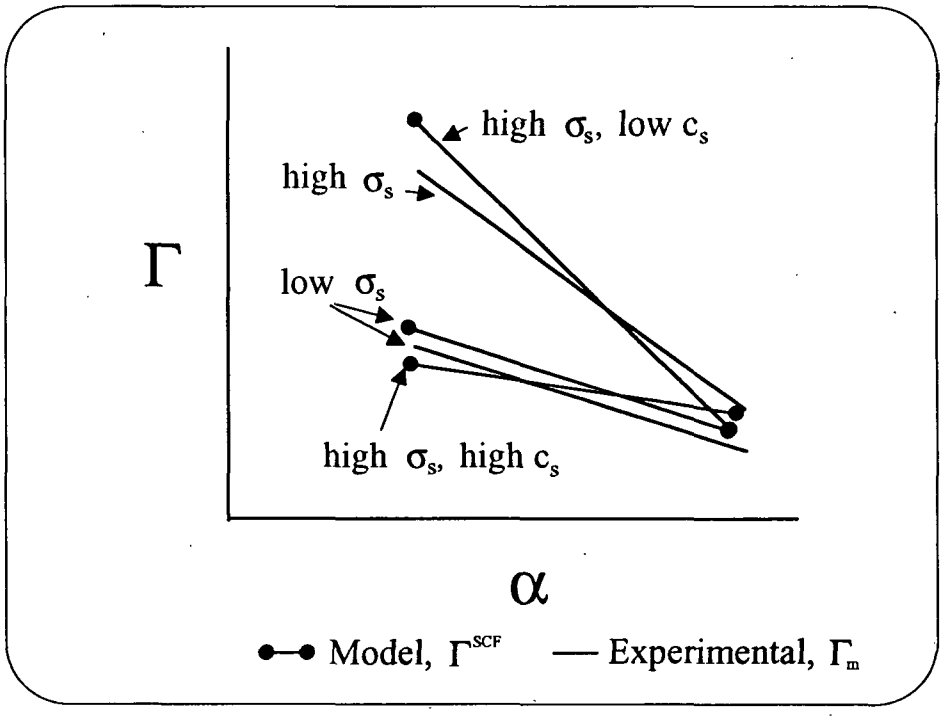

Figure 36. A sketch representing the effect of first order interactions involving σ_s and α for both model and experimental data.

The changes in Γ^{SCF} caused by interactions between $M_{(n)}$ and σ_s are small when compared with those for the experimental data. At high α, increasing $M_{(n)}$ has no noticeable effect at both high and low σ_s. At high α and low c_s, Γ^{SCF} does increase with increasing $M_{(n)}$. However, the change in Γ^{SCF} is negligible at high α and low c_s. Γ^{SCF} values are compared in Tables 26 and 27.

Table 26. MULPOL Γ^{SCF} values which illustrate the interaction between $M_{(n)}$ and σ_s, at high α (with treatment numbers in parentheses).

Γ^{SCF} (mg/m^2)	low σ_s:		high σ_s:	
(high α)	low salt	high salt	low salt	high salt
high $M_{(n)}$	0.061 (9)	0.071 (3)	0.114 (13)	0.126 (15)
low $M_{(n)}$	0.060 (1)	0.066 (11)	0.114 (5)	0.121 (7)
net change	0.001	0.005	0.000	0.005

Table 27. MULPOL Γ^{SCF} values which illustrate the interaction between $M_{(n)}$ and σ_s, at low α (with treatment numbers in parentheses).

Γ^{SCF} (mg/m^2)	low σ_s:		high σ_s:	
(low α)	low salt	high salt	low salt	high salt
high $M_{(n)}$	1.320 (10)	1.187 (4)	1.585 (14)	1.160 (16)
low $M_{(n)}$	0.391 (2)	0.323 (12)	0.558 (6)	0.303 (8)
net change	0.929	0.864	1.027	0.857

In general, the trends found in the Γ^{SCF} values are similar to those found experimentally, with three exceptions. First, at low α, increasing $M_{(n)}$ causes a larger increase in Γ^{SCF} than that shown for the experimental data. Second, at high σ_s and low α, Γ^{SCF} decreases with increased c_s, due to a shift to the screening-reduced adsorption regime described by van de Steeg et al.[48] Third, the effects due to interactions between $M_{(n)}$ and σ_s are small when compared with those for the experimental data.

Van de Steeg, et al.[48] have used MULPOL to investigate the effects α (α is used to conform to notation used in this thesis, the author's use τ), σ_s, and c_s, on purely electrostatic

adsorption (where $\chi = 0.5$ and $\chi_s = 0$) on an oppositely charged surface. Their results agree with those reported here for both Γ_m and Γ^{SCF}. They showed that at low α (< 0.10), large increases in the adsorbed amount occurred with increasing σ_s. The magnitude of this increase dropped as τ increased. They also showed that effects of c_s on the adsorbed amount were negligible for $\alpha >$ 0.10.

The absolute differences in Γ_m and Γ^{SCF} range from approximately 5 to 140%. Most of the cases with large differences occur at pH 8.5. In fact, the Γ^{SCF} values at pH 8.5 are higher than those at pH 10.0, indicating that a plot of Γ^{SCF} versus pH would give a maximum. The experimental results indicate that Γ_m increases with increasing pH.

Blaakmeer, et al.[50] compared experimental results for adsorption of poly(acrylic acid) to positively charged polystyrene latex particles with predictions made using MULPOL. Plots of both experimental and predicted values for adsorbed amount versus pH contained maxima. As α decreases, the adsorbed amount reaches a maximum where decreased repulsion between charges is offset by decreased attraction for the surface. Further decreases in α result in decreases in the adsorbed amount. A more detailed study of the effects of pH on PAAm adsorption is warranted.

FT-IR-ATR ANALYSIS

FT-IR-ATR experiments were performed to study PAAm adsorption to the ZnSe IRE as a function of concentration and time. This section will emphasize the results of the analyses.

Spectrum reduction techniques were discussed in the methods section above. The primary peaks found in all aqueous spectra are present in the spectrum of Nanopure® water shown in Figure 37 below. The large peak in the 3800 - 2800 cm^{-1} region is made up of a series of transitions which originate from the asymmetric and symmetric stretching modes of water.[141,142] The 2600 - 1850 cm^{-1} region contains a small combination peak due to rotation and deformation modes of the water molecule.[148] The moderate peak in the 1850 - 1350 cm^{-1} region is attributed to the deformation mode of water.[148] Each vibrational mode is depicted in the insets in Figure 37.

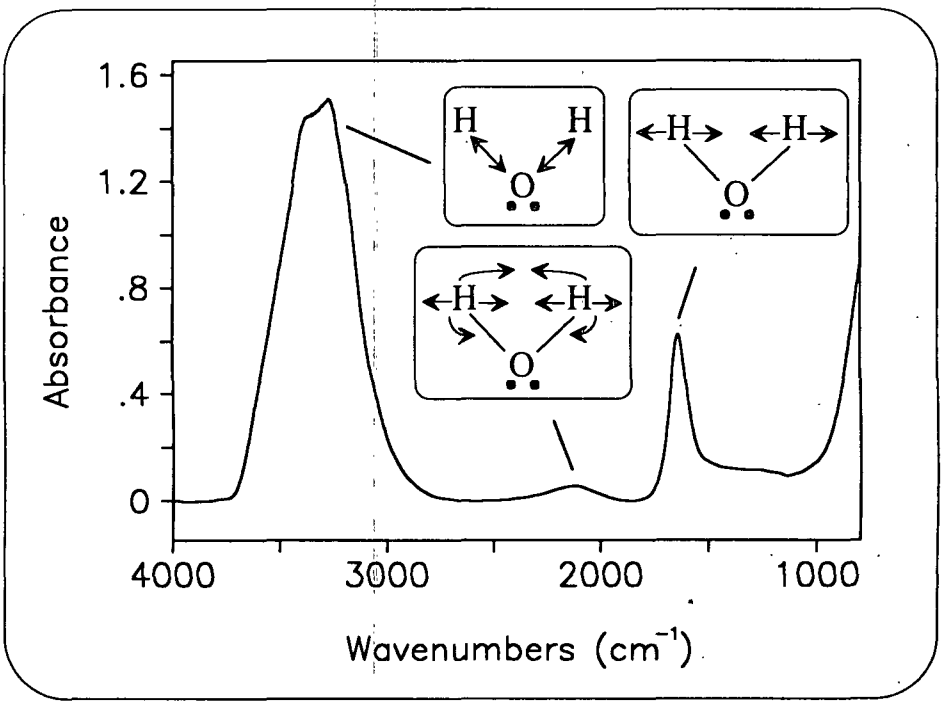

Figure 37. A water spectrum with schematics of the vibrational modes.

For reference, a neat film spectrum of PAAm is shown in Figure 38 below. The spectrum was prepared by adding successive drops of 0.72 % (w/w) PAAm in water to a KBr plate and drying with an infrared lamp. After allowing time to cool, 100 scans were collected at 4 cm^{-1}

wavenumber resolution. Happ-Genzel apodization was used to fourier transform the interferogram. The spectrum was then converted to absorbance.

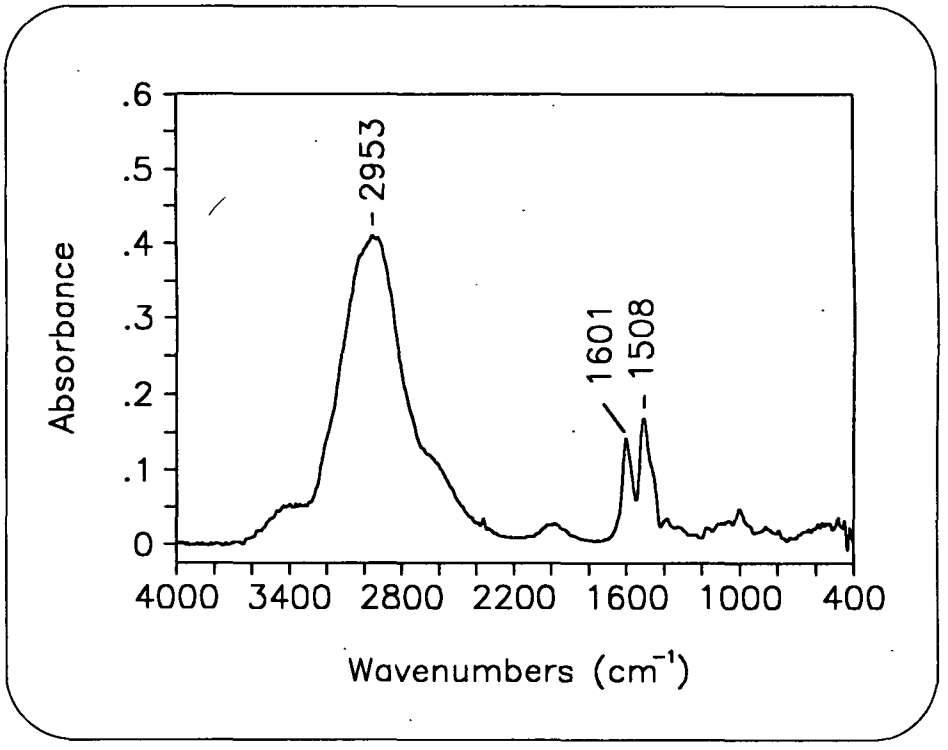

Figure 38. A spectrum of neat PAAm.

The spectrum contains three prominant peaks at 2953, 1601, and 1508 cm^{-1}. The first peak at 2953 cm^{-1} is due to CH_2 streching. The latter are due to the assymmetric and symmetric bending modes of the NH_3^+ group, respectively[148,149,150].

After cleaning, the Circle™ cell was calibrated between each set of experiments. The area of the D_2O stretching peak in the 2732 - 2286 cm^{-1} region (see Figure 28) was determined using INTEGRAT, a LABCALC® subprogram. The calibration data for the four sets of experiments presented below are shown in Table 28. The area (A) and D_2O (C) concentration values were

used to calculate the internal reflection incidence angle (θ) and the number of internal reflections (N) according to the technique of Sperline, et al.[85] The data show that the Circle™ cell can be repositioned reproducibly.

Table 28. Calibration results for the Circle™ cell using the technique of Sperline, et al.[85]

Experiment	A	C (% w/w)	θ	N	d_p (μm)
A	4.310	0.9987	51.39	7.076	0.3499
B	4.338	0.9987	51.32	7.094	0.3503
C	4.249	0.9987	51.55	7.036	0.3491
D	4.319	1.054	51.96	6.932	0.3469

The depth of penetration (d_p) at 2508 cm^{-1} was estimated using the equation defined by Harrick.[77] Figure 39 is a diagram of the evenescent wave. The equation for d_p is given below: where $\lambda_1 = \lambda/\eta_1$ is the wavelength in the denser medium and $\eta_{21} = \eta_2/\eta_1$ is the ratio of the refractive index of the rarer medium divided by that of the denser.

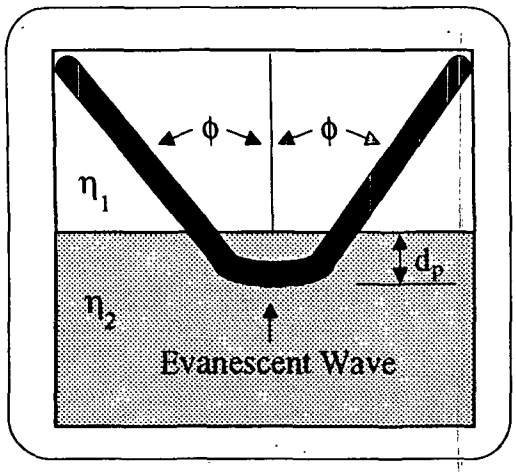

$$d_p = \frac{\lambda_1}{2\pi\left(\sin^2\theta - \eta_{21}^2\right)^{\frac{1}{2}}} \qquad \{17\}$$

Figure 39. A diagram of the evanescent wave with Harrick's[77] equation for the depth of penetration.

Two different experiments were performed to study the adsorption of PAAm to the ZnSe IRE. In the first, sets of spectra were collected at pH 4.0, 8.5, and 10.0 (experiments A, B, and C, respectively). Each set consisted of a series of PAAm solutions of increasing concentration. Collection of the spectrum was begun immediately after injection of the PAAm sample. It took approximately 8 minutes to collect 1000 scans. After each PAAm spectrum was collected, the cell was flushed, filled with water at the appropriate pH, and a second spectrum was collected. These spectra represent PAAm adsorbed to the ZnSe IRE without interference from PAAm in the bulk. A spectrum of pH 8.5 PAAm at 6900 ppm is shown in Figure 40. The spectrum was smoothed using the 23 point Savitsky-Golay[151,152] smoothing function in LABCALC™.

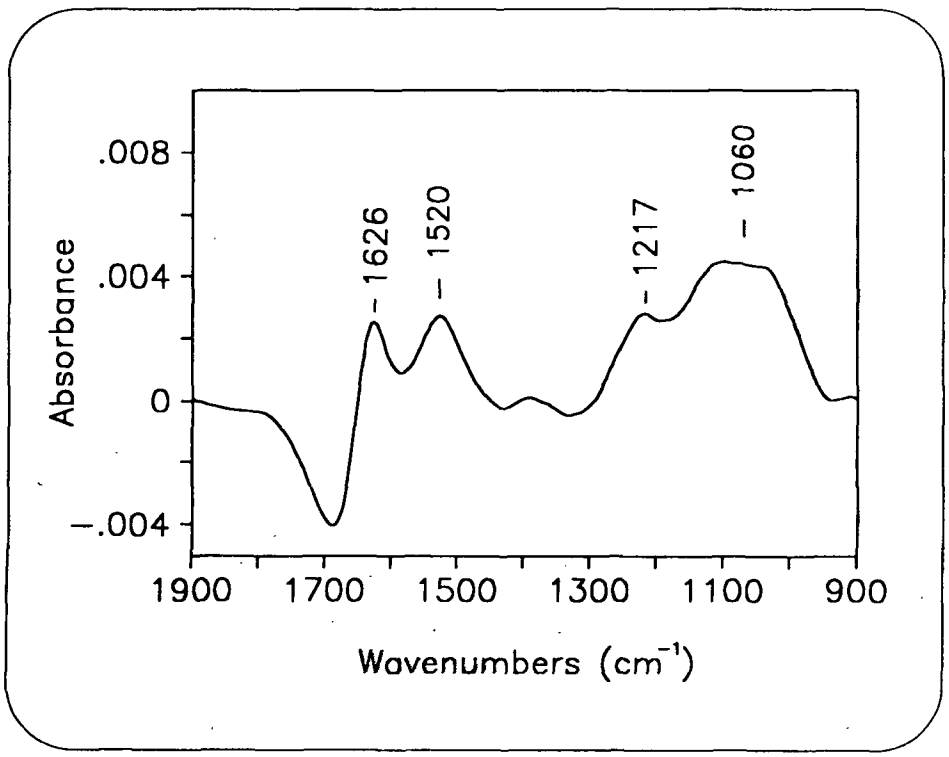

Figure 40. A spectrum of pH 8.5 PAAm at 6900 ppm.

Spectra of pH 8.5 PAAm at all concentrations are plotted as a function of concentration on the z axis in Figure 41. The 1626 cm^{-1} peak is, at least, partially due to assymmetric bending of the NH_3^+ group. A positive peak due to shifting of the water deformation peak may also be present in this region. Shifting of the water deformation peak is discussed in greater detail below. The NH_3^+ symmetric deformation peak seen in Figure 38 shifts to 1520 cm^{-1} as a result of interaction with the water. Similar shifts to higher frequencies on bonding have been reported elsewhere.[148,149,150] The peak at 1060 cm^{-1} is due to stretching of the C-N bond.[153] The peak at 1217 cm^{-1} is currently unidentified. The area of the peaks at 1060 and 1520 cm^{-1} were determined using CURVEFIT and are shown plotted versus concentration in Figures 42 and 43, respectively.

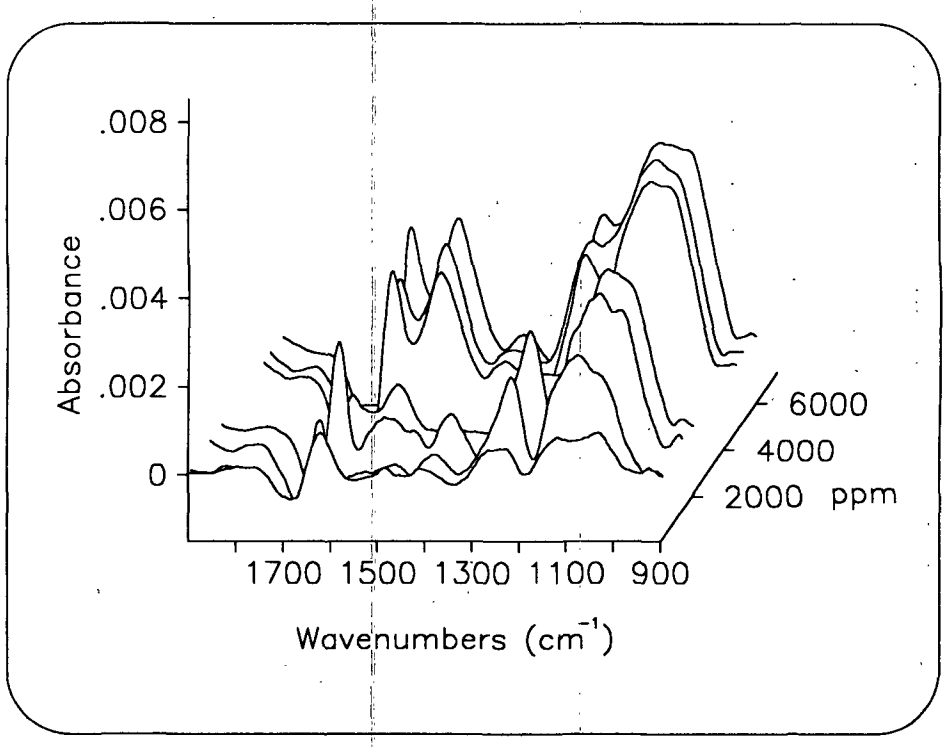

Figure 41. Spectra of PAAm at pH 8.5 plotted as a function of concentration.

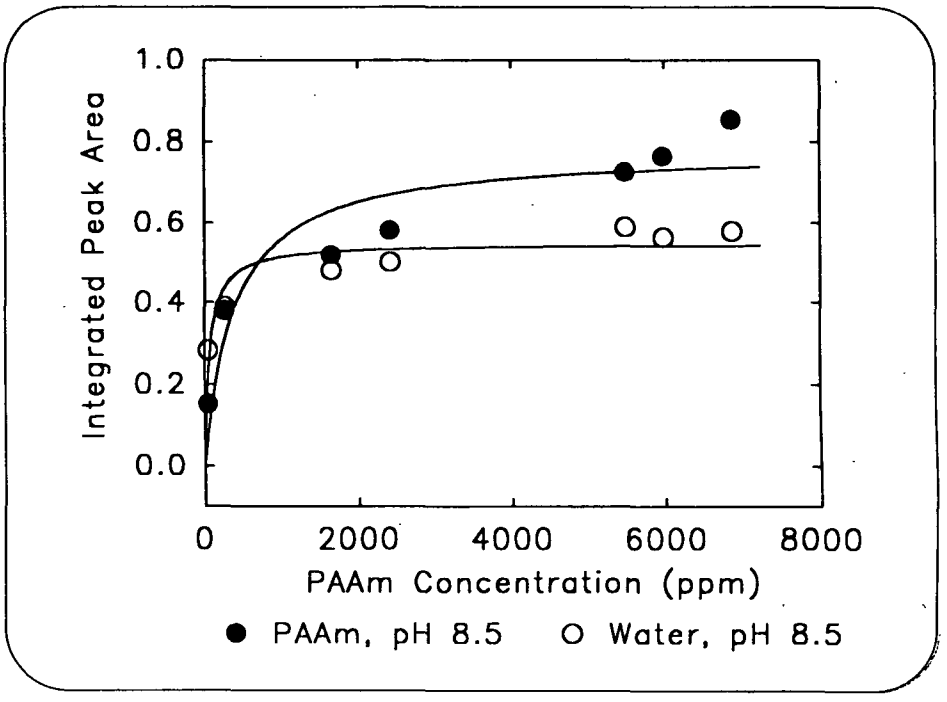

Figure 42. Area of the 1060 cm^{-1} peak plotted versus concentration for spectra with either PAAm solution or water in the bulk at pH 8.5.

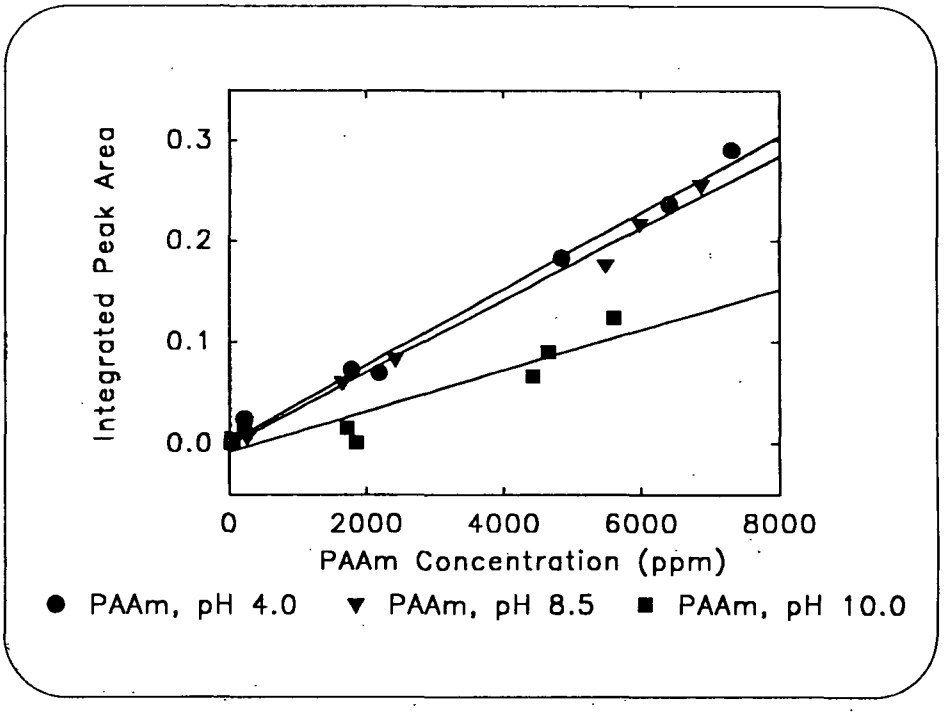

Figure 43. Area of the 1520 cm^{-1} peak plotted versus concentration with PAAm solutions in the bulk.

Both the 1520 and 1060 cm^{-1} peaks increase with concentration and exposure to PAAm. The latter appears to level off at higher concentrations. Similar trends were observed for PAAm spectra collected at the other pH values (8.5 and 10.0).

The increase in the area of the 1520 cm^{-1} peak with increased concentration for the pH 4.0 and 8.5 samples is linear in the 50 to 8000 ppm range. For the pH 10 case, the area of the 1520 cm^{-1} peak is essentially zero in the 50 to 2000 ppm range. At higher concentrations, the area of the 1520 cm^{-1} peak can be determined. Presumably, the reduction in peak area when compared with the results at pH 4.0 and 8.5 is due to the reduced number of charged amine groups at pH 10.0.

The 1520 cm^{-1} peak was absent in all spectra of adsorbed PAAm with pH-adjusted water in the bulk, whereas the 1060 cm^{-1} peak remained constant or diminished slightly. This observation supports the conclusion that the 1060 cm^{-1} peak is due primarily to adsorption of PAAm on the IRE and the 1520 cm^{-1} peak is due primarily to PAAm in the bulk.

Buckley, et al.[154] reported that the N-H stretching peak at approximately 3200 cm^{-1} increases in intensity when protonated aliphatic amines complex with nickel arsenate via ionic bonding. They also report that the NH_3^+ deformation peak at 1520 cm^{-1} decreases in intensity on complexation. This type of behavior may explain the trends observed in the data presented here. For PAAm in the bulk, the NH_3^+ deformation peak is moderate in intensity. On adsorption, the amine functional groups of the PAAm complex with the ZnSe via ionic bonding. As a result, the intensity of the NH_3^+ deformation peak decreases while the intensity of the C-N stretching

peak increases. So, the change in intensity of the respective peaks reflects a change in environment, rather than the absence of the associated modes of vibration.

In the second experiment (D), adsorption of PAAm at pH 8.5 and 5900 ppm was studied as a function of time. The observed trends were similar to those found for the concentration experiment. Figure 44 below shows spectra of PAAm at pH 8.5 plotted versus time. All spectra shown were smoothed using the 23 point Savitsky-Golay[151,152] smoothing function in LABCALC®.

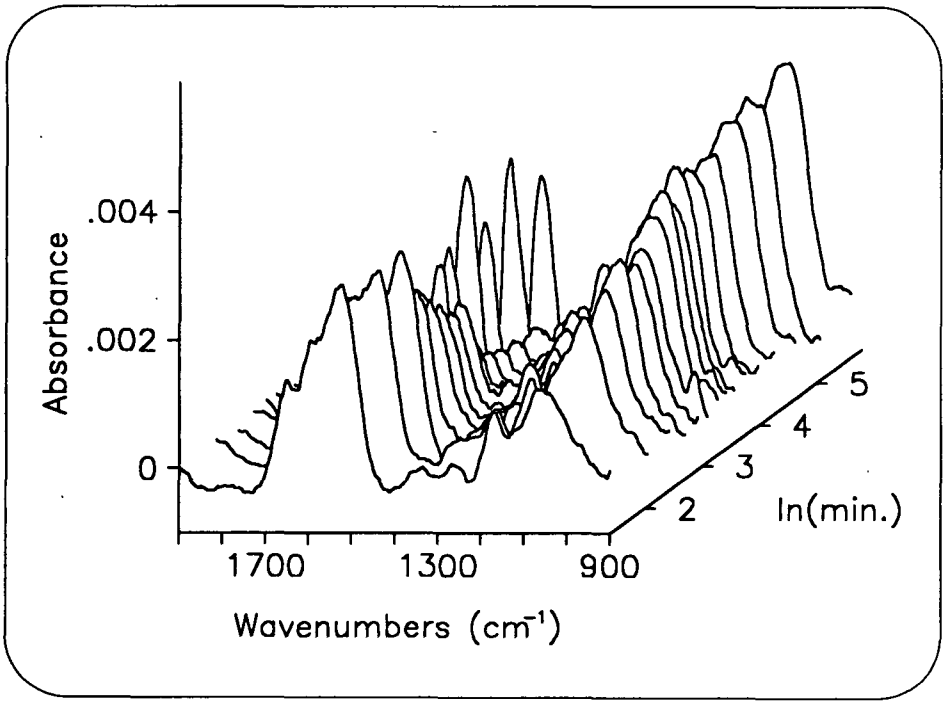

Figure 44. Spectra of PAAm at pH 8.5 plotted as a function of time.

Figure 45 shows the area of the peaks at 1520 and 1060 cm^{-1} plotted as a function of time. The C-N stretching peak intensity at 1060 cm^{-1} increases steadily and levels off as time increases. The NH_3^+ deformation peak at 1520 cm^{-1} starts out strong and then decreases as PAAm adsorbs to the IRE. The decrease in the NH_3^+ deformation peak is most likely due to the

combined effects of a reduction in the intensity of the evanescent wave as PAAm adsorbs to the IRE surface and of depletion of PAAm in the bulk.

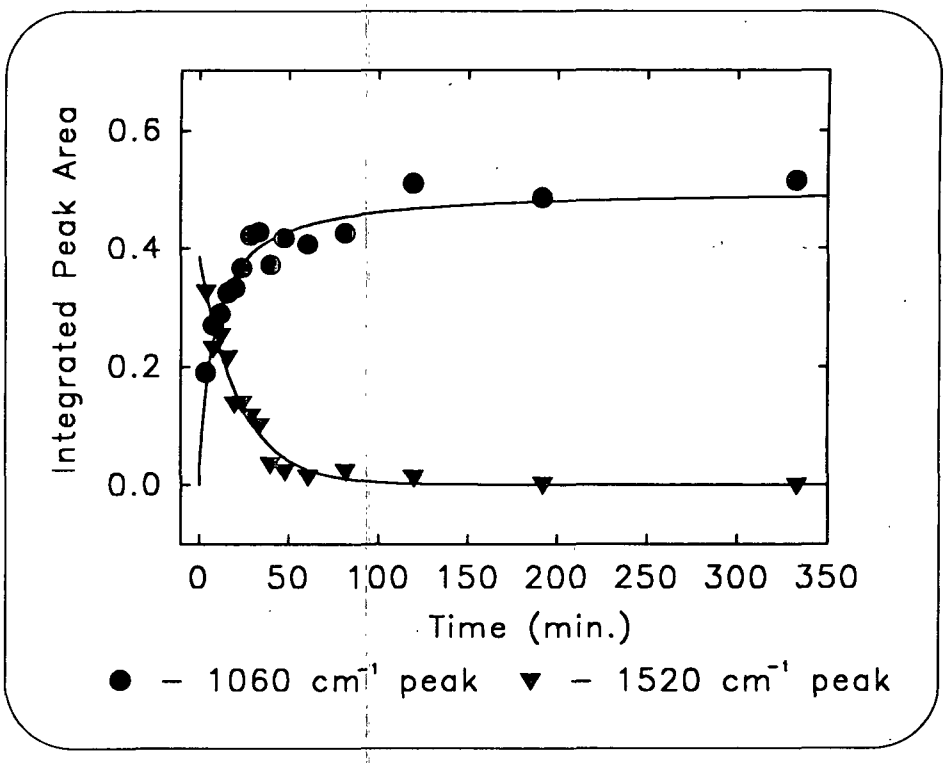

Figure 45. Area of the 1520 and 1060 cm^{-1} peaks plotted versus time (pH 8.5).

Other effects are also evident in the PAAm difference spectra. A negative peak near 1695 cm^{-1} and a positive peak near 1610 cm^{-1} emerge and increase in absolute intensity with time. The spectra in Figure 44 are shown in Figure 46 with the z axis inverted, that is, time increases from top to bottom in the figure. The peaks are due to a shift in the deformation mode of water toward lower frequencies as the level of hydrogen bonding decreases.[143] This effect may be the result of displacment of water molecules from the vicinity of the IRE as PAAm adsorbs. As the concentration of PAAm decreases, water molecules would be transferred from hydration shells to the bulk solvent environment. This type of transfer would also cause changes in hydrogen

bonding levels. Determination of the origin of the shift in the water deformation peak would require detailed experiments designed to study the spectrum of PAAm in water and D_2O. Experiments of this type were not performed as part of this thesis.

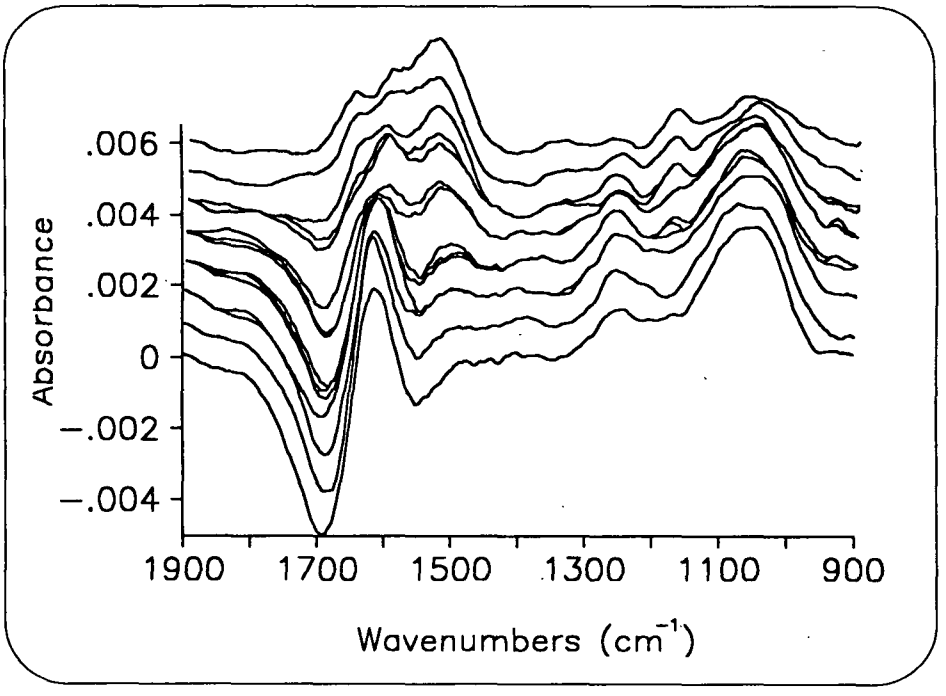

Figure 46. Spectra of PAAm at pH 8.5 plotted as a function of time with z axis inverted (decreasing time from top to bottom).

After the last timed measurement, a sample was injected which contained PSL (0.0062 C/m^2) with PAAm (12,600 $M_{(n)}$) adsorbed at pH 8.5 with no added NaCl. All excess PAAm had been washed from the sample (see methods section for preparation technique). A spectrum of Nanopure® water at pH 8.5 was collected prior to injection of the PSL sample and subsequent toremoving the PSL sample by flushing with Nanopure® water at pH 8.5. All three spectra are shown in Figure 47 below. The C-N stretching peak at 1060 cm^{-1} increases in intensity when the PSL sample is injected (B). When the sample is removed (C), the intensity drops back to the

previous level (A). So, it appears that it is possible to study PAAm adsorption in the bulk as well.

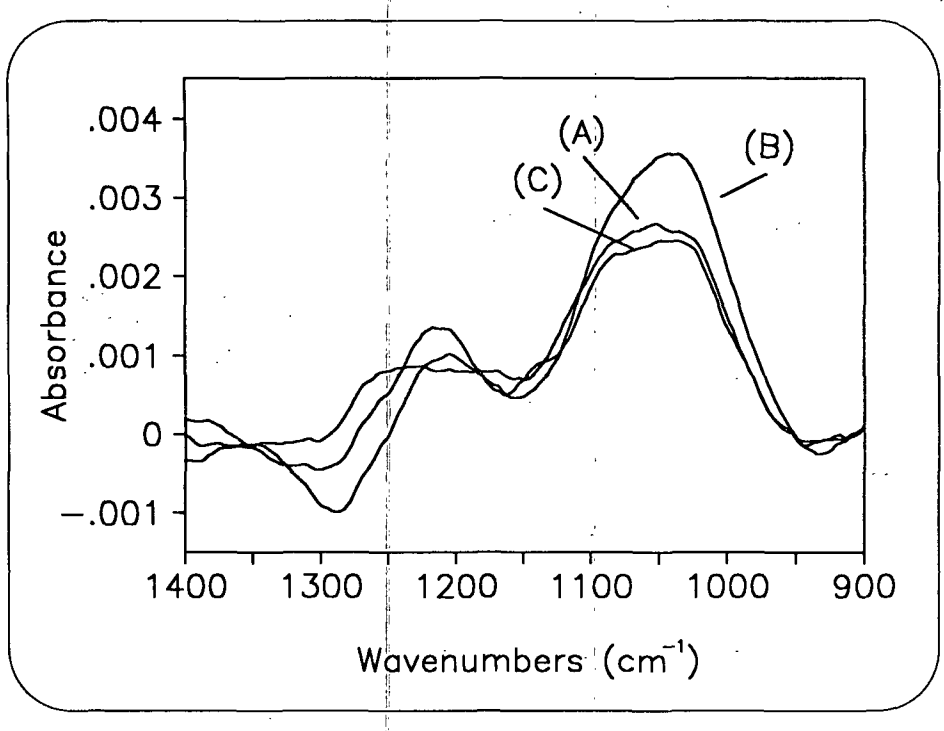

Figure 47. A spectrum of a PSL suspension with PAAm adsorbed at pH 8.5 (B). Spectra of pH 8.5 water taken before (A) and after (C) are also shown.

Unfortunately, attempts to reproduce the data taken as a function of time, and to study PAAm adsorption with time at other pH levels, were unsuccessful. With time, the ZnSe IRE became irreversibly damaged due to the repeated polishing and plasma treatment used in the cleaning process.

CONCLUSIONS

The adsorption of polyallylamine hydrochloride (PAAm) on polystyrene latex particles (PSL) was used as a model system for studying polyelectrolyte adsorption. The effects of polymer charge density (α), number average molecular weight ($M_{(n)}$), salt concentration (c_s), and particle surface charge density (σ_s) on the amount of PAAm adsorbed (Γ_m) were investigated. The dominant variable is polymer charge density. Adsorbed amounts of PAAm increased by a factor of ten or more when α decreased from 80 to 5%.

The balance of electrostatic forces also plays an important role. At low α, increasing $M_{(n)}$ or σ_s causes an increase in Γ_m due to increased looping and increased ability to neutralize charge, respectively. These effects diminish at high α due to formation of a patch configuration. At low σ_s, increasing $M_{(n)}$ causes a small increase in Γ_m. This increase is greater at high σ_s due to increased charge neutralization which provides greater opportunity for looping.

The experimental results were compared directly with predictions made using MULPOL a version of the self-consistent-field model developed by Böhmer, et al.[47] In general, the trends found in the predicted amount of PAAm adsorbed (Γ_{SCF}) are similar to those found experimentally, with three exceptions. First, at low α, increasing $M_{(n)}$ causes a larger increase in Γ_{SCF} than that shown for Γ_m. Second, at high c_s and low α, Γ_{SCF} decreases slightly with increased σ_s, due to a shift to the screening-reduced adsorption regime described by van de Steeg et al.[48] Third, the effects on Γ_{SCF} due to interactions between $M_{(n)}$ and σ_s are small when compared with those for Γ_m. The absolute differences in Γ_{SCF} and Γ_m range from approximately 5 to 140%. At

pH 8.5, Γ_{SCF} values are higher than Γ_{SCF} at pH 10. This is opposite of the observed trend in the experimental data.

Progress has been made in the development of an FT-IR-ATR technique for studying polyamine adsorption in aqueous media. An algorithm was developed which objectively subtracts water spectra from aqueous sample spectra, allowing the user to study solute peaks. The algorithm was used to analyze spectra of PAAm in solution and adsorbed to the ZnSe internal reflection element. Features of the PAAm difference spectra have been identified. Spectra of aqueous PAAm exhibit a peak near 1520 cm^{-1} due to the symmetric bending deformation of the NH_3^+ group. Adsorbed PAAm exhibits a peak near 1060 cm^{-1} due to changes in the C-N stretch on complexation.

FUTURE WORK

The effects of several process variables, and their interactions, on the amount of polymer adsorbed have been investigated in this thesis. The experiments were designed to obtain the most information from a limited number of experiments. The key variables and interactions have been identified. Expanded experiments, designed to study these variables and interactions in depth are warranted.

Comparisons of experimental data with analyses made using MULPOL showed that the SCF model can adequately predict adsorption trends. Future experimental studies might benefit from use of the model. Variables and theories can be explored using the model, before experiments are actually performed.

One adsorption variable not studied in this thesis is polymer branching. Branching increases steric hindrance, which limits the ability of the polymer to adopt a looped configuration. Many synthetic retention aids are branched. Their adsorption behavior may be considerably different than the straight chain PAAm studied here. A study of the effects of branching on retention aide adsorption would be valuable. Arai and Norde[155] have published a paper on this topic based on work done with proteins at Wageningen Agricultural University.

The use of FT-IR-CIR spectroscopy to study polyelectrolyte adsorption from solution has been demonstrated here. However, the technique would benefit from additional development. To study adsorption in the bulk, the polyelectrolyte must be prevented from adsorbing to the surface of the IRE. ZnSe has a high refractive index, which maximizes the penetration of the IR

beam, but it attracts cationic polyelectrolytes. Other commercially available crystals, such as silicon, have surfaces which can be readily modified,[156] but they have low refractive indices.

ACKNOWLEDGMENTS

I would like to thank the Institute of Paper Science and Technology, the Board of Trustees, all member companies, and individual contributers who have made it possible for me to continue my education these past few years. I am especially grateful for the help and guidance provided by my advisor, Dr. Robert A. Stratton, and all those have served on my thesis advisory committee.

I would like to individually acknowledge those who have made contributions to my thesis research. Ms. Susan Vorhies of Reiley Industries for donation of a polyvinylpyridine standard. Ms. Inga Vaden and Dr. Geoffrey V.F. Seaman of Interfacial Dynamics Corporation for preparation of polystyrene latex samples and consultations on charaterization techniques. The late Dr. Jan Scheutjens, as well as Dr. Frans Leermakers, for making MULPOL available and providing technical help regarding its use. Mr. Stephen Hardaker for use of the FT- IR chamber. Dr. Robert Braga for use of and training on the Nicolet 60SXR FT-IR. Dr. James Duckworth and Mr. John McKibben for assistance in programming LABCALC®.

I extend a special thanks to all those who have made my time here enjoyable. My colleagues in colloid and surface science, Matt Lang and Chris Luettgen, the host of Green Bay Packer fans, and all the students and families through the years.

I am most grateful to my wife Chris. I could always count on her patience, love, and encouragement.

LITERATURE REVIEW

[1] Fleer, G.J.; Lyklema, J. Adsorption of Polymers. In G.G. Parfitt and C.H. Rochester (Eds.). Adsorption from Solution at the Solid/Liquid Interface. Academic Press Inc. 111 Fifth Avenue, New York 10003. 1983:153-218.

[2] Ruehrwein, R.D.; Ward, D.W. Soil Science. 73:485-92 (1952).

[3] LaMer, V.K.; Healy, T.W. Rev. Pure Appl. Chem. 13:112-33(1963).

[4] Eggert, A.R. Role of particle size of colloidal polystyrene latex in flocculation studies by a cationic polymer. Doctor's Dissertation. Appleton, Wisconsin, The Institute of Paper Chemistry, 1976. 190 p.

[5] Kane, J.C.; LaMer, V.K.; Linford, H.B. J. Phys. Chem. 67:1977-1981 (1963).

[6] Kane, J.C.; LaMer, V.K.; Linford, H.B. J. Phys. Chem. 68:2273-2277 (1964).

[7] Kane, J.K.; LaMer, V.K.; Linford, H.B. J. Phys. Chem. 68:3539-3544 (1964).

[8] Kane, J.C.; LaMer, V.K.; Linford, H.B. J. Am. Chem. Soc. 86:3450-3453 (1964).

[9] Lindquist, G.M. The role of polyelectrolyte charge density and molecular weight on the adsorption and flocculation of colloidal silica with polyethylenimine. Doctor's Dissertation. Appleton, Wisconsin, The Institute of Paper Chemistry, 1975. 239 p.

[10] Lindquist, G.M.; Stratton, R.A. J. Colloid Interface Sci. 55:45-59 (1976).

[11] Sikora, M.D. The role of polyelectrolyte charge density in the mechanism of hydrodynamic shear-induced restabilization of a flocculated colloidal dispersion. Doctor's Dissertation. Appleton, Wisconsin, The Institute of Paper Chemistry, 1978. 170 p.

[12] Kasper, D.R. Theoretical and experimental investigations of the flocculation of charged particles in aqueous solutions by polyelectrolytes of opposite charge. Doctor's Dissertation. California Institute of Technology, 1971. 201 p.

[13] Gregory, J. J. Colloid Interface Sci. 42(2):448-56 (1973).

[14] van der Linden, C.C.; Leermakers, A.M. Macromolecules. 25:3449-53 (1992).

[15] de Gennes, P.G. Scaling Concepts in Polymer Physics. Cornell University Press, Ithaca, NY, 1979.

[16] de Gennes, P.G. Macromolecules. 114:1637-44 (1981).

[17] Scheutjens, J.M.H.M.; Fleer, G.J. J. Phys. Chem. 83:1619-1635 (1979).

[18] Scheutjens, J.M.H.M.; Fleer, G.J. J. Phys. Chem. 84:178-190(1980).

[19] Scheutjens, J.M.H.M.; Fleer, G.J. In Th.F. Thadros(Ed.) The Effect of Polymers on Dispersion Properties. Academic Press. London. 1982:145-168.

[20] Dickinson, E.; Lal, M. Adv. Molec. Relax. Process. 17:1- (1980).

[21] Vincent, B.; Whittington, S. In E. Matijevic (Ed.). Surface and Colloid Science. Vol. 12. Wiley, New York. 1981.

[22] Hoeve, C.A.J. J. Chem. Phys. 44:1505-1509(1966).

[23] Hoeve, C.A.J. J. Polym. Sci., Part C. 30:361-367 (1970).

[24] Hoeve, C.A.J. J. Polm. Sci., Part C. 34:1-10(1971).

[25] Silberberg, A. J. Chem. Phys. 48:2835-2851(1968).

[26] Roe, R.J. J. Chem. Phys. 60:4192-4207 (June 1974).

[27] Simha, R.; Frisch, H.L.; Eirich, F.R. J. Phys. Chem. 57:584-589(1953).

[28] Frisch, H.L.; Simha, R. J. Chem. Phys. 24:652-655 (1956)

[29] Frisch, H.L.; Simha, R. J. Chem. Phys. 27:702-706 (1957).

[30] Silberberg, A. J. Phys. Chem. 66:1872-1883,1884-1907 (1964).

[31] Silberberg, A. J. Chem. Phys. 46:1105-1114(1967).

[32] DiMarzio, E.A. J. Phys. Chem. 42:2101-2106(1965).

[33] DiMarzio, E.A.; McCracklin, F.L. J. Phys. Chem. 43:539-547(1965).

[34] Hoeve, C.A.J.; DiMarzio, E.A.; Peyser, P. J. Phys. Chem. 42:2558-2563(1965).

[35] Rubin, R.J. J. Chem. Phys. 43:2392-2407(1965).

[36] Roe, R.J. J. Chem. Phys. 43:1591-1598(1965).

[37] Roe, R.J.; J. Chem. Phys. 44:4264-4272(1966).

[38] Motomura, K.; Matuura, R. J. Chem. Phys. 50:1281-1287(1969).

[39] Motomura, K.; Sekita, K.; Matuura. Bull. Chem. Soc. Jpn. 44:1243-1248(1971).

[40] Motomura, K.; Moroi, Y.; Matuura, R. Bull. Chem. Soc. Jpn. 44:1248-1252(1971).

[41] Young, R.J. Introduction to Polymers. Chapman and Hall. 733 Third Avenue, New York, Ny 10017. 1981.

[42] Hesselink, F.Th. J. Coll. Inter. Sci. 60(3):448-66 (1977).

[43] VanDerSchee, H.A.; Lyklema, J. J. Phys. Chem. 88:6661-6667 (1984).

[44] Papenhuijzen, J.; VanDerSchee, H.A.; Fleer, G.J. J. Coll. Inter. Sci. 104:540-552 (1985).

[45] Papenhuijzen, J.; Fleer, G.J.; Bijsterboschs, B.H. J. Coll. Inter. Sci. 104:553-561 (1985).

[46] Evers, O.A.; Fleer, G.J.; Scheutjens, J.M.H.M.; Lyklema, J. J. Coll. Inter. Sci. 111:446-454 (1985).

[47] Böhmer, M.R.; Evers, O.A.; Schuetjens, J.M.H.M. Macromolecules. 23:2288-301 (1990).

[48] van de Steeg, H.G.M.; Cohen Stuart, M.A.; de Keizer, A.; Bijsterbosch, B.H. Langmuir. 8:2538-46 (1992).

[49] Tadros, Th.F. In Th.F. Thadros(Ed.) The Effect of Polymers on Dispersion Properties. Academic Press. 1982:1-38.

[50] Blaakmeer, J.; Cohen Stuart, M.A.; Fleer, G.J. Macromolecules 23(8):2301-2309 (1990).

[51] Blaakmeer, J.; Cohen Stuart, M.A.; Fleer, G.J. J. Colloid Interface Sci. 140(2):314-325 (1990).

[52] Mirabella, F. Jr. J. Poly. Sci.: Poly. Phys. Ed. 20:2309-2315 (1982).

[53] Colletti, R.; Gold, H.S.; Dybowski, C. Appl. Spec. 41:1185-1189 (1987).

[54] Barnett, K.G.; Cosgrove, T.; Vincent, B.; Burgess, A.N.; Crowley, T.L.; King, T.; Turner, J.D.; Tadros, Th.F. Polymer. 22:283-5 (March, 1981).

[55] Barnett, K.G.; Cosgrove, T.; Vincent, B.; Sissons, D.S.; Cohen-Stuart, M. Macromolecules. 14:1018-1020 (1981).

[56] Cosgrove, T.; Ryan, K. Langmuir. 6(1):136-42 (1990).

[57] Chandar, P.; Somasundaran, P.; Turro, N.J.; Waterman, K.C. Langmuir. 3:298-300 (1987).

[58] Cosgrove, T.; Obey, T.M.; Vincent, B. J. Coll. Inter. Sci. 111:409-418 (1986).

[59] Cate, M.C.; Robb, I.D. J. Coll. Inter. Sci. 86:411-421 (1982).

[60] Sakai, H.; Imamura, Y. Bull. Chem. Soc. Jpn. 53(6):1749-50 (1980).

[61] Sakai, H.; Fujimori, T.; Imamura, Y. Bull. Chem. Soc. Jpn. 53(12):3457-61 (1980).

[62] Kobayashi, K.; Araki, K.; Imamura, Y. Bull. Chem. Soc. Jpn. 62(11):3421-5 (1989).

[63] Cosgrove, T.; Heath, T.G.; Ryan, K.; Crowley, T.L. Macromolecules. 20(11):2879-82 (1987).

[64] Rochester, C.H. Adv. Colloid Interface Sci. 12:43-82 (1980).

[65] Schueing, D.R. In D.R. Schueing (Ed.). Fourier Transform Infrared Spectroscopy in Colloid and Interface Science. American Chemical Society, Washington, DC 1991. pp.1-21.

[66] Fontana, B.J.; Thomas, J.R. J. Phys. Chem. 65:480-487 (1961).

[67] Korn, M.; Killman, E.; Eisenlauer, J. J. Colloid Interface Sci. 76(1):7-18 (1980).

[68] Korn, M.; Killman, E. J. Colloid Interface Sci. 76(1):19-31 (1980).

[69] Kawaguchi, M.; Hayakawa, K.; Takahashi, A. Polymer J. 12(4):265-270 (1980).

[70] Kawaguchi, M.; Sano, T.; Takahashi, A. Polymer J. 13(?):1019- (1981).

[71] Kawaguchi, M.; Aoki, M.; Takahashi, A. Macromolecules. 16:635-640 (1983).

[72] Kawaguchi, M.; Maeda, K.; Kato, T.; Takahashi, A. Macromolecules. 17:1666-1671 (1984).

[73] Sakai, H.; Imamura, Y. Bull. Chem. Soc. Jpn. 53:1749-50 (1980).

[74] Sakai, H.; Fujimori, T.; Imamura, Y. Bull. Chem. Soc. Jpn. 53:3457-61 (1980).

[75] Kobayashi, K.; Araki, K.; Imamura, Y. Bull. Chem. Soc. Jpn. 62:3421-5 (1989).

[76] Rein, A.J.; Wilks, P.A. Am. Lab. 14(10):152,154-5 (1982).

[77] Harrick, N.J. Internal Reflection Spectroscopy. Harrick Scientific Corporation, Ossining, New York. 1987.

[78] Julian, B.; Carter, J. FTIR-CIR Spectral Lines. Nicolet Instrument Corporation. Madison, WI. 6(1):15-7 (Feb. 1985).

[79] Braue, E.H., Jr.; Pannella, M.G. Appl. Spec. 41(7):1213-6 (1987).

[80] Braue, E.H., Jr.; Pannella, M.G. Appl. Spec. 41(6):1057-67 (1987).

[81] Sperline, R.P.; Muralidharan, S.; Freiser, H. Appl. Spec. 40(7):1019-22 (1986).

[82] Iwamoto, R.; Ohta, K. Appl. Spec. 38(3):359-65 (1984).

[83] Mirabella, F., Jr. Appl. Spec. 42(7):1258-65 (1988).

[84] van der Beek, G.P.; Cohen Stuart, M.A.; Fleer, G.J. Macromolecules. 24:3553-61 (1991).

[85] Sperline, R.P.; Muralidharan, S.; Freiser, H. Langmuir 3:198-202 (1987).

[86] Scheuing, D.R. Appl. Spec. 41:1343-1346 (1987).

[87] Scheuing, D.R.; Hsieh, J.C.L. Langmuir. 4:1277-1283 (1988).

[88] Parry, D.B.; Harris, J.M. Appl. Spec. 42(6):997-1004 (1988).

[89] Kuys, K.J.; Roberts, N.K. Coll. and Surf. 24:1-17 (1987).

[90] Tejedor-Tejedor, M.I.; Anderson, M.A. Langmuir. 2(2):203-210 (1986).

[91] Zeltner, W.A.; Yost, E.C.; Machesky, M.L.; Tejedor-Tejedor, M.I.; Anderson, M.A. ACS Symp. Ser. 323 (Geochem. Processes Miner. Surf.) :142-161 (1986).

[92] Urban, M.W.; Koenig, J.L.; Shih, L.B.; Allaway, J.R. Appl. Spec. 41(4):590-596 (1987).

[93] Braue, E.H.; Pannella, M.G. Appl. Spec. 44(9):1513-20 (1990).

[94] Kung, K.S.; Hayes, K.F. Langmuir 9(1):263-7 (1993).

[95] Wigsten, A.L. Polymer Adsorption and Flocculation of Particles in Turbulent Flow. Doctor's Dissertation. Appleton, Wisconsin, The Institute of Paper Chemistry. 1983. 127 p.

[96] Arquette, R.E. An Investigation of the Relations Between Polymer Adsorption and the Electrphoretic Mobility of Polystyrene Latex. A291 Project. Appleton, Wisconsin, The Institute of Paper Chemistry. 1982. 30 p.

[97] Miller, C.E. An Investigation of the Effects of Polymer Partitioning on Fines Retention. Doctor's Dissertation. Appleton, Wisconsin, The Institute of Paper Chemistry. 1989. 169 p.

[98] G.V.F. Seaman. President, Interfacial Dynamics Corporation, P.O. Box 279, Portland, OR, 97207. Personal Communication. August, 1989.

[99] Harada, S.; Hasegawa, S. Makromol. Chem., Rapid Commun. 5:27-31 (1984).

[100] Kobayashi, S.; Tokunoh, M.; Saegusa, T.; Mashio, F. Macromolecules. 18:2357-2361 (1985).

[101] Gooding, D.L.; Schmuck, N.; Gooding, K.M. J. Liq. Chrom. 5(12):2259-2270 (1982)

[102] Nagy, D.L.; Terwilliger, D.A. J. Liq. Chrom. 12(8):1431-1449 (1989).

[103] Young, R. J. Introduction to Polymers. Chapman and Hall. 733 Third Avenue, New York, NY 10017. 1983. p137.

[104] Katchalsky, A.; Shavit, N.; Eisenberg, H. J. Polymer Sci. 13:69- (1954).

[105] Bloys van Treslong, C.J.; Staverman, A.J. Rec. Trav. Chim. 93(6):171-8 (1974).

[106] Shepherd, E.J.; Kitchener, J.A. J. Chem. Soc. 2448-52 (1956).

[107] Katchalsky, A.; Mazur, J.; Spitnik, P. J. Polym. Sci. 23: 513-532 (1957).

[108] Nagasawa, M.; Holtzer, A. J. Amer. Chem. Soc. 86:538-43 (1964).

[109] Nagasawa, M.; Murase, T.; Kondo, K. J. Phys. Chem. 69:4005-12 (1964).

[110] Kenchington, A.W. Analytical information from titration curves. In A laboratory manual of analytical methods of protein chemistry. Vol. 2, Chapter 10. Pergamon Press. New York. 1960. pp 353-88.

[111] Tanford, C. J. Amer. Chem. Soc. 72:441-451(1950).

[112] Tanford, C. Hydrogen ion titration curves of proteins. In Electrochemistry in Biology and Medicine. Wiley. pp 248.

[113] Tanford, C.; Swanson, S.A.; Shore, W.S. J. Amer. Chem. Soc. 77:6416- (1955).

[114] Tanford, C. J. Amer. Chem. Soc. 79:3931- (1957).

[115] Tanford, C. J. Amer. Chem. Soc. 79:5333- (1957).

[116] Kobayashi, S.; Tokunoh, M.; Saegusa, T.; Mashio, F. Macromolecules. 18(12):2357-61 (1985).

[117] Yoshikawa, Y.; Matsuoka, H.; Ise, N. Brit. Polymer J. 18(4):242-6 (1986).

[118] Ochiai, H.; Anabuki, Y.; Kojima, O.; Tominaga, K.; Murakami, I. J. Polymer Sci.: Part B: Polymer Phys. 28:233-40 (1990).

[119] Beirmann, C.J. TAPPI J. 75(5):166-71 (1992).

[120] Terayama, H. J. Polymer Sci. 8(2):243-53 (1952)

[121] Kawamura, S.; Tanaka, Y. Water and Sewage works. 113:348-57 (Sept.,1966).

[122] Kawamura, S. Water and Sewage Works. 114:324-7 (Sept., 1967).

[123] Halabisky, D.D. Unpublished work. TAPPI Retention and Drainage Short Course. Minneapolis, MN. (Oct., 1976).

[124] Halabisky, D.D. TAPPI J. 60(12):125-27 (Dec., 1977).

[125] Onabe, F. International Symposium on Wood and Pulping Chemistry. Vol. 3:138-43 (May 23-27, 1983).

[126] St. John, M.R.; Gallagher, T.M. TAPPI Proceedings, 1992 Papermakers Conf. p. 479-95.

[127] Dr. Charles Potter. Hercules Inc. Personal communication. February, 1989.

[128] Onabe, F. Mokuzai Gakkaishi. 28(7):437-44 (1982).

[129] Tanaka, H. Japan TAPPI. 37(10):74-84 (1983).

[130] Baulsir, C. Spectra-Tech Inc. 652 Glenbrook Rd. Bldg. 8 Stamford, CT, 06906. Personal Communication. May, 1992.

[131] Koenig, J.L.; Kormos, D. Appl. Spec. 33(4):349-50 (1979).

[132] Antoon, M.K.; D'Esposito, L.; Koenig, J.L. Appl. Spec. 33(4):351-7 (1979).

[133] Haaland, D.M.; Easterling, R.G. Appl. Spec. 34(5):539-48 (1980).

[134] Gillette, P.C.; Koenig, J.L. Appl. Spec. 38(3):334-7 (1984).

[135] Liu, J.; Koenig, J.L. Appl. Spec. 41(3):447-9 (1987).

[136] Lacey, R.F. Appl. Spec. 43(7):1135-9 (1989).

[137] Powell, J.R.; Wasacz, F.M.; Jakobsen, R.J. Appl. Spec. 40(3):339-44 (1986).

[138] Dousseau, F.; Therrien, M.; Pézolet, M. Appl. Spec. 43(3):538-42 (1989).

[139] Banerjee, S.; Li, D. Appl. Spec. 45(6):1047-9 (1991).

[140] Friese, M.A.; Banerjee, S. Appl. Spec. 46(2):246-8 (1992).

[141] Hecht, D.; Tadesse, L.; Walters, L. J. Am. Chem. Soc. 114(11):339-44 (1992).

[142] Herzberg, G. Molecular Spectra and Molecular Structure. Volume II. Infrared and Raman Spectra of Polyatomic Molecules. D. Van Nostrand Company, Inc. New York, NY. 1945. p. 280-2.

[143] Pimentel, G.C.; McClellan, A.L. The Hydrogen Bond. W.H. Freeman and Company. San Francisco, CA. 1960. p. 196-7.

[144] Israelachvili, J.N.; Tandon, R.K.; White, L.R. J Colloid Interface Sci. 78(2):430-43 (1980).

[145] Joppien, G.R. J. Phys. Chem. 82(20):2210-4 (1978).

[146] Pefferkorn, E.; Jean-Chronberg, A.C.; Varoqui, R. Macromolecules 23(6):1735-41 (1990).

[147] Leermakers. F. Wageningen Agricultural University, Wageningen, The Netherlands. Personal communication. April, 1993.

[148] Colthup, N.B.; Daly, L.H.; Wiberley, S.E. Introduction to Infrared and Raman Spectroscopy. Academic Press Inc. New York, NY. 1964. p. 373.

[149] Bellamy, L.J. The Infra-red Spectra of Complex Molecules. Third Edition. Chapman and Hall. London. 1975.

[150] Thompson, H.W.; Nicholson, D.L.; Short, L.N. Disc. Faraday Soc. 9:222-35 (1950).

[151] Savitsky, A.; Golay, J.E. Anal. Chem. 36(8):1627-39 (1964).

[152] Nevius, T.A.; Pardue, H.L. Anal. Chem. 56(12):2249-51 (1984).

[153] Stewart, J.E. J. Chem. Phys. 30(5):1259-65 (1959).

[154] Buckley, A.M.; Bramwell, S.T.; Visser, D.; Day, P. J. Solid State Chem. 69:240-51 (1987).

[155] Arai, T.; Norde, W. Colloids Surf. 51:1-15 (1990).

[156] Törnkvist, C.; Liedberg, B.; Lundström, I. Langmuir. 7(3):470-85 (1991).

LIST OF SYMBOLS AND ABBREVIATIONS

ATR	attenuated total reflectance, a sampling technique used in FT-IR spectroscopy
BASELN2	a LABCALC® subprogram used to correct baseline drift in FT-IR spectra
BTC	benzethonium chloride, primary standard used in colloid titrations
C_c	the calculated concentration of PAAm standards for calibration of the colloid titration technique
Ce	the concentration of polymer in the bulk at adsorption equilibrium
c_s	the concentration of salt (NaCl) used for adsorptions
C_t	the titrated concentration of PAAm standards for calibration of the colloid titration technique
CURVEFIT	a LABCALC® subprogram used to obtain the areas of overlapping peaks in FT-IR spectra
d	the thickness of a lattice layer in the SCF adsorption model, nm
DEWIGGLE	a LABCALC® subprogram used to objectively subtract FT-IR spectra
d_p	the depth of penetration of the evanescent wave in internal reflection spectroscopy
FT-IR	fourier transform infrared spectroscopy
FT-IR-ATR	fourier transform infrared attenuated total reflection spectroscopy
i	a specific layer in the adsorption lattice
INTEGRAT	a LABCALC® subprogram used to obtain the area of peaks in FT-IR spectra via integration using the trapezoid method
IPST	the Institute of Paper Science and Technology
IRE	internal reflection elements, crystals used in FT-IR-ATR spectroscopy
LABCALC®	a software product of Galactic Industries Corporation for analyzing FT-IR spectra
M_n	number average molecular weight
M_w	weight average molecular weight
MW	molecular weight
N	the number of internal reflections for a ATR sample cell
Nanopure®	a water purification system by Barnstead/Thermolyne Corporation
n_{sp}/c	the reduced specific viscosity, equal to $\frac{(t-t_0)}{t_0 c}$

OFFSET2	a LABCALC® subprogram used to zero the baseline of FT-IR spectra
p	the fraction of polymer segments in i = 1 (trains) in the SCF adsorption model
PAAm	polyallylamine
pK	the apparent dissociation constant of PAAm, $pK = pH - \log\left(\frac{1-\alpha}{\alpha}\right)$
$pK_{½}$	the apparent dissociation constant of PAAm at $\alpha = 0.5$
PSL	polystyrene latex particles
PVP	poly(2-vinyl pyridine)
r	the number of monomer segments per polymer molecule in the SCF adsorption model
SCF	the self-consistent-field theory pioneered by Scheutjens and Fleer
SEC	size exclusion chromatography
t	measured time for the sample in capillary viscosity tests
TB	o-toluidine blue , the indicator used in colloid titrations
TFA	trifluoroacetic acid
t_r	the retention time of samples in size exclusion chromatography
t_0	measured time for the solvent in capillary viscosity tests

Greek Characters:

α	the degree of ionization of a polyelectrolyte
Γ	the total surface coverage for adsorbed polymer layers
Γ^{exc}	the excess surface coverage for adsorbed polymer layers
Γ_m	the maximum amount of adsorbed polymer in the plateau region of the adsorption isotherm
θ	the internal reflection incidence angle in ATR sample cells
$\varepsilon/\varepsilon_0$	the relative dielectric constant of the components in the SCF adsorption model
$[\eta]$	the intrinsic viscosity
η_1	the refractive index of the denser medium when calculating d_p
η_2	the refractive index of the rarer medium when calculating d_p
η_{21}	the refractive index ratio, η_2/η_1
λ	the infrared wavelength when calculating d_p, μm

λ_1	λ in the denser medium, λ/η_1
σ_s	the surface charge of the adsorbate
ϕ_1	the volume fraction of polymer segments in the first layer in the SCF adsorption model
ϕ_b	the initial volume fraction of polymer segments in the bulk in the SCF adsorption model
ϕ_i	the volume fraction of polymer segments in layer i in the SCF adsorption model
ϕ_i^f	the volume fraction of free polymer segments in layer i in the SCF adsorption model
ϕ_*	is the volume fraction of polymer segments in the bulk solution at equilibrium
χ	the Flory-Huggins interaction parameter which represents the segment-solvent interaction energy in the SCF adsorption model
χ_s	the Silberberg interaction parameter which represents the non-electrostatic segment-surface interaction energy in the SCF adsorption model

LIST OF FIGURES

LIST OF TABLES

APPENDIX I - SEC FRACTIONATION PROCEDURE

The following is a step by step description of the procedure used during the fractionation of the polydisperse Aldrich PAAm by size exclusion chromatography.

1. Eluent, which was 0.1 % (w/w) TFA and 0.2 M $NaNO_3$, was prepared in batches of approximately 6 liters. The solutions were mixed thoroughly and filtered through a Millipore® suction flask with a TYPE HV 0.45 μm filter. The error in solute concentrations from batch to batch was estimated to be less than 0.25% in each case (± 0.00025 % (w/w) and ± 0.0005 M $NaNO_3$, respectively). A 2 liter flask, used to supply eluent to the HPLC pump, was refilled periodically with the 6 liter stock supply.

2. Injections onto the analytical column (250 x 4.6 mm) were done using a 10 μl injection loop. Injections onto the semi-preparative column were done using a 250 μl injection loop. Tables I-1 and I-2 below list the HPLC settings for the analytical and the semi-preparative injections, respectively.

Table I-1. HPLC parameter settings for injections on the analytical column.

Time	Parameter	Value	Comments
-	PMAX	200	maximum column pressure
-	PMIN	2	minimum column pressure
-	TEMP	35°C	column heater set temp.
0	FLOW	0.4	pump flow rate (ml/min.)
0	%	100	% flow, reservoir A/B
0	RSVR	A	reservoir A eluent only
0	EVNT	0	no events set

Table I-2. HPLC parameter settings for injections on the semi-preparative column.

Time	Parameter	Value	Comments
-	PMAX	200	maximum column pressure
-	PMIN	2	minimum column pressure
-	TEMP	25°C	column heater off
0	FLOW	10	pump flow rate (ml/min.)
0	%	100	% flow, reservoir A/B
0	RSVR	A	reservoir A eluent only
0	EVNT	0	no events set
6	EVNT	8	turn on fraction collector
9.9	EVNT	0	turn off fraction collector

3. Prior to use the detector was allowed to stabilize and then was balanced according to the directions in the manual. Detector range settings (RIU/FS) varied depending on the concentration of the sample. The polarity was set to positive (+) and the LCD readout was set on recorder.

4. When injections were made on the analytical column, output from the detector flow cell was sent to a waste bottle. When injections were made on the semi-preparative column, the flow cell output was directed to the Gilson FC-100K Fractionator. The time delay switch was set to 0.2 minutes and the power switch on the front panel was left on. Two racks of twenty 20 ml test tubes were in the first two positions on the fractionator. The first test tube slots in each rack were fitted with tubes which would provide continuous drainage to a 50 gal. waste barrel. Everything that eluted before 6.0 minutes and after 9.8 minutes ran through these tubes. After thirteen injections, the fractioned polymer

from twelve of the tubes were collected in 1 liter sample jars. Prior to use the test tubes and sample jars were treated with 1 % (v/v) dichlorodimethylsilane in toluene, allowed to dry, and then rinsed exhaustively with Nanopure® water. This was done to minimize polymer adsorption on the glass surfaces.

5. In both analytical and semi-preparative cases above, a volume slightly larger than the injection loop was drawn into a Valco compatible syringe, and any bubbles were removed. The syringe was then inserted into the syringe port, with the valve to the column in the closed position, and the sample was injected into the sample loop.

6. When ready, the operator began a mental count to three, i.e., " one thousand one, one thousand two, one thousand three ". On the number "one" the operator activated the data save on the computer with the F10 key. On the number "three" the operator simultaneously hit the HPLC start key and opened the sample loop valve. The start key activates the programmed run and starts the clock. The start key also makes a contact closure via a wire between the program start output port on the HPLC and the marker input port on the detector. This contact closure causes the detector to insert a 6 millisecond marker or signal into the data file, signifying the start of the program.

7. After 16.5 minutes the data collection was stopped by hitting F9. The program was reset by typing "Q", followed by "CODAS C:FILENAME.DAT 100K". The HPLC and the fractionator arm were also reset.

8. All chromatograms were scaled to a detector range setting of 4.

APPENDIX II - INTRINSIC VISCOSITY DATA : PAAm FRACTIONS

This appendix contains the data and regression analysis results for the intrinsic viscosity measurements discussed in the PAAm characterization section above. A number of PAAm fractions were selected for analysis so that their respective intrinsic viscosities would span the entire range of expected values for all the fractions.

The intrinsic viscosity, $[\eta]$, is defined as the y-intercept of the line obtained when the reduced specific viscosity (η_{sp}/c) is plotted against sample concentration. For dilute solutions, $\eta_{sp}/c = \frac{t - t_0}{t_0\, c}$, where t and t_0 represent the time it takes for the sample and solvent to pass between the capillary viscometer markings, respectively, and c is the fraction concentration. In each case five t measurements at each of the five concentrations were averaged. The relative viscosity, η_r, is equal to $\frac{t}{t_0}$ and the specific viscosity, η_{sp}, is equal to η_r - 1 for dilute solutions.

The first table shown below gives the data for the measurement of t_0 for the solvent, an aqueous 0.1% TFA solution with 0.2 M $NaNO_3$. The remaining tables show the data collected for intrinsic viscosity determinations for PAAm fractions H4, H5, H7, L6, L9, and H14.

Table II-1. Measurement of t_0 for the PAAm fraction solvent.

time (seconds)	average t
99.04	
99.03	
99.13	
99.13	
99.01	99.07

Table II-2. Data for the intrinsic viscosity determination of PAAm fraction H4.

Fraction H4	concentration (% w/w)	time (seconds)	average time	η_r	η_{sp}	η_{sp}/c
Sample 1	0.234	122.350				
		122.450				
		122.350				
		122.450				
		122.260	122.370	1.235	0.235	1.004
Sample 2	0.188	117.580				
		117.490				
		117.590				
		117.630				
		117.610	117.580	1.187	0.187	0.997
Sample 3	0.156	114.470				
		114.450				
		114.410				
		114.460				
		114.510	114.460	1.155	0.155	0.995
Sample 4	0.134	112.480				
		111.850				
		112.160				
		112.190				
		112.160	112.170	1.132	0.132	0.988
Sample 5	0.117	111.340				
		110.560				
		110.800				
		110.440				
		110.510				
		110.490	110.690	1.117	0.117	1.001
Sample 6	0.104	109.250				
		109.270				
		109.590				
		109.150				
		109.590				
		109.270	109.350	1.104	0.104	0.997

Linear Regression Analysis, H4: $\eta_{sp}/c = 0.9891 + 0.04903c \quad R^2 = 0.177$

(intrinsic viscosity, $[\eta]$ = y-intercept)

Table II-3. Data for the intrinsic viscosity determination of PAAm fraction H5.

Fraction H5	concentration (% w/w)	time (seconds)	average time	η_r	η_{sp}	η_{sp}/c
Sample 1	0.423	136.460				
		136.750				
		136.590				
		136.520				
		136.550	136.570	1.379	0.379	0.895
Sample 2	0.339	129.070				
		128.590				
		129.190				
		128.810				
		128.720	128.880	1.301	0.301	0.889
Sample 3	0.282	123.510				
		123.550				
		123.550				
		123.740				
		123.480	123.570	1.247	0.247	0.877
Sample 4	0.242	119.950				
		119.940				
		119.990				
		119.870				
		120.150	119.980	1.211	0.211	0.873
Sample 5	0.212	117.190				
		117.170				
		117.020				
		117.340				
		117.180	117.180	1.183	0.183	0.864
Sample 6	0.188	115.260				
		114.950				
		115.090				
		114.930				
		115.130	115.070	1.162	0.162	0.859

Linear Regression Analysis, H5: $\eta_{sp}/c = 0.8328 + 0.1537c$ $R^2 = 0.954$

(intrinsic viscosity, $[\eta]$ = y-intercept)

Table II-4. Data for the intrinsic viscosity determination of PAAm fraction H7.

Fraction H7	concentration (% w/w)	time (seconds)	average time	η_r	η_{sp}	η_{sp}/c
Sample 1	0.448	128.680				
		129.080				
		128.790				
		128.930				
		128.910	128.880	1.301	0.301	0.672
Sample 2	0.358	122.540				
		122.700				
		123.030				
		122.700				
		122.620	122.720	1.239	0.239	0.666
Sample 3	0.299	118.340				
		118.440				
		118.470				
		118.740				
		118.340	118.470	1.196	0.196	0.656
Sample 4	0.256	115.470				
		115.530				
		115.300				
		116.040				
		115.600	115.590	1.167	0.167	0.652
Sample 5	0.224	113.310				
		113.390				
		113.340				
		113.170				
		113.250	113.290	1.144	0.144	0.641
Sample 6	0.199	111.590				
		111.610				
		111.450				
		111.570				
		111.630	111.570	1.126	0.126	0.634

Linear Regression Analysis, H7: $\eta_{sp}/c = 0.6090 + 0.1495c$ $R^2 = 0.925$

(intrinsic viscosity, $[\eta]$ = y-intercept)

Table II-5. Data for the intrinsic viscosity determination of PAAm fraction L6.

Fraction L6	concentration (% w/w)	time (seconds)	average time	η_r	η_{sp}	η_{sp}/c
Sample 1	0.133	107.200				
		107.170				
		107.140				
		107.130				
		107.200	107.170	1.082	0.082	0.617
Sample 2	0.106	105.490				
		105.570				
		105.660				
		105.390				
		105.480	105.520	1.065	0.065	0.614
Sample 3	0.088	104.270				
		104.440				
		104.310				
		104.160				
		104.210	104.280	1.053	0.053	0.595
Sample 4	0.076	103.650				
		103.550				
		103.480				
		103.590				
		103.420	103.540	1.045	0.045	0.596
Sample 5	0.066	102.990				
		103.020				
		102.960				
		102.810				
		102.870	102.930	1.039	0.039	0.588
Sample 6	0.059	102.470				
		102.490				
		102.500				
		102.520				
		102.370	102.470	1.034	0.034	0.583

Linear Regression Analysis, L6: $\eta_{sp}/c = 0.5565 + 0.4777c$ $R^2 = 0.915$

(intrinsic viscosity, $[\eta]$ = y-intercept)

Table II-6. Data for the intrinsic viscosity determination of PAAm fraction L9.

Fraction L9	concentration (% w/w)	time (seconds)	average time	η_r	η_{sp}	η_{sp}/c
Sample 1	0.816	123.780				
		123.730				
		123.700				
		123.740				
		123.560	123.700	1.249	0.249	0.305
Sample 2	0.653	118.990				
		118.590				
		119.160				
		118.770				
		118.700	118.840	1.200	0.200	0.306
Sample 3	0.544	115.590				
		115.280				
		115.370				
		115.290				
		115.340	115.370	1.165	0.165	0.303
Sample 4	0.466	113.100				
		113.070				
		112.990				
		113.150				
		113.090	113.080	1.141	0.141	0.303
Sample 5	0.408	111.130				
		111.060				
		111.060				
		111.270				
		111.200	111.140	1.122	0.122	0.299
Sample 6	0.363	109.660				
		109.830				
		109.920				
		110.580				
		109.790	109.960	1.110	0.110	0.303

Linear Regression Analysis, L9: $\eta_{sp}/c = 0.2980 + 0.009160c \quad R^2 = 0.417$

(intrinsic viscosity, $[\eta]$ = y-intercept)

Table II-7. Data for the intrinsic viscosity determination of PAAm fraction H14.

Fraction H14	concentration (% w/w)	time (seconds)	average time	η_r	η_{sp}	η_{sp}/c
Sample 1	0.438	113.030				
		113.860				
		114.450				
		113.030				
		113.190				
		113.220				
		113.060	113.410	1.145	0.145	0.330
Sample 2	0.351	110.330				
		110.320				
		110.240				
		110.450				
		110.980	110.460	1.115	0.115	0.328
Sample 3	0.292	108.500				
		108.560				
		108.620				
		108.520				
		108.560	108.550	1.096	0.096	0.328
Sample 4	0.250	107.390				
		107.020				
		107.340				
		107.110				
		107.340				
		107.100	107.220	1.082	0.082	0.329
Sample 5	0.219	106.060				
		106.080				
		106.080				
		106.260				
		106.610	106.220	1.072	0.072	0.330
Sample 6	0.195	105.550				
		105.400				
		105.640				
		105.270				
		105.250				
		105.270	105.400	1.064	0.064	0.328

Linear Regression Analysis, H14: $\eta_{sp}/c = 0.3272 + 0.00536c$ $R^2 = 0.247$

(intrinsic viscosity, $[\eta]$ = y-intercept)

APPENDIX III - CALCULATION PROCEDURE FOR $M_{(n)}$ AND $M_{(w)}$

The determination of molecular weight by size exclusion chromatography was discussed in the methods section above. To obtain an estimate for the weight average ($M_{(w)}$) and number average ($M_{(n)}$) molecular weights, as well as the polydispersity ($M_{(w)}/M_{(n)}$) for each sample, the chromatograms for each fraction were analyzed further. A description of the procedure used is given below.

Prior to analysis, the baseline of each chromatogram was corrected to account for detector drift. A multiple point correction technique was used. In each chromatogram, a number of points (5 - 12) were selected along the x axis which were thought to represent the true baseline of the chromatogram. These points were entered into a modified LABCALC® program called BASELN2 which creates a new curve by drawing a straight line between neighboring points. The new curve is then subtracted from the old to give a flat baseline. The baseline is then set to zero using the OFFSET program in LABCALC®. Where possible the same points were used in each chromatogram. Figure III-1 below shows an example of a baseline correction.

In every case, the fraction chromatograms contained two peaks. The first and largest peak represents the elution of the PAAm sample. The second, small peak represents very small differences in the concentration of the TFA and $NaNO_3$ in the eluent and the sample solvent. In some cases there is significant overlap of the two peaks. Since this overlap would interfere with the technique for estimating $M_{(w)}$ and $M_{(n)}$, it was necessary to isolate the PAAm peak.

CURVEFIT, a LABCALC® program, was used to fit Log-Normal curves to the PAAm peaks in each chromatogram. Figure III-2 below shows an example of a fitted curve. The fitted curves for each fraction were used to calculate $M_{(w)}$ and $M_{(n)}$.

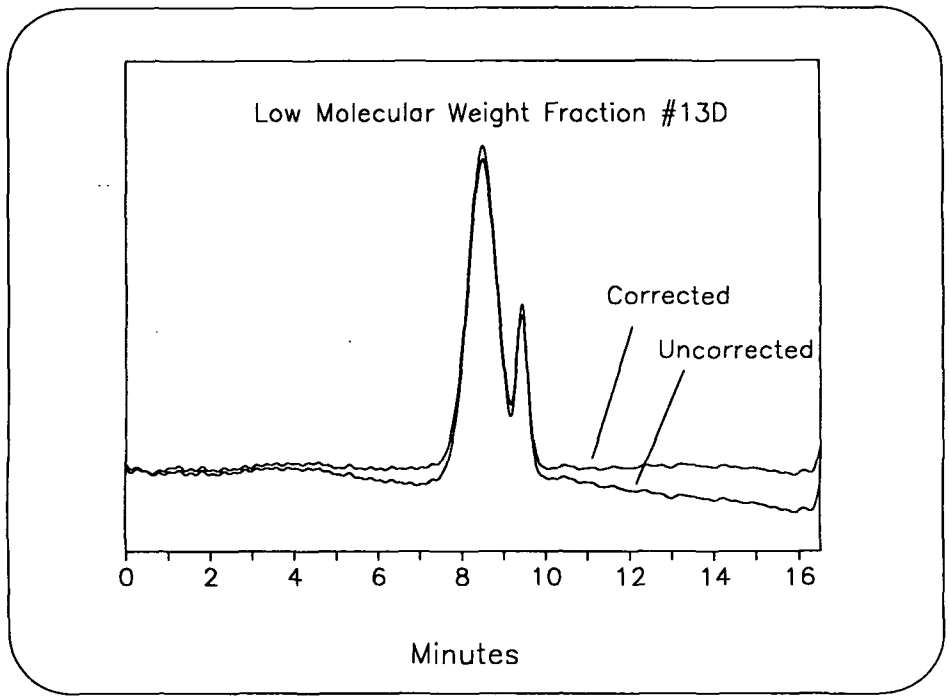

Figure III-1. An example of a multiple point baseline correction.

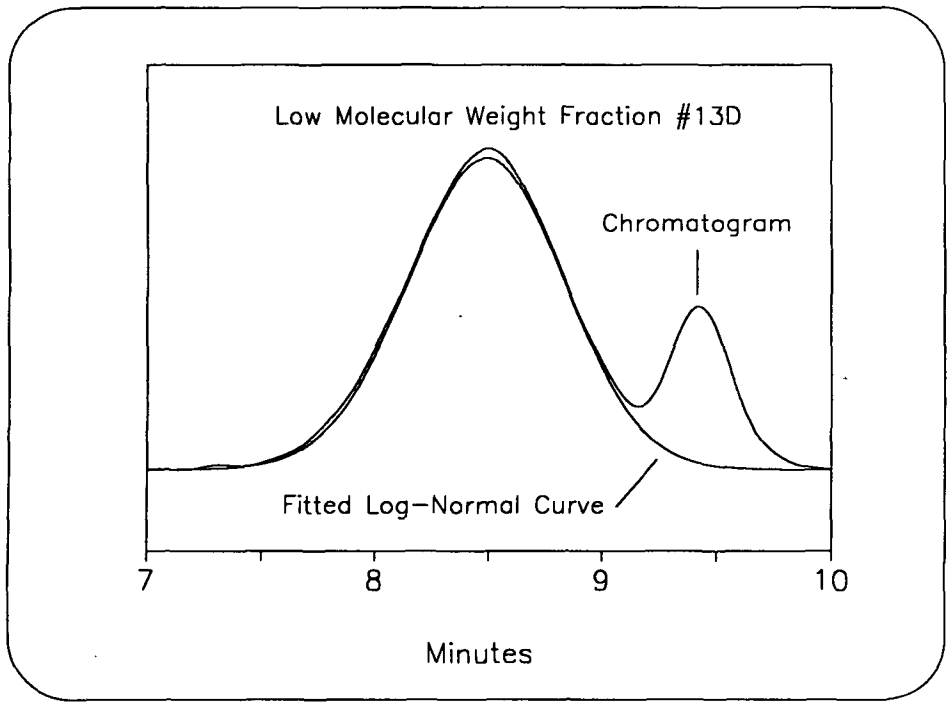

Figure III-2. An example a Log-Normal curve fitted to a PAAm peak.

In each case, the curve was divided into a set number of bins. The area under the curve for each bin is determined by way of a modified LABCALC® program called INTGAUTO. The program reads the filename of the curve, the number of bins to use, and values for the left and right end points from a text file. Using a trapezoid approximation technique it determines the area between each point in the first bin, the first and second, the first, second and third, etc. At each step, the data are written to a text file. The area of each bin is then calculated by difference.

The median retention time for each bin was used to calculate its molecular weight by means of Equation III-1 below (Equation 4 in the methods section).

$$MW = e^{(23.6-1.66t_r)} \qquad \{III\text{-}1\}$$

Estimates of $M_{(w)}$ and $M_{(n)}$ were made for each fraction using Equations III-2 and III-3 shown below:

$$M_{(n)} = \frac{\sum_{i=1}^{n} A_i}{\sum_{i=1}^{n} \frac{A_i}{MW_i}} \qquad \{III\text{-}2\}$$

$$M_{(w)} = \frac{\sum_{i=1}^{n} A_i MW_i}{\sum_{i=1}^{n} A_i} \qquad \{III\text{-}3\}$$

where MW_i is the calculated molecular weight of bin i (Equation III-1), n is the total number of bins, and A_i is the total area in bin i (which is proportional to the mass of polymer in the i^{th} bin).

A study of the effect of the number of bins used, showed that a consistent value for $M_{(w)}$ and $M_{(n)}$ was obtained when 20 or more bins were used. All calculations were performed using 50 bins.

APPENDIX IV - $M_{(n)}$ AND $M_{(w)}$ DATA FOR PAAm FRACTIONS

The molecular weight characterization data for all PAAm fractions are summarized in Table IV-1. The procedure used to determine these values is described in detail in Appendix III.

Table IV-1. Molecular weight characterization data for all of the PAAm fractions.

Fraction	t_r	MW[a]	$M_{(w)}$	$M_{(n)}$	$M_{(w)}/M_{(n)}$
H4	7.09	152,000	154,000	109,000	1.40
H5	7.28	106,000	124,000	82,800	1.49
H6	7.48	77,200	100,000	64,600	1.55
H7	7.60	60,600	82,400	50,400	1.64
H8	7.74	50,400	65,300	38,900	1.68
H9	7.90	38,300	58,600	30,300	1.93
H10	8.02	31,500	51,400	24,400	2.10
H11	8.08	28,700	44,200	22,000	2.01
H12	8.07	29,000	43,200	22,500	2.05
H13	8.10	27,800	41,500	20,300	2.05
H14	8.14	24,900	54,000	22,400	2.41
H15	8.17	24,600	48,800	20,200	2.42
L5	7.49	75,400	72,300	58,000	1.25
L6	7.66	55,800	56,500	42,600	1.33
L7	7.82	44,300	43,600	34,400	1.27
L8	7.97	34,100	33,600	25,800	1.30
L9	8.13	28,400	25,300	19,300	1.31
L10	8.27	20,700	20,300	14,900	1.36
L11	8.37	17,600	18,200	12,600	1.45
L12	8.43	16,100	16,100	10,900	1.48
L13	8.50	14,200	14,200	9,620	1.48
L14	8.58	12,400	15,800	8,940	1.77
L15	8.51	14,000	15,900	9,150	1.74
L16	8.40	16,800	15,600	8,990	1.74

a - calculated using equation 4 in the methods section.

APPENDIX V - DERIVATION OF THE DEGREE OF IONIZATON EQUATION

An equation for the degree of ionization, α, of charged polymers has been given by Bloys van Treslong, et al.[105] and Sikora.[11]

The equation for any pH appears as follows:

$$\alpha = \frac{(C_H)_{added} - (C_H)_{free} + (C_{OH})_{free}}{C_M} \qquad \{1\}$$

where $(C_H)_{added}$ is the proton concentration after addition of HCl; $(C_H)_{free}$ and $(C_{OH})_{free}$ are the concentrations of free proton and hydroxyl ions, and C_M is the polymer concentration in monomeric units.

Attempts to find a derivation of this equation in the literature have so far been unsuccessful. The following is a derivation of equation {1} using PAAm as an example. The derivation begins with the statement of the electo-neutrality equation in general terms below:

$$\sum z_a[A^+] - \sum z_b[B^-] = 0 \qquad \{2\}$$

where $[A^+]$ and $[B^-]$ represent the concentration of each positive and negative ion present, and z_a and z_b represent their respective charges.

The following equilibria apply when one considers the specific case of the titration of aqueous PAAm with HCl, both being 0.1 N in NaCl.

Solution:

$$[H_2O] \Leftrightarrow [H^+]_{free} + [OH^-]_{free}$$

$$[AmHCl] \Rightarrow [AmH^+] + [Cl^-]_{amine} \Leftrightarrow [H^+]_{free} + [Am] + [Cl^-]_{amine}$$

$$[NaCl] \Rightarrow [Na^+]_{b1} + [Cl^-]_{b1}$$

Titrant:

$$[H_2O] \Leftrightarrow [H^+]_{free} + [OH^-]_{free}$$

$$[HCl] \Rightarrow [H^+]_{added} + [Cl^-]_{added}$$

$$[NaCl] \Rightarrow [Na^+]_{b2} + [Cl^-]_{b2}$$

where b1 and b2 represent the background salt added. Using equation {2} and the equilibria above the electro-neutrality condition prior to titrant addition would be as follows.

$$[H^+]^0_{free} + [AmH^+]^0 + [Na^+]^0 - [OH^-]^0_{free} - [Cl^-]^0_{amine} - [Cl^-]^0_{b1} = 0 \qquad \{3\}$$

At equilibrium, following addition of an aliquot of the titrant, the electro-neutrality condition could be described as follows:

$$[H^+]^1_{free} + [AmH^+]^1 + [Na^+]^1_{total} - [OH^-]^1_{free} - [Cl^-]^1_{total} = 0 \qquad \{4\}$$

If y represents the volume of titrant added and x represents the original volume of the sample, the following equation holds:

$$(x+y)\left[[H^+]^1_{free}+[AmH^+]^1+[Na^+]^1_{total}-[OH^-]^1_{free}-[Cl^-]^1_{total}\right]-$$

$$(x)\left[[H^+]^0_{free}+[AmH^+]^0+[Na^+]^0-[OH^-]^0_{free}-[Cl^-]^0_{amine}-[Cl^-]^0_{b1}\right]=$$

$$(y)[[H^+]_{added}+[Na^+]_{b2}-[Cl^-]_{added}-[Cl^-]_{b1}] \qquad \{5\}$$

Substituting in the following equations for the total molar concentrations of sodium and chloride ions in equation {5}:

$$[Na^+]^1_{total}=\frac{(x)[Na^+]^0_{b2}+(y)[Na^+]^1_{b2}}{(x+y)} \qquad \{6\}$$

$$[Cl^-]^1_{total}=\frac{(x)[Cl^-]^0_{amine}+(x)[Cl^-]^0_{b1}+(y)[Cl^-]^1_{added}+(y)[Cl^-]^1_{b2}}{(x+y)} \qquad \{7\}$$

results in the cancellation of all the sodium and chloride terms, leaving the following:

$$(x+y)\left[[H^+]^1_{free}+[AmH^+]^1-[OH^-]^1_{free}\right]-$$

$$(x)\left[[H^+]^0_{free}+[AmH^+]^0-[OH^-]^0_{free}\right]=(y)[H^+]_{added} \qquad \{8\}$$

The derivative of equation {8} with respect to y is equation {8} for infinitely small changes in y, the volume of titrant added. The derivative is as follows:

$$[AmH^+]^1=[H^+]_{added}-[H^+]^1_{free}+[OH^-]^1_{free} \qquad \{9\}$$

Dividing both sides of equation {9} by C_M gives equation {1} for the degree of ionization of PAAm. The result is shown below.

$$\alpha_{amine} = \frac{[AmH^+]^1}{C_M} = \frac{[H^+]_{added} - [H^+]^1_{free} + [OH^-]^1_{free}}{C_M} \quad \{10\}$$

The equation for the titration of a blank sample could be written as follows:

$$\alpha_{blank} = \frac{[AmH^+]^2}{C_M} = \frac{[H^+]_{added} - [H^+]^2_{free} + [OH^-]^2_{free}}{C_M} \quad \{11\}$$

Subtracting equation {11} from {10} at any given pH leaves:

$$\alpha_{amine} = \frac{[H^+]^{amine}_{added} - [H^+]^{blank}_{added}}{C_M} \quad \{12\}$$

since the $[H^+]_{free}$ and $[OH^-]_{free}$ terms cancel at equal pH and since $\alpha_{blank} = 0$.

Equation {12} represents a practical relation which can be used to calculate α, using data from strong acid or base titrations of a blank and the polyallylamine in question.

APPENDIX VI - POTENTIOMETRIC TITRATION TECHNIQUE

Polyallylamine is a polybase which can accept hydrogen ions to form a positively charged polyelectrolyte. The reaction is depicted below:

$$R-(CH_2CH_2NH_2)_a + bH^+ \Leftrightarrow R-(CH_2CH_2NH_3^+)_c + R-(CH_2CH_2NH_2)_{a-c} + (b-c)H^+$$

The degree of protonation (α) is the fraction of amine functional groups that are protonated, or ($\frac{c}{a}$) as shown in the reaction above. Potentiometric titrations can be used to study α as a function of pH. The procedure used in this thesis was as follows:

1. Poly(methylpentene) volumetric flasks were used to prepare all polymer solutions. The non-ionic character of these flasks reduces losses of polymer by adsorption to the surface of the flasks.

2. CO_2 was removed from Nanopure® distilled H_2O by bubbling N_2 through overnight. This H_2O was used for preparation of all the solutions below.

3. Dry NaCl, Na_2CO_3, Potassium biphthalate, and PAAm to constant weight.

4. Prepare 0.5 L of titrant by adding 2.922 gm of NaCl and the appropriate amount of HCl or NaOH to make a 0.1 M solution.

5. Prepare 0.25 L of PAAm solution by diluting approx. 0.2339 gm of PAAm and approx. 1.461 gm NaCl with H_2O from step 2 which has been adjusted to the desired pH (e.g. pH 11 for titration with HCl or pH 3 for titration with NaOH). Record the pH of the final solution.

6. Prepare 0.25 L of blank by diluting approx. 1.461 gm of NaCl with H_2O from step 2 which has been adjusted to the desired pH.

7. Prepare 0.25 L of the primary standard by dissolving the appropriate amount (enough so that approximately 13 ml of 0.1 m titrant will neutralize 50 ml of the primary standard solution) with H_2O from step 2.

8. Rinse pipette twice with the solution to be pipetted. Then pipette 50 ml of primary standard, PAAm, or Blank into a 100 ml poly(propylene) sample jar with four holes drilled in the cap. Insert the stopper, thermometer, N_2 blanket tube, and pH electrode (just above solution). Allow the system to reach constant temperature (approx. 21°C). Then insert the electrode completely, insert the titrant feed tube to the bottom of the flask, and start the titration immediately with the "record" switch on the automatic titrator. Stop the titration when approximately 20 ml of titrant have been added (pH ≈2).

9. Remove the titrant feed tube immediately, and rinse all tubes and flask.

10. Repeat as necessary.

The titrator was a Brinkmann 536. The electrode was the combination pH electrode provided with the instrument. The titrator settings are as follows:

<u>Na_2CO_3 titrations:</u>

mm/100% vol. =	200.00	pH span =	10.00
stop %U =	off	%U =	4.88
auto control =	off	Temp, °C =	room temp.
min./100% vol. =	10.00	mV/pH =	88.00
mV x 100 =	pH 2	selector =	mV, pH

Potassium Biphthalate:

mm/100% vol. =	200.00	pH span =	14.00
stop %U =	off	%U =	4.87
auto control =	off	Temp, °C =	room temp.
min./100% vol. =	10.00	mV/pH =	97.50
mV x 100 =	pH 0	selector =	mV, pH

PAAm and H_2O:

mm/100% vol. =	200.00	pH span =	10.00
stop %U =	off	%U =	4.88
auto control =	off	Temp, °C =	room temp.
min./100% vol. =	60.00	mV/pH =	97.50
mV x 100 =	pH 0	selector =	mV, pH

The titration curves were recorded on the back side of the recorder chart paper. The curves were analyzed as follows:

1. The corner axes of each curve was marked clearly with ink. A reduced photocopy of each curve was taken so that each curve fit well inside an 8.5 x 11 in. sheet of paper.

2. The curves were digitized using a Hewlett-Packard ColorPro plotter and UnPlotIt® hardware and software being sure that pH was read as the X axis. ASCII X, Y data files containing curve points at 0.01 in. increments were stored from the collected data.

3. The files were edited to remove all but the actual numbers and then imported into LABCALC® using the XYIMPORT function.

4. All duplicate files were averaged and saved to a new file using standard LABCALC® functions.

5. The X and Y value of the first point on the averaged PAAm titration curve was noted. Then the OFFSET2 function was used to shift the entire curve in the Y direction so that the corresponding X point in the H_2O curve lined up with the first PAAm point.

6. The PAAm curve was transformed from ml of titrant versus pH to monomer concentration versus pH by the following LABCALC® equation:

   #s = ((inverse(#s+50))*50*[PAAm])

   and saved to a new file.

7. The PAAm and H_2O curve were transformed from ml of titrant versus pH to titrant concentration versus pH by the following LABCALC® equation:

   #s = ((inverse(#s+50))*#s*[titrant])

8. The H_2O curve was then subtracted from the PAAm curve and divided by the monomer concentration curve. For titrations from pH 3 with NaOH, the resulting curve is subtracted from 1 (e.g. #s = -#s + 1). This final curve is the degree of protonation, α, versus pH.

APPENDIX VII - POTENTIOMETRIC TITRATION DATA

Table VII-1. Potentiometric titration data for PAAm with no added NaCl.

pH	α	pK	pH	α	pK	pH	α	pK	pH	α	pK
3.012	0.824	3.682	3.661	0.795	4.250	4.310	0.776	4.848	4.959	0.762	5.465
3.028	0.819	3.685	3.677	0.796	4.267	4.326	0.775	4.864	4.975	0.762	5.480
3.045	0.820	3.702	3.694	0.796	4.285	4.342	0.774	4.877	4.991	0.761	5.495
3.061	0.819	3.718	3.710	0.795	4.299	4.359	0.773	4.890	5.008	0.761	5.511
3.077	0.818	3.731	3.726	0.795	4.316	4.375	0.772	4.906	5.024	0.761	5.526
3.093	0.816	3.740	3.742	0.795	4.330	4.391	0.772	4.921	5.040	0.761	5.542
3.109	0.816	3.755	3.758	0.794	4.345	4.407	0.772	4.936	5.056	0.760	5.558
3.126	0.817	3.776	3.775	0.794	4.361	4.424	0.771	4.952	5.073	0.760	5.573
3.142	0.816	3.789	3.791	0.794	4.377	4.440	0.771	4.966	5.089	0.760	5.590
3.158	0.813	3.797	3.807	0.794	4.393	4.456	0.770	4.980	5.105	0.760	5.606
3.174	0.810	3.804	3.823	0.793	4.407	4.472	0.769	4.996	5.121	0.761	5.623
3.191	0.814	3.831	3.840	0.793	4.423	4.488	0.769	5.011	5.137	0.761	5.640
3.207	0.812	3.841	3.856	0.793	4.438	4.505	0.769	5.027	5.154	0.760	5.655
3.223	0.810	3.852	3.872	0.792	4.453	4.521	0.768	5.041	5.170	0.760	5.670
3.239	0.809	3.865	3.888	0.792	4.468	4.537	0.768	5.056	5.186	0.760	5.686
3.255	0.807	3.877	3.904	0.791	4.483	4.553	0.767	5.072	5.202	0.760	5.704
3.272	0.807	3.894	3.921	0.792	4.501	4.570	0.767	5.088	5.219	0.760	5.719
3.288	0.806	3.905	3.937	0.792	4.517	4.586	0.768	5.105	5.235	0.759	5.734
3.304	0.804	3.916	3.953	0.791	4.531	4.602	0.768	5.121	5.251	0.759	5.749
3.320	0.804	3.932	3.969	0.791	4.547	4.618	0.767	5.135	5.267	0.759	5.765
3.337	0.804	3.950	3.986	0.791	4.563	4.635	0.766	5.150	5.283	0.759	5.781
3.353	0.804	3.966	4.002	0.790	4.578	4.651	0.766	5.165	5.300	0.759	5.797
3.369	0.802	3.977	4.018	0.789	4.592	4.667	0.765	5.179	5.316	0.758	5.813
3.385	0.802	3.993	4.034	0.788	4.606	4.683	0.765	5.195	5.332	0.758	5.827
3.401	0.801	4.007	4.050	0.788	4.621	4.699	0.765	5.212	5.348	0.757	5.842
3.418	0.801	4.022	4.067	0.787	4.635	4.716	0.765	5.227	5.365	0.758	5.861
3.434	0.800	4.036	4.083	0.786	4.649	4.732	0.765	5.243	5.381	0.758	5.876
3.450	0.800	4.052	4.099	0.785	4.662	4.748	0.764	5.259	5.397	0.757	5.891
3.466	0.800	4.068	4.115	0.785	4.677	4.764	0.764	5.274	5.413	0.757	5.907
3.483	0.799	4.082	4.132	0.784	4.692	4.781	0.764	5.291	5.429	0.757	5.923
3.499	0.799	4.098	4.148	0.783	4.706	4.797	0.765	5.308	5.446	0.757	5.939
3.515	0.798	4.113	4.164	0.782	4.719	4.813	0.764	5.323	5.462	0.757	5.955
3.531	0.798	4.127	4.180	0.781	4.733	4.829	0.764	5.339	5.478	0.757	5.971
3.547	0.797	4.142	4.196	0.781	4.747	4.845	0.764	5.356	5.494	0.757	5.987
3.564	0.798	4.160	4.213	0.780	4.762	4.862	0.764	5.372	5.511	0.756	6.002
3.580	0.797	4.175	4.229	0.778	4.775	4.878	0.764	5.387	5.527	0.755	6.016
3.596	0.797	4.191	4.245	0.778	4.789	4.894	0.763	5.401	5.543	0.755	6.031
3.612	0.796	4.205	4.261	0.777	4.805	4.910	0.763	5.417	5.559	0.755	6.047
3.629	0.796	4.219	4.278	0.777	4.819	4.927	0.762	5.432	5.575	0.755	6.064
3.645	0.796	4.235	4.294	0.776	4.833	4.943	0.762	5.448	5.592	0.754	6.079

Table VII-1. Potentiometric titration data for PAAm with no added NaCl.

pH	α	pK	pH	α	pK	pH	α	pK	pH	α	pK
5.608	0.753	6.093	6.257	0.727	6.682	6.906	0.661	7.195	7.555	0.541	7.626
5.624	0.753	6.109	6.273	0.726	6.696	6.922	0.658	7.206	7.571	0.538	7.637
5.640	0.753	6.125	6.289	0.725	6.711	6.938	0.656	7.218	7.587	0.533	7.644
5.657	0.753	6.141	6.306	0.724	6.724	6.955	0.654	7.230	7.603	0.529	7.655
5.673	0.752	6.155	6.322	0.723	6.738	6.971	0.651	7.242	7.620	0.526	7.665
5.689	0.752	6.170	6.338	0.721	6.750	6.987	0.650	7.256	7.636	0.522	7.675
5.705	0.751	6.185	6.354	0.720	6.764	7.003	0.647	7.266	7.652	0.518	7.683
5.722	0.751	6.201	6.370	0.719	6.779	7.019	0.644	7.276	7.668	0.514	7.693
5.738	0.751	6.217	6.387	0.718	6.793	7.036	0.642	7.289	7.685	0.511	7.704
5.754	0.750	6.232	6.403	0.717	6.807	7.052	0.639	7.301	7.701	0.507	7.713
5.770	0.750	6.249	6.419	0.716	6.820	7.068	0.637	7.312	7.717	0.502	7.721
5.786	0.750	6.263	6.435	0.714	6.832	7.084	0.633	7.322	7.733	0.498	7.730
5.803	0.749	6.278	6.452	0.713	6.846	7.101	0.630	7.332	7.749	0.495	7.741
5.819	0.749	6.292	6.468	0.711	6.860	7.117	0.628	7.344	7.766	0.492	7.752
5.835	0.748	6.308	6.484	0.710	6.873	7.133	0.625	7.355	7.782	0.489	7.762
5.851	0.747	6.323	6.500	0.708	6.886	7.149	0.622	7.366	7.798	0.485	7.773
5.868	0.747	6.338	6.516	0.707	6.899	7.165	0.619	7.377	7.814	0.482	7.783
5.884	0.746	6.352	6.533	0.706	6.912	7.182	0.617	7.388	7.831	0.479	7.794
5.900	0.745	6.367	6.549	0.704	6.925	7.198	0.613	7.398	7.847	0.475	7.803
5.916	0.745	6.382	6.565	0.702	6.938	7.214	0.610	7.409	7.863	0.471	7.813
5.932	0.745	6.397	6.581	0.701	6.951	7.230	0.607	7.420	7.879	0.468	7.823
5.949	0.744	6.411	6.598	0.699	6.963	7.247	0.604	7.430	7.896	0.464	7.832
5.965	0.743	6.425	6.614	0.697	6.976	7.263	0.601	7.441	7.928	0.456	7.851
5.981	0.742	6.439	6.630	0.695	6.987	7.279	0.598	7.451	7.944	0.452	7.861
5.997	0.741	6.454	6.646	0.693	7.000	7.295	0.595	7.462	7.960	0.449	7.871
6.014	0.741	6.469	6.662	0.692	7.013	7.311	0.590	7.470	7.977	0.444	7.879
6.030	0.740	6.484	6.679	0.690	7.026	7.328	0.587	7.481	7.993	0.440	7.889
6.046	0.739	6.498	6.695	0.688	7.038	7.344	0.585	7.493	8.009	0.437	7.899
6.062	0.738	6.513	6.711	0.686	7.051	7.360	0.582	7.503	8.025	0.434	7.910
6.078	0.738	6.528	6.727	0.685	7.064	7.376	0.578	7.512	8.042	0.430	7.919
6.095	0.737	6.543	6.744	0.682	7.075	7.393	0.574	7.523	8.058	0.426	7.928
6.111	0.736	6.556	6.760	0.680	7.087	7.409	0.571	7.533	8.074	0.422	7.937
6.127	0.735	6.571	6.776	0.677	7.098	7.425	0.568	7.544	8.090	0.418	7.946
6.143	0.735	6.586	6.792	0.675	7.111	7.441	0.565	7.554	8.106	0.413	7.955
6.160	0.734	6.599	6.809	0.673	7.123	7.457	0.561	7.565	8.123	0.411	7.966
6.176	0.733	6.613	6.825	0.672	7.137	7.474	0.558	7.575	8.139	0.407	7.975
6.192	0.732	6.628	6.841	0.670	7.149	7.490	0.554	7.585	8.155	0.403	7.985
6.208	0.731	6.642	6.857	0.669	7.162	7.506	0.552	7.596	8.171	0.399	7.993
6.224	0.729	6.655	6.873	0.666	7.174	7.522	0.548	7.606	8.188	0.396	8.004
6.241	0.728	6.668	6.890	0.663	7.184	7.539	0.545	7.616	8.204	0.391	8.012

Table VII-1. Potentiometric titration data for PAAm with no added NaCl.

pH	α	pK	pH	α	pK	pH	α	pK	pH	α	pK
8.220	0.388	8.021	8.869	0.237	8.361	9.518	0.111	8.614	10.167	0.026	8.590
8.236	0.384	8.031	8.885	0.234	8.370	9.534	0.107	8.614	10.183	0.024	8.569
8.252	0.380	8.040	8.901	0.230	8.378	9.550	0.105	8.620	10.199	0.022	8.557
8.269	0.376	8.049	8.918	0.226	8.384	9.567	0.102	8.624	10.216	0.021	8.547
8.285	0.372	8.058	8.934	0.223	8.390	9.583	0.100	8.629	10.232	0.020	8.538
8.301	0.369	8.068	8.950	0.220	8.400	9.599	0.098	8.632	10.248	0.019	8.525
8.317	0.366	8.079	8.966	0.217	8.409	9.615	0.095	8.637	10.264	0.017	8.506
8.334	0.363	8.089	8.983	0.212	8.413	9.631	0.094	8.645	10.280	0.016	8.485
8.350	0.358	8.096	8.999	0.210	8.422	9.648	0.091	8.650	10.297	0.014	8.443
8.366	0.354	8.105	9.015	0.205	8.427	9.664	0.089	8.653	10.313	0.013	8.427
8.382	0.350	8.114	9.031	0.202	8.435	9.680	0.086	8.653	10.329	0.011	8.389
8.398	0.346	8.121	9.047	0.199	8.442	9.696	0.083	8.655	10.345	0.011	8.373
8.415	0.342	8.130	9.064	0.195	8.447	9.713	0.082	8.663	10.362	0.009	8.308
8.431	0.337	8.137	9.080	0.191	8.454	9.729	0.080	8.667	10.378	0.007	8.220
8.447	0.333	8.146	9.096	0.189	8.462	9.745	0.078	8.670	10.394	0.006	8.188
8.463	0.330	8.156	9.112	0.186	8.471	9.761	0.075	8.672	10.410	0.006	8.168
8.480	0.326	8.165	9.129	0.183	8.479	9.777	0.072	8.665	10.426	0.005	8.083
8.496	0.322	8.173	9.145	0.180	8.487	9.794	0.070	8.668	10.443	0.004	8.050
8.512	0.319	8.183	9.161	0.177	8.494	9.810	0.068	8.670	10.459	0.003	7.973
8.528	0.316	8.192	9.177	0.174	8.501	9.826	0.065	8.666	10.475	0.002	7.756
8.544	0.312	8.201	9.193	0.171	8.506	9.842	0.063	8.668	10.491	0.001	7.451
8.561	0.308	8.209	9.210	0.168	8.514	9.859	0.061	8.671			
8.577	0.304	8.218	9.226	0.164	8.519	9.875	0.059	8.675			
8.593	0.301	8.226	9.242	0.161	8.526	9.891	0.057	8.673			
8.609	0.297	8.235	9.258	0.159	8.534	9.907	0.055	8.676			
8.626	0.294	8.245	9.275	0.156	8.540	9.924	0.053	8.673			
8.642	0.290	8.253	9.291	0.153	8.546	9.940	0.051	8.669			
8.658	0.285	8.258	9.307	0.150	8.552	9.956	0.049	8.665			
8.674	0.281	8.267	9.323	0.146	8.556	9.972	0.046	8.658			
8.690	0.278	8.275	9.339	0.144	8.563	9.988	0.045	8.660			
8.707	0.273	8.281	9.356	0.141	8.571	10.005	0.043	8.654			
8.723	0.270	8.291	9.372	0.138	8.576	10.021	0.040	8.644			
8.739	0.266	8.298	9.388	0.134	8.578	10.037	0.039	8.643			
8.755	0.262	8.306	9.404	0.131	8.584	10.053	0.037	8.642			
8.772	0.258	8.314	9.421	0.129	8.590	10.070	0.035	8.630			
8.788	0.255	8.323	9.437	0.124	8.588	10.086	0.033	8.622			
8.804	0.252	8.331	9.453	0.122	8.596	10.102	0.032	8.616			
8.820	0.248	8.338	9.469	0.120	8.604	10.118	0.030	8.613			
8.836	0.244	8.345	9.485	0.117	8.608	10.134	0.030	8.620			
8.853	0.241	8.354	9.502	0.114	8.612	10.151	0.027	8.601			

Table VII-2. Potentiometric titration data for PAAm with 0.001 M NaCl.

pH	α	pK	pH	α	pK	pH	α	pK	pH	α	pK
3.010	0.754	3.497	3.653	0.789	4.225	4.296	0.780	4.845	4.939	0.766	5.453
3.026	0.758	3.522	3.669	0.788	4.238	4.312	0.779	4.860	4.955	0.765	5.467
3.042	0.755	3.532	3.685	0.788	4.254	4.328	0.779	4.874	4.971	0.765	5.482
3.058	0.764	3.568	3.701	0.790	4.275	4.344	0.778	4.888	4.987	0.764	5.497
3.074	0.767	3.591	3.717	0.789	4.290	4.360	0.777	4.902	5.003	0.764	5.513
3.090	0.771	3.618	3.733	0.788	4.303	4.376	0.776	4.915	5.019	0.764	5.530
3.106	0.768	3.627	3.749	0.789	4.322	4.392	0.775	4.929	5.035	0.764	5.546
3.122	0.770	3.647	3.765	0.789	4.337	4.408	0.775	4.945	5.051	0.763	5.560
3.138	0.772	3.668	3.781	0.790	4.356	4.424	0.774	4.960	5.067	0.764	5.576
3.154	0.772	3.685	3.797	0.790	4.372	4.440	0.774	4.976	5.083	0.763	5.591
3.170	0.774	3.706	3.813	0.791	4.390	4.457	0.774	4.990	5.100	0.763	5.606
3.187	0.775	3.725	3.830	0.790	4.406	4.473	0.773	5.004	5.116	0.763	5.622
3.203	0.775	3.740	3.846	0.790	4.420	4.489	0.772	5.019	5.132	0.763	5.638
3.219	0.777	3.760	3.862	0.789	4.435	4.505	0.772	5.034	5.148	0.762	5.654
3.235	0.778	3.780	3.878	0.790	4.452	4.521	0.771	5.049	5.164	0.762	5.669
3.251	0.777	3.792	3.894	0.790	4.470	4.537	0.771	5.065	5.180	0.762	5.684
3.267	0.779	3.813	3.910	0.790	4.484	4.553	0.771	5.080	5.196	0.762	5.700
3.283	0.777	3.826	3.926	0.789	4.500	4.569	0.770	5.095	5.212	0.762	5.716
3.299	0.781	3.852	3.942	0.790	4.518	4.585	0.770	5.109	5.228	0.761	5.732
3.315	0.782	3.869	3.958	0.790	4.534	4.601	0.770	5.125	5.244	0.761	5.747
3.331	0.783	3.889	3.974	0.790	4.550	4.617	0.769	5.140	5.260	0.760	5.762
3.347	0.782	3.902	3.990	0.790	4.566	4.633	0.769	5.156	5.276	0.761	5.778
3.363	0.783	3.920	4.006	0.790	4.582	4.649	0.769	5.172	5.292	0.761	5.795
3.379	0.782	3.933	4.022	0.790	4.598	4.666	0.768	5.186	5.309	0.761	5.812
3.395	0.783	3.952	4.039	0.790	4.614	4.682	0.768	5.202	5.325	0.761	5.828
3.412	0.782	3.966	4.055	0.790	4.630	4.698	0.769	5.219	5.341	0.761	5.843
3.428	0.783	3.986	4.071	0.789	4.644	4.714	0.768	5.234	5.357	0.760	5.858
3.444	0.785	4.005	4.087	0.789	4.658	4.730	0.768	5.249	5.373	0.760	5.874
3.460	0.785	4.022	4.103	0.789	4.674	4.746	0.768	5.266	5.389	0.759	5.888
3.476	0.786	4.041	4.119	0.788	4.690	4.762	0.767	5.280	5.405	0.760	5.904
3.492	0.786	4.056	4.135	0.788	4.706	4.778	0.767	5.295	5.421	0.759	5.919
3.508	0.786	4.072	4.151	0.788	4.720	4.794	0.766	5.309	5.437	0.759	5.935
3.524	0.786	4.088	4.167	0.787	4.734	4.810	0.766	5.326	5.453	0.759	5.951
3.540	0.785	4.104	4.183	0.786	4.748	4.826	0.766	5.342	5.469	0.758	5.965
3.556	0.787	4.123	4.199	0.785	4.762	4.842	0.766	5.358	5.485	0.758	5.982
3.572	0.788	4.141	4.215	0.785	4.777	4.858	0.766	5.373	5.501	0.758	5.998
3.588	0.787	4.156	4.231	0.783	4.790	4.874	0.766	5.389	5.518	0.757	6.011
3.604	0.787	4.172	4.248	0.783	4.804	4.891	0.765	5.404	5.534	0.756	6.026
3.621	0.788	4.190	4.264	0.781	4.816	4.907	0.765	5.420	5.550	0.757	6.043
3.637	0.788	4.206	4.280	0.780	4.829	4.923	0.766	5.436	5.566	0.756	6.057

Table VII-2. Potentiometric titration data for PAAm with 0.001 M NaCl.

pH	α	pK	pH	α	pK	pH	α	pK	pH	α	pK
5.582	0.755	6.071	6.225	0.728	6.653	6.868	0.664	7.163	7.511	0.548	7.594
5.598	0.755	6.087	6.241	0.727	6.666	6.884	0.661	7.175	7.527	0.544	7.604
5.614	0.754	6.102	6.257	0.725	6.678	6.900	0.659	7.186	7.543	0.540	7.613
5.630	0.755	6.118	6.273	0.724	6.693	6.916	0.657	7.199	7.559	0.537	7.624
5.646	0.754	6.133	6.289	0.723	6.706	6.932	0.655	7.210	7.575	0.533	7.633
5.662	0.754	6.148	6.305	0.722	6.720	6.948	0.653	7.223	7.591	0.531	7.644
5.678	0.753	6.164	6.321	0.721	6.734	6.964	0.651	7.234	7.607	0.526	7.653
5.694	0.753	6.179	6.337	0.720	6.748	6.980	0.648	7.246	7.624	0.524	7.665
5.710	0.753	6.194	6.353	0.719	6.761	6.997	0.646	7.257	7.640	0.520	7.674
5.727	0.752	6.208	6.370	0.717	6.774	7.013	0.642	7.267	7.656	0.516	7.684
5.743	0.752	6.225	6.386	0.716	6.787	7.029	0.639	7.277	7.672	0.512	7.693
5.759	0.752	6.240	6.402	0.715	6.800	7.045	0.637	7.289	7.688	0.508	7.702
5.775	0.750	6.252	6.418	0.713	6.813	7.061	0.634	7.299	7.704	0.505	7.712
5.791	0.750	6.267	6.434	0.712	6.828	7.077	0.631	7.310	7.720	0.500	7.721
5.807	0.749	6.282	6.450	0.711	6.841	7.093	0.629	7.322	7.736	0.497	7.731
5.823	0.749	6.298	6.466	0.710	6.855	7.109	0.626	7.333	7.752	0.493	7.740
5.839	0.748	6.312	6.482	0.709	6.868	7.125	0.623	7.344	7.768	0.490	7.750
5.855	0.748	6.327	6.498	0.707	6.881	7.141	0.620	7.354	7.784	0.486	7.760
5.871	0.747	6.342	6.514	0.705	6.893	7.157	0.617	7.365	7.800	0.482	7.769
5.887	0.747	6.356	6.530	0.703	6.905	7.173	0.614	7.375	7.816	0.479	7.780
5.903	0.745	6.370	6.546	0.702	6.918	7.189	0.612	7.386	7.832	0.475	7.790
5.919	0.744	6.384	6.562	0.701	6.932	7.206	0.609	7.397	7.849	0.471	7.799
5.936	0.744	6.400	6.579	0.700	6.946	7.222	0.605	7.407	7.865	0.468	7.808
5.952	0.744	6.415	6.595	0.698	6.958	7.238	0.603	7.419	7.881	0.464	7.818
5.968	0.742	6.427	6.611	0.695	6.968	7.254	0.600	7.430	7.897	0.461	7.828
5.984	0.742	6.442	6.627	0.695	6.984	7.270	0.597	7.440	7.913	0.457	7.837
6.000	0.742	6.458	6.643	0.693	6.996	7.286	0.594	7.451	7.929	0.453	7.847
6.016	0.741	6.472	6.659	0.691	7.008	7.302	0.590	7.461	7.945	0.449	7.855
6.032	0.740	6.487	6.675	0.688	7.019	7.318	0.587	7.471	7.961	0.445	7.865
6.048	0.739	6.500	6.691	0.688	7.034	7.334	0.584	7.481	7.977	0.441	7.874
6.064	0.738	6.513	6.707	0.686	7.045	7.350	0.581	7.493	7.993	0.437	7.883
6.080	0.737	6.528	6.723	0.683	7.057	7.366	0.577	7.502	8.009	0.434	7.894
6.096	0.736	6.542	6.739	0.681	7.069	7.382	0.574	7.512	8.025	0.430	7.902
6.112	0.735	6.554	6.755	0.679	7.080	7.398	0.571	7.522	8.041	0.425	7.910
6.128	0.734	6.569	6.771	0.676	7.091	7.415	0.567	7.532	8.057	0.422	7.921
6.145	0.733	6.582	6.788	0.675	7.104	7.431	0.564	7.543	8.074	0.418	7.930
6.161	0.732	6.597	6.804	0.673	7.117	7.447	0.561	7.554	8.090	0.414	7.938
6.177	0.731	6.611	6.820	0.670	7.128	7.463	0.557	7.563	8.106	0.409	7.946
6.193	0.730	6.624	6.836	0.668	7.139	7.479	0.554	7.573	8.122	0.405	7.955
6.209	0.729	6.638	6.852	0.666	7.152	7.495	0.550	7.582	8.138	0.402	7.965

Table VII-2. Potentiometric titration data for PAAm with 0.001 M NaCl.

pH	α	pK	pH	α	pK	pH	α	pK	pH	α	pK
8.154	0.398	7.973	8.797	0.246	8.310	9.440	0.118	8.566	10.083	0.026	8.506
8.170	0.393	7.982	8.813	0.242	8.318	9.456	0.115	8.570	10.099	0.024	8.490
8.186	0.389	7.989	8.829	0.239	8.327	9.472	0.112	8.571	10.115	0.022	8.476
8.202	0.385	7.998	8.845	0.235	8.333	9.488	0.109	8.574	10.131	0.021	8.456
8.218	0.381	8.008	8.861	0.232	8.340	9.504	0.107	8.581	10.147	0.019	8.432
8.234	0.378	8.018	8.877	0.228	8.349	9.520	0.104	8.583	10.163	0.017	8.411
8.250	0.374	8.027	8.894	0.225	8.356	9.537	0.100	8.584	10.180	0.016	8.392
8.267	0.370	8.035	8.910	0.221	8.363	9.553	0.097	8.585	10.196	0.015	8.378
8.283	0.366	8.044	8.926	0.218	8.371	9.569	0.095	8.587	10.212	0.014	8.351
8.299	0.363	8.055	8.942	0.215	8.379	9.585	0.093	8.594	10.228	0.013	8.349
8.315	0.360	8.064	8.958	0.211	8.385	9.601	0.090	8.597	10.244	0.011	8.303
8.331	0.355	8.072	8.974	0.207	8.390	9.617	0.088	8.601	10.260	0.009	8.221
8.347	0.352	8.082	8.990	0.204	8.399	9.633	0.086	8.606	10.276	0.008	8.175
8.363	0.348	8.090	9.006	0.201	8.408	9.649	0.083	8.607	10.292	0.007	8.111
8.379	0.344	8.099	9.022	0.198	8.414	9.665	0.081	8.608	10.308	0.005	8.032
8.395	0.340	8.107	9.038	0.195	8.422	9.681	0.078	8.608	10.324	0.004	7.905
8.411	0.337	8.117	9.054	0.191	8.426	9.697	0.076	8.610	10.340	0.003	7.772
8.427	0.333	8.125	9.070	0.187	8.432	9.713	0.073	8.608	10.356	0.001	7.382
8.443	0.328	8.132	9.086	0.185	8.441	9.729	0.070	8.608			
8.459	0.323	8.139	9.102	0.182	8.450	9.746	0.068	8.610			
8.476	0.320	8.148	9.118	0.179	8.457	9.762	0.066	8.608			
8.492	0.317	8.157	9.135	0.175	8.463	9.778	0.063	8.605			
8.508	0.312	8.165	9.151	0.172	8.469	9.794	0.061	8.606			
8.524	0.309	8.174	9.167	0.170	8.477	9.810	0.059	8.603			
8.540	0.306	8.183	9.183	0.166	8.483	9.826	0.056	8.601			
8.556	0.301	8.189	9.199	0.163	8.490	9.842	0.055	8.604			
8.572	0.298	8.199	9.215	0.161	8.497	9.858	0.053	8.608			
8.588	0.295	8.210	9.231	0.157	8.503	9.874	0.052	8.610			
8.604	0.291	8.217	9.247	0.155	8.510	9.890	0.050	8.608			
8.620	0.287	8.225	9.263	0.151	8.514	9.906	0.047	8.594			
8.636	0.283	8.232	9.279	0.148	8.519	9.922	0.044	8.589			
8.652	0.279	8.240	9.295	0.144	8.522	9.938	0.043	8.592			
8.668	0.275	8.247	9.311	0.141	8.528	9.954	0.041	8.582			
8.685	0.271	8.256	9.328	0.138	8.532	9.971	0.039	8.577			
8.701	0.267	8.262	9.344	0.135	8.539	9.987	0.037	8.571			
8.717	0.263	8.270	9.360	0.132	8.542	10.003	0.034	8.548			
8.733	0.260	8.279	9.376	0.129	8.547	10.019	0.033	8.545			
8.749	0.256	8.286	9.392	0.127	8.553	10.035	0.031	8.538			
8.765	0.253	8.294	9.408	0.124	8.559	10.051	0.029	8.524			
8.781	0.249	8.301	9.424	0.121	8.561	10.067	0.028	8.521			

Table VII-3. Potentiometric titration data for PAAm with 0.01 M NaCl.

pH	α	pK	pH	α	pK	pH	α	pK	pH	α	pK
3.011	0.683	3.345	3.662	0.753	4.146	4.313	0.752	4.794	4.964	0.744	5.426
3.027	0.688	3.371	3.678	0.754	4.166	4.329	0.751	4.808	4.980	0.744	5.443
3.043	0.690	3.391	3.694	0.754	4.181	4.345	0.750	4.823	4.996	0.744	5.458
3.060	0.690	3.408	3.711	0.755	4.199	4.362	0.750	4.838	5.012	0.743	5.472
3.076	0.694	3.431	3.727	0.755	4.216	4.378	0.750	4.855	5.029	0.742	5.488
3.092	0.697	3.455	3.743	0.756	4.234	4.394	0.750	4.871	5.045	0.742	5.504
3.109	0.701	3.479	3.759	0.757	4.252	4.410	0.750	4.887	5.061	0.743	5.521
3.125	0.705	3.504	3.776	0.756	4.267	4.427	0.749	4.902	5.077	0.743	5.539
3.141	0.708	3.526	3.792	0.757	4.285	4.443	0.749	4.918	5.094	0.743	5.555
3.157	0.709	3.543	3.808	0.759	4.305	4.459	0.749	4.933	5.110	0.743	5.570
3.174	0.715	3.574	3.825	0.759	4.323	4.475	0.748	4.948	5.126	0.743	5.586
3.190	0.715	3.589	3.841	0.759	4.340	4.492	0.747	4.962	5.143	0.743	5.604
3.206	0.717	3.611	3.857	0.760	4.357	4.508	0.747	4.978	5.159	0.743	5.621
3.222	0.719	3.631	3.873	0.760	4.374	4.524	0.746	4.993	5.175	0.743	5.636
3.239	0.719	3.647	3.890	0.760	4.390	4.541	0.746	5.008	5.191	0.743	5.652
3.255	0.719	3.664	3.906	0.760	4.407	4.557	0.747	5.026	5.208	0.743	5.669
3.271	0.721	3.685	3.922	0.761	4.424	4.573	0.747	5.043	5.224	0.743	5.684
3.288	0.725	3.709	3.938	0.761	4.442	4.589	0.747	5.059	5.240	0.742	5.699
3.304	0.726	3.727	3.955	0.761	4.458	4.606	0.746	5.073	5.256	0.743	5.716
3.320	0.728	3.747	3.971	0.761	4.473	4.622	0.746	5.089	5.273	0.742	5.732
3.336	0.731	3.770	3.987	0.761	4.490	4.638	0.746	5.106	5.289	0.742	5.748
3.353	0.733	3.790	4.004	0.761	4.507	4.654	0.746	5.122	5.305	0.742	5.764
3.369	0.733	3.808	4.020	0.761	4.523	4.671	0.745	5.136	5.322	0.742	5.780
3.385	0.734	3.826	4.036	0.761	4.538	4.687	0.745	5.152	5.338	***	0.000
3.401	0.735	3.845	4.052	0.760	4.553	4.703	0.745	5.168	0.000	***	0.000
3.418	0.737	3.866	4.069	0.760	4.568	4.719	0.744	5.184	0.000	0.000	***
3.434	0.739	3.886	4.085	0.759	4.583	4.736	0.744	5.199	0.000	***	0.000
3.450	0.740	3.905	4.101	0.759	4.599	4.752	0.744	5.216	0.000	0.000	5.860
3.467	0.741	3.923	4.117	0.758	4.614	4.768	0.745	5.234	5.419	0.741	5.876
3.483	0.742	3.941	4.134	0.758	4.629	4.785	0.745	5.250	5.435	0.741	5.892
3.499	0.743	3.960	4.150	0.758	4.646	4.801	0.744	5.264	5.452	0.741	5.908
3.515	0.744	3.978	4.166	0.757	4.659	4.817	0.744	5.280	5.468	0.741	5.924
3.532	0.745	3.997	4.183	0.755	4.672	4.833	0.744	5.298	5.484	0.741	5.941
3.548	0.745	4.014	4.199	0.755	4.687	4.850	0.745	5.315	5.501	0.741	5.957
3.564	0.747	4.035	4.215	0.755	4.704	4.866	0.744	5.330	5.517	0.741	5.972
3.580	0.748	4.052	4.231	0.754	4.718	4.882	0.744	5.345	5.533	0.740	5.987
3.597	0.748	4.070	4.248	0.753	4.733	4.898	0.744	5.361	5.549	0.739	6.001
3.613	0.750	4.089	4.264	0.753	4.747	4.915	0.744	5.378	5.566	0.739	6.019
3.629	0.750	4.107	4.280	0.752	4.762	4.931	0.744	5.394	5.582	0.739	6.034
3.646	0.751	4.124	4.296	0.752	4.779	4.947	0.744	5.410	5.598	0.739	6.050

Table VII-3. Potentiometric titration data for PAAm with 0.01 M NaCl.

pH	α	pK	pH	α	pK	pH	α	pK	pH	α	pK
5.614	0.739	6.066	6.265	0.721	6.677	6.916	0.664	7.212	7.567	0.559	7.670
5.631	0.738	6.081	6.282	0.720	6.691	6.932	0.663	7.226	7.583	0.555	7.679
5.647	0.738	6.097	6.298	0.719	6.705	6.949	0.661	7.238	7.600	0.551	7.689
5.663	0.738	6.113	6.314	0.717	6.718	6.965	0.659	7.250	7.616	0.548	7.699
5.680	0.738	6.129	6.330	0.716	6.732	6.981	0.656	7.262	7.632	0.545	7.711
5.696	0.738	6.145	6.347	0.715	6.746	6.998	0.654	7.275	7.648	0.542	7.722
5.712	0.738	6.162	6.363	0.715	6.762	7.014	0.651	7.285	7.665	0.539	7.732
5.728	0.738	6.179	6.379	0.713	6.774	7.030	0.649	7.297	7.681	0.535	7.742
5.745	0.738	6.194	6.396	0.712	6.789	7.046	0.647	7.310	7.697	0.533	7.754
5.761	0.738	6.210	6.412	0.711	6.803	7.063	0.645	7.322	7.714	0.529	7.764
5.777	0.737	6.225	6.428	0.710	6.817	7.079	0.642	7.332	7.730	0.526	7.775
5.793	0.737	6.240	6.444	0.709	6.831	7.095	0.640	7.345	7.746	0.523	7.785
5.810	0.737	6.257	6.461	0.709	6.847	7.111	0.638	7.357	7.762	0.518	7.793
5.826	0.736	6.272	6.477	0.708	6.861	7.128	0.636	7.370	7.779	0.515	7.804
5.842	0.735	6.286	6.493	0.706	6.874	7.144	0.634	7.382	7.795	0.511	7.814
5.859	0.736	6.303	6.509	0.705	6.888	7.160	0.632	7.394	7.811	0.508	7.825
5.875	0.735	6.319	6.526	0.704	6.901	7.177	0.629	7.407	7.827	0.504	7.835
5.891	0.735	6.334	6.542	0.702	6.915	7.193	0.627	7.418	7.844	0.500	7.845
5.907	0.735	6.350	6.558	0.701	6.929	7.209	0.624	7.430	7.860	0.497	7.855
5.924	0.734	6.364	6.575	0.699	6.940	7.225	0.622	7.441	7.876	0.494	7.865
5.940	0.733	6.379	6.591	0.698	6.954	7.242	0.619	7.453	7.893	0.490	7.876
5.956	0.732	6.393	6.607	0.696	6.968	7.258	0.616	7.463	7.909	0.487	7.886
5.972	0.732	6.409	6.623	0.695	6.981	7.274	0.613	7.474	7.925	0.484	7.897
5.989	0.732	6.424	6.640	0.693	6.994	7.290	0.611	7.486	7.941	0.480	7.906
6.005	0.731	6.439	6.656	0.692	7.007	7.307	0.607	7.496	7.958	0.477	7.917
6.021	0.731	6.455	6.672	0.690	7.021	7.323	0.604	7.507	7.974	0.473	7.926
6.038	0.730	6.469	6.688	0.689	7.034	7.339	0.602	7.520	7.990	0.469	7.936
6.054	0.730	6.485	6.705	0.688	7.047	7.356	0.599	7.531	8.006	0.466	7.947
6.070	0.730	6.501	6.721	0.686	7.059	7.372	0.597	7.542	8.023	0.462	7.957
6.086	0.729	6.516	6.737	0.683	7.071	7.388	0.594	7.553	8.039	0.458	7.966
6.103	0.728	6.530	6.754	0.682	7.085	7.404	0.590	7.562	8.055	0.454	7.975
6.119	0.728	6.546	6.770	0.680	7.097	7.421	0.588	7.574	8.072	0.451	7.985
6.135	0.727	6.561	6.786	0.678	7.109	7.437	0.585	7.586	8.088	0.447	7.995
6.151	0.727	6.576	6.802	0.677	7.124	7.453	0.582	7.596	8.104	0.443	8.005
6.168	0.726	6.591	6.819	0.676	7.138	7.469	0.579	7.607	8.120	0.440	8.016
6.184	0.725	6.606	6.835	0.674	7.151	7.486	0.575	7.617	8.137	0.437	8.026
6.200	0.725	6.621	6.851	0.672	7.163	7.502	0.572	7.628	8.153	0.433	8.036
6.217	0.723	6.634	6.867	0.670	7.175	7.518	0.568	7.638	8.169	0.429	8.045
6.233	0.722	6.647	6.884	0.668	7.188	7.535	0.565	7.649	8.185	0.425	8.055
6.249	0.722	6.663	6.900	0.666	7.199	7.551	0.563	7.660	8.202	0.421	8.063

Table VII-3. Potentiometric titration data for PAAm with 0.01 M NaCl.

pH	α	pK
8.218	0.417	8.073
8.234	0.414	8.083
8.251	0.409	8.091
8.267	0.405	8.100
8.283	0.402	8.110
8.299	0.398	8.119
8.316	0.395	8.131
8.332	0.392	8.142
8.348	0.388	8.151
8.364	0.384	8.159
8.381	0.380	8.169
8.397	0.377	8.179
8.413	0.373	8.187
8.430	0.368	8.194
8.446	0.364	8.204
8.462	0.361	8.215
8.478	0.357	8.223
8.495	0.353	8.232
8.511	0.349	8.240
8.527	0.345	8.248
8.543	0.342	8.259
8.560	0.337	8.267
8.576	0.334	8.277
8.592	0.330	8.285
8.608	0.326	8.293
8.625	0.322	8.302
8.641	0.318	8.310
8.657	0.314	8.319
8.674	0.311	8.328
8.690	0.308	8.338
8.706	0.304	8.345
8.722	0.300	8.353
8.739	0.295	8.361
8.755	0.291	8.369
8.771	0.288	8.378
8.787	0.284	8.385
8.804	0.281	8.396
8.820	0.278	8.405
8.836	0.274	8.414
8.852	0.270	8.420
8.869	0.266	8.428
8.885	0.263	8.437
8.901	0.259	8.445
8.918	0.255	8.453
8.934	0.252	8.460
8.950	0.248	8.468
8.966	0.245	8.477
8.983	0.241	8.485
8.999	0.237	8.492
9.015	0.233	8.498
9.031	0.229	8.505
9.048	0.226	8.514
9.064	0.222	8.519
9.080	0.219	8.528
9.097	0.216	8.536
9.113	0.213	8.546
9.129	0.210	8.554
9.145	0.207	8.563
9.162	0.203	8.568
9.178	0.199	8.574
9.194	0.196	8.581
9.211	0.192	8.586
9.227	0.188	8.593
9.243	0.186	8.601
9.259	0.183	8.609
9.276	0.179	8.613
9.292	0.175	8.618
9.308	0.171	8.623
9.324	0.168	8.630
9.341	0.165	8.635
9.357	0.162	8.642
9.373	0.159	8.649
9.390	0.156	8.656
9.406	0.152	8.660
9.422	0.148	8.662
9.438	0.145	8.668
9.455	0.141	8.670
9.471	0.138	8.675
9.487	0.135	8.681
9.503	0.132	8.684
9.520	0.129	8.689
9.536	0.126	8.693
9.552	0.123	8.698
9.569	0.120	8.702
9.585	0.118	8.710
9.601	0.115	8.715
9.617	0.112	8.716
9.634	0.109	8.720
9.650	0.106	8.723
9.666	0.103	8.726
9.682	0.101	8.732
9.699	0.099	8.738
9.715	0.096	8.740
9.731	0.093	8.743
9.748	0.091	8.745
9.764	0.088	8.749
9.780	0.086	8.753
9.796	0.083	8.752
9.813	0.080	8.753
9.829	0.077	8.752
9.845	0.076	8.757
9.861	0.073	8.758
9.878	0.071	8.758
9.894	0.069	8.763
9.910	0.066	8.762
9.927	0.064	8.761
9.943	0.061	8.757
9.959	0.059	8.755
9.975	0.057	8.755
9.992	0.054	8.747
10.008	0.051	8.739
10.024	0.049	8.737
10.040	0.047	8.735
10.057	0.046	8.735
10.073	0.043	8.720
10.089	0.040	8.713
10.105	0.038	8.701
10.122	0.036	8.691
10.138	0.034	8.685
10.154	0.032	8.669
10.171	0.029	8.648
10.187	0.028	8.653
10.203	0.026	8.628
10.219	0.023	8.593
10.236	0.021	8.575
10.252	0.020	8.550
10.268	0.018	8.537
10.284	0.017	8.518
10.301	0.015	8.482
10.317	0.013	8.448
10.333	0.012	8.404
10.350	0.010	8.365
10.366	0.008	8.250
10.382	0.006	8.172
10.398	0.005	8.081
10.415	0.004	7.970
10.431	0.002	7.819
10.447	0.001	7.402

Table VII-4. Potentiometric titration data for PAAm with 0.1 M NaCl.

pH	α	pK	pH	α	pK	pH	α	pK	pH	α	pK
3.011	0.745	3.477	3.739	0.753	4.223	4.467	0.744	4.930	5.195	0.742	5.653
3.029	0.746	3.496	3.757	0.753	4.242	4.485	0.744	4.947	5.213	0.741	5.670
3.047	0.747	3.518	3.775	0.753	4.260	4.503	0.744	4.965	5.231	0.741	5.688
3.065	0.749	3.540	3.793	0.753	4.277	4.521	0.745	4.986	5.249	0.741	5.705
3.084	0.749	3.558	3.812	0.752	4.294	4.539	0.745	5.005	5.267	0.741	5.724
3.102	0.750	3.578	3.830	0.751	4.309	4.558	0.744	5.021	5.286	0.742	5.745
3.120	0.750	3.598	3.848	0.750	4.326	4.576	0.744	5.038	5.304	0.742	5.762
3.138	0.750	3.615	3.866	0.751	4.345	4.594	0.744	5.057	5.322	0.741	5.778
3.156	0.750	3.634	3.884	0.751	4.364	4.612	0.744	5.076	5.340	0.741	5.796
3.175	0.751	3.655	3.903	0.750	4.381	4.630	0.745	5.096	5.358	0.740	5.813
3.193	0.752	3.675	3.921	0.749	4.396	4.649	0.744	5.111	5.377	0.740	5.832
3.211	0.753	3.696	3.939	0.749	4.414	4.667	0.743	5.128	5.395	0.741	5.851
3.229	0.753	3.713	3.957	0.749	4.432	4.685	0.743	5.147	5.413	0.741	5.870
3.247	0.752	3.729	3.975	0.749	4.450	4.703	0.742	5.163	5.431	0.741	5.888
3.266	0.752	3.748	3.993	0.749	4.468	4.721	0.742	5.180	5.449	0.742	5.907
3.284	0.752	3.766	4.012	0.748	4.485	4.740	0.742	5.198	5.468	0.742	5.925
3.302	0.753	3.785	4.030	0.748	4.502	4.758	0.742	5.217	5.486	0.741	5.943
3.320	0.753	3.804	4.048	0.748	4.520	4.776	0.742	5.235	5.504	0.741	5.961
3.338	0.753	3.823	4.066	0.747	4.536	4.794	0.742	5.253	5.522	0.741	5.979
3.357	0.754	3.842	4.084	0.746	4.553	4.812	0.742	5.272	5.540	0.740	5.995
3.375	0.754	3.862	4.103	0.747	4.572	4.831	0.743	5.291	5.559	0.740	6.012
3.393	0.754	3.880	4.121	0.748	4.593	4.849	0.743	5.310	5.577	0.741	6.033
3.411	0.754	3.898	4.139	0.748	4.612	4.867	0.743	5.327	5.595	0.741	6.050
3.429	0.755	3.917	4.157	0.747	4.628	4.885	0.743	5.346	5.613	0.739	6.066
3.448	0.755	3.937	4.175	0.747	4.645	4.903	0.744	5.366	5.631	0.739	6.083
3.466	0.755	3.955	4.194	0.747	4.664	4.922	0.744	5.384	5.650	0.739	6.102
3.484	0.755	3.973	4.212	0.746	4.680	4.940	0.744	5.402	5.668	0.740	6.122
3.502	0.756	3.994	4.230	0.746	4.698	4.958	0.743	5.420	5.686	0.740	6.141
3.520	0.757	4.014	4.248	0.746	4.715	4.976	0.742	5.436	5.704	0.740	6.159
3.539	0.757	4.031	4.266	0.745	4.732	4.994	0.742	5.453	5.722	0.740	6.177
3.557	0.756	4.049	4.285	0.745	4.749	5.013	0.742	5.471	5.741	0.740	6.194
3.575	0.757	4.068	4.303	0.745	4.768	5.031	0.742	5.489	5.759	0.739	6.210
3.593	0.757	4.087	4.321	0.746	4.789	5.049	0.742	5.508	5.777	0.739	6.228
3.611	0.757	4.105	4.339	0.746	4.807	5.067	0.743	5.527	5.795	0.738	6.245
3.630	0.757	4.122	4.357	0.745	4.824	5.085	0.743	5.546	5.813	0.738	6.263
3.648	0.757	4.141	4.376	0.746	4.843	5.104	0.743	5.565	5.831	0.738	6.282
3.666	0.756	4.157	4.394	0.746	4.861	5.122	0.743	5.583	5.850	0.738	6.299
3.684	0.756	4.175	4.412	0.746	4.879	5.140	0.742	5.600	5.868	0.737	6.315
3.702	0.755	4.192	4.430	0.744	4.895	5.158	0.742	5.617	5.886	0.737	6.333
3.721	0.753	4.206	4.448	0.744	4.912	5.176	0.742	5.635	5.904	0.737	6.352

Table VII-4. Potentiometric titration data for PAAm with 0.1 M NaCl.

pH	α	pK	pH	α	pK	pH	α	pK	pH	α	pK
5.922	0.738	6.371	6.650	0.710	7.038	7.378	0.638	7.625	8.106	0.516	8.134
5.941	0.737	6.389	6.669	0.709	7.055	7.397	0.636	7.639	8.124	0.512	8.146
5.959	0.737	6.407	6.687	0.708	7.071	7.415	0.633	7.652	8.143	0.509	8.159
5.977	0.737	6.424	6.705	0.706	7.086	7.433	0.631	7.667	8.161	0.505	8.170
5.995	0.737	6.442	6.723	0.706	7.103	7.451	0.628	7.680	8.179	0.501	8.182
6.013	0.737	6.461	6.741	0.704	7.119	7.469	0.626	7.693	8.197	0.497	8.193
6.032	0.737	6.480	6.760	0.703	7.134	7.488	0.623	7.706	8.215	0.493	8.204
6.050	0.736	6.496	6.778	0.702	7.149	7.506	0.620	7.719	8.234	0.489	8.215
6.068	0.737	6.515	6.796	0.699	7.163	7.524	0.618	7.734	8.252	0.485	8.226
6.086	0.736	6.531	6.814	0.698	7.178	7.542	0.615	7.745	8.270	0.482	8.238
6.104	0.735	6.548	6.832	0.698	7.195	7.560	0.612	7.758	8.288	0.478	8.250
6.123	0.735	6.565	6.851	0.696	7.211	7.579	0.608	7.770	8.306	0.474	8.262
6.141	0.735	6.583	6.869	0.694	7.225	7.597	0.606	7.783	8.325	0.470	8.273
6.159	0.734	6.600	6.887	0.693	7.240	7.615	0.602	7.795	8.343	0.466	8.284
6.177	0.734	6.617	6.905	0.692	7.256	7.633	0.601	7.811	8.361	0.463	8.296
6.195	0.733	6.634	6.923	0.689	7.269	7.651	0.598	7.825	8.379	0.458	8.307
6.214	0.732	6.651	6.942	0.688	7.285	7.669	0.596	7.838	8.397	0.456	8.321
6.232	0.731	6.667	6.960	0.686	7.298	7.688	0.593	7.850	8.416	0.453	8.333
6.250	0.731	6.684	6.978	0.683	7.312	7.706	0.589	7.863	8.434	0.448	8.343
6.268	0.730	6.700	6.996	0.682	7.328	7.724	0.587	7.877	8.452	0.444	8.354
6.286	0.730	6.718	7.014	0.680	7.341	7.742	0.584	7.890	8.470	0.441	8.367
6.305	0.730	6.737	7.033	0.678	7.356	7.760	0.580	7.900	8.488	0.438	8.380
6.323	0.730	6.754	7.051	0.678	7.374	7.779	0.577	7.913	8.507	0.434	8.391
6.341	0.729	6.770	7.069	0.677	7.390	7.797	0.573	7.925	8.525	0.430	8.402
6.359	0.727	6.784	7.087	0.675	7.404	7.815	0.570	7.937	8.543	0.425	8.412
6.377	0.727	6.804	7.105	0.673	7.419	7.833	0.567	7.950	8.561	0.421	8.423
6.396	0.727	6.821	7.124	0.671	7.433	7.851	0.564	7.964	8.579	0.417	8.434
6.414	0.725	6.834	7.142	0.668	7.446	7.870	0.561	7.977	8.598	0.413	8.445
6.432	0.724	6.851	7.160	0.666	7.459	7.888	0.557	7.988	8.616	0.409	8.456
6.450	0.723	6.867	7.178	0.664	7.474	7.906	0.554	8.000	8.634	0.405	8.466
6.468	0.722	6.882	7.196	0.662	7.489	7.924	0.551	8.013	8.652	0.401	8.477
6.487	0.721	6.899	7.215	0.660	7.503	7.942	0.548	8.025	8.670	0.397	8.488
6.505	0.720	6.914	7.233	0.658	7.517	7.961	0.544	8.038	8.689	0.392	8.499
6.523	0.718	6.930	7.251	0.656	7.531	7.979	0.540	8.049	8.707	0.387	8.508
6.541	0.717	6.945	7.269	0.653	7.544	7.997	0.536	8.060	8.725	0.383	8.518
6.559	0.717	6.963	7.287	0.651	7.557	8.015	0.532	8.072	8.743	0.380	8.530
6.578	0.716	6.978	7.306	0.649	7.572	8.033	0.529	8.084	8.761	0.376	8.541
6.596	0.714	6.993	7.324	0.646	7.585	8.052	0.525	8.096	8.780	0.372	8.552
6.614	0.713	7.009	7.342	0.644	7.599	8.070	0.522	8.108	8.798	0.369	8.564
6.632	0.711	7.023	7.360	0.640	7.610	8.088	0.518	8.119	8.816	0.363	8.572

Table VII-4. Potentiometric titration data for PAAm with 0.1 M NaCl.

pH	α	pK
8.834	0.359	8.583
8.852	0.356	8.594
8.871	0.350	8.602
8.889	0.346	8.612
8.907	0.342	8.622
8.925	0.337	8.632
8.943	0.333	8.643
8.962	0.329	8.652
8.980	0.324	8.660
8.998	0.321	8.672
9.016	0.316	8.681
9.034	0.311	8.688
9.053	0.307	8.699
9.071	0.304	8.710
9.089	0.300	8.721
9.107	0.295	8.729
9.125	0.290	8.736
9.144	0.286	8.747
9.162	0.282	8.756
9.180	0.278	8.765
9.198	0.273	8.773
9.216	0.268	8.781
9.235	0.264	8.790
9.253	0.260	8.799
9.271	0.255	8.806
9.289	0.251	8.814
9.307	0.246	8.821
9.326	0.241	8.828
9.344	0.237	8.837
9.362	0.234	8.846
9.380	0.231	8.858
9.398	0.227	8.867
9.417	0.223	8.873
9.435	0.218	8.880
9.453	0.213	8.886
9.471	0.208	8.891
9.489	0.206	8.904
9.507	0.202	8.910
9.526	0.197	8.916
9.544	0.192	8.919
9.562	0.188	8.926
9.580	0.183	8.931
9.598	0.179	8.938
9.617	0.175	8.943
9.635	0.171	8.949
9.653	0.167	8.954
9.671	0.163	8.959
9.689	0.157	8.961
9.708	0.154	8.968
9.726	0.151	8.974
9.744	0.146	8.978
9.762	0.142	8.982
9.780	0.139	8.988
9.799	0.135	8.992
9.817	0.131	8.995
9.835	0.126	8.992
9.853	0.122	8.996
9.871	0.118	8.999
9.890	0.114	8.997
9.908	0.109	8.997
9.926	0.106	9.001
9.944	0.103	9.002
9.962	0.099	9.003
9.981	0.096	9.007
9.999	0.092	9.004
10.017	0.088	9.000
10.035	0.084	8.998
10.053	0.081	8.997
10.072	0.078	8.997
10.090	0.073	8.983
10.108	0.070	8.985
10.126	0.066	8.977
10.144	0.063	8.970
10.163	0.060	8.964
10.181	0.056	8.950
10.199	0.053	8.945
10.217	0.049	8.927
10.235	0.046	8.920
10.254	0.042	8.898
10.272	0.039	8.885
10.290	0.036	8.856
10.308	0.032	8.826
10.326	0.030	8.810
10.345	0.027	8.780
10.363	0.022	8.716
10.381	0.020	8.690
10.399	0.016	8.614
10.417	0.013	8.546
10.436	0.011	8.468
10.454	0.007	8.329
10.472	0.005	8.206
10.490	0.003	7.944

APPENDIX VIII - CONDUCTIMETRIC TITRATION TECHNIQUE

Prior to analysis, a 0.01M KCl solution was prepared and used to calibrate the conductivity meter. The meter was adjusted to read 1408 micromhos/cm. PAAm samples were analyzed by adding 50 ml of sample at approximately 10 meq./L to the reaction vessel. The probes were put into position and the nitrogen blanket was started. After the vessel reached a constant temperature, the titration was started by immersing the probes (with the conductivity probe in place of the thermometer) and pressing the titrator start switch. An eyedropper bulb was used to continuously pump fresh solution into the conductivity probe by hand. Every 0.2 ml the pumping was stopped and the conductivity was recorded. The Metrohm Potentiograph Recording Titrator, model 536, recorded pH throughout the duration of the titration. The Dosimat 665 dispensed 0.1M HCl at a constant rate of $\frac{1}{3}$ ml/ min.

The pH curves were digitized in the same manner as the potentiometric titration curves (see APPENDIX VI). First the x and y axis were marked at the corner of each curve. Then, a reduced photocopy of each curve was taken so that they would fit well inside the borders of an 8.5 x 11 in. sheet of paper. The curves were then digitized using a Hewlett-Packard ColorPro plotter and Unplotit® hardware and software, with pH read as the y axis. The sensitivity was set to read data points every 0.01 in. on the x axis.

APPENDIX IX - CONDUCTIMETRIC TITRATION DATA

Tables IX-1 through IX-4 below list data from the conductimetric titration of PAAm. The technique used is discussed in Appendix VIII above. The results are discussed in the PAAm - characterization section.

Table IX-1. Conductimetric titration data for PAAm with no added NaCl.

ml	mmhos	pH
0.00	3.30	
0.20	3.30	
0.40	3.20	
0.60	3.20	
0.80	3.10	
1.00	3.00	11.30
1.20	3.00	11.30
1.40	2.90	11.30
1.60	2.90	11.30
1.80	2.80	11.30
2.00	2.80	11.20
2.20	2.70	11.20
2.40	2.70	11.20
2.60	2.60	11.20
2.80	2.60	11.10
3.00	2.50	11.10
3.20	2.50	11.10
3.40	2.40	11.00
3.60	2.40	11.00
3.80	2.30	10.90
4.00	2.30	10.80
4.20	2.20	10.80
4.40	2.20	10.70
4.80	2.10	10.50
5.00	2.10	10.30
5.20	2.10	10.20
5.40	2.06	9.99
5.60	2.06	9.80
5.80	2.06	9.60
6.00	2.07	9.43
6.20	2.07	9.27
6.40	2.08	9.09
6.60	2.08	8.94
6.80	2.09	8.80
7.00	2.09	8.66
7.20	2.09	8.52
7.40	2.09	8.38
7.60	2.09	8.22
7.80	2.10	8.08
8.00	2.10	7.94
8.20	2.10	7.79
8.40	2.10	7.65
8.60	2.10	7.49
8.80	2.10	7.33
9.00	2.09	7.15
9.20	2.09	6.95
9.40	2.09	6.71
9.60	2.09	6.39
9.80	2.09	5.92
10.00	2.12	4.51
10.20	2.23	3.95
10.40	2.34	3.76
10.80	2.55	3.54
11.00	2.66	3.46
11.20	2.78	3.39
11.40	2.92	3.34
11.60	3.06	3.29
11.80	3.21	3.25
12.00	3.34	3.21
12.20	3.45	3.17
12.40	3.56	3.15
12.60	3.66	3.12
12.80	3.75	3.09
13.00	3.83	3.06
13.40	4.02	3.01
13.80	4.22	2.97
14.00	4.34	

Table IX-2. Conductimetric titration data for PAAm in 0.001 M NaCl.

ml	mmhos	pH
0.00	2.80	
0.20	2.80	11.20
0.40	2.70	11.20
0.60	2.70	11.20
1.00	2.50	11.10
1.20	2.50	11.10
1.40	2.40	11.10
1.60	2.40	11.00
1.80	2.30	11.00
2.00	2.30	10.90
2.20	2.20	10.90
2.40	2.20	10.80
2.60	2.20	10.80
2.80	2.10	10.70
3.00	2.10	10.60
3.20	2.00	10.50
3.40	2.00	10.40
3.60	2.00	10.20
3.80	2.00	10.00
4.00	2.00	9.90
4.20	2.00	9.70
4.40	2.00	9.50
4.60	2.00	9.30
5.00	1.99	9.01
5.20	2.00	8.87
5.40	2.01	8.73
5.60	2.01	8.59
5.80	2.02	8.44
6.00	2.02	8.29
6.20	2.02	8.16
6.40	2.03	8.02
6.60	2.03	7.88
6.80	2.03	7.74
7.00	2.03	7.59
7.20	2.03	7.43
7.40	2.03	7.26
7.60	2.03	7.09
7.80	2.03	6.86
8.00	2.03	6.58
8.20	2.03	6.24
8.40	2.02	5.81
8.60	2.03	4.80
8.80	2.11	4.06
9.00	2.22	3.82
9.20	2.34	3.67
9.40	2.46	3.58
9.60	2.58	3.50
9.80	2.71	3.43
10.00	2.84	3.37
10.20	2.96	3.32
10.40	3.08	3.28
10.80	3.31	3.21
11.00	3.43	3.17
11.20	3.54	3.14
11.40	3.65	3.11
11.60	3.76	3.09
11.80	3.88	3.07
12.00	3.99	3.04

Table IX-3. Conductimetric titration data for PAAm in 0.01 M NaCl.

ml	mmhos	pH
0.00	5.40	
0.20	5.40	
0.40	5.30	
0.80	5.20	
1.00	5.10	11.40
1.40	5.00	11.40
1.60	4.90	11.40
1.80	4.90	11.40
2.00	4.80	11.40
2.20	4.80	11.40
2.60	4.70	11.30
3.00	4.50	11.30
3.40	4.40	11.30
3.60	4.40	11.20
3.80	4.30	11.20
4.00	4.30	11.20
4.20	4.20	11.20
4.40	4.20	11.10
4.60	4.10	11.10
5.00	4.00	11.00
5.20	3.97	11.00
5.40	3.92	10.96
5.60	3.87	10.92
5.80	3.83	10.86
6.00	3.78	10.80
6.20	3.74	10.74
6.40	3.69	10.66
6.60	3.66	10.56
6.80	3.62	10.46
7.00	3.59	10.33
7.20	3.57	10.18
7.40	3.56	10.02
7.60	3.55	9.85
7.80	3.55	9.68
8.00	3.55	9.51
8.20	3.55	9.36
8.40	3.56	9.21
8.60	3.56	9.06
9.00	3.57	8.78
9.20	3.57	8.65
9.40	3.57	8.51
9.60	3.57	8.38
9.80	3.57	8.23
10.00	3.57	8.09
10.20	3.57	7.94
10.40	3.57	7.79
10.60	3.57	7.64
10.80	3.57	7.48
11.00	3.57	7.30
11.20	3.57	7.08
11.40	3.56	6.82
11.60	3.56	6.46
11.80	3.56	5.66
12.00	3.61	4.18
12.20	3.71	3.89
12.40	3.83	3.75
12.60	3.94	3.64
12.80	4.04	3.56
13.00	4.15	3.49
13.20	4.27	3.43
13.40	4.38	3.38
13.60	4.48	3.33
13.80	4.60	3.30
14.00	4.72	3.26
14.20	4.84	3.23
14.40	4.94	3.20
14.60	5.04	
14.80	5.14	
15.00	5.23	

Table IX-4. Conductimetric titration data for PAAm in 0.1 M NaCl.

ml	mmhos	pH
0.20	15.10	
0.40	15.10	
0.60	15.00	11.50
0.80	15.00	11.50
1.00	14.90	11.50
1.20	14.90	11.50
1.40	14.80	11.50
1.60	14.80	11.40
1.80	14.70	11.40
2.00	14.60	11.40
2.20	14.60	11.40
2.40	14.50	11.40
2.60	14.50	11.40
2.80	14.40	11.40
3.00	14.40	11.30
3.20	14.30	11.30
3.40	14.30	11.30
3.60	14.20	11.30
3.80	14.20	11.30
4.00	14.10	11.20
4.20	14.09	11.23
4.40	14.03	11.21
4.60	13.98	11.18
5.00	13.90	11.13
5.20	13.86	11.10
5.60	13.77	11.04

ml	mmhos	pH
5.80	13.72	11.01
6.00	13.69	10.97
6.40	13.61	10.88
6.60	13.57	10.83
6.80	13.53	10.78
7.00	13.49	10.72
7.20	13.45	10.64
7.40	13.42	10.57
7.60	13.39	10.48
7.80	13.37	10.38
8.00	13.35	10.28
8.20	13.34	10.16
8.40	13.33	10.04
8.60	13.33	9.92
8.80	13.33	9.78
9.00	13.34	9.66
9.20	13.34	9.53
9.40	13.33	9.41
9.60	13.35	9.28
9.80	13.36	9.15
10.00	13.36	9.02
10.20	13.37	8.90
10.40	13.36	8.77
10.60	13.38	8.65
10.80	13.39	8.52
11.00	13.39	8.39

ml	mmhos	pH
11.20	13.39	8.24
11.40	13.38	8.09
11.80	13.42	7.77
12.00	13.41	7.60
12.20	13.42	7.39
12.40	13.41	7.14
12.60	13.41	6.84
12.80	13.41	6.36
13.00	13.50	4.08
13.20	13.60	3.76
13.40	13.69	3.60
13.60	13.80	3.49
13.80	13.92	3.39
14.00	14.01	3.33
14.20	14.09	3.27
14.40	14.14	3.22
14.60	14.21	3.18
14.80	14.32	3.13
15.00	14.46	3.10
15.20	14.61	3.07
15.40	14.77	3.03
15.60	14.91	3.01
15.80	15.05	2.98
16.00	15.17	

APPENDIX X - COLLOID TITRATION TECHNIQUE

The following is a detailed description of the colloid titration technique used to quantify the amount of PAAm in solution.

Preparation

1. Estimate the approximate concentration range of the unknown samples to be titrated.

2. Calculate the PVSK titrant concentration necessary to neutralize 1.0 gm of PAAm solution at mid-range using 10 ml of titrant. The following equation applies:

$$M_s \times C_s = V_t \times N_t$$

where: M_s = the mass of sample
C_s = the concentration of the sample in equivalents/gm
V_t = the volume of titrant
N_t = the normality of the titrant

Note: Prepare all positively charged polyelectrolyte solutions in non-adsorbing flasks (ie. polypropylene or polymethyl pentene).

Titrations

Table X-1. Brinkman titrator settings for colloid titrations.

mm/100% vol. =	200.00	mV span =	500.00
stop %U =	off	%U =	8.30
auto control =	off	damping =	on
min./100% vol. =	20.00	mV/pH =	100.00
mV x 100 =	6.00	selector =	mV, pH

1. Prepare the PVSK solution according to the concentration calculated in the preparation section (steps 1 and 2) using pH 4, Nanopure® water for dilution.

2. Prepare a BTC solution at approximately the same concentration as that calculated for the mid-range in the PAAm unknown solutions calculated in step 2 in the preparations section above.

3. Weigh 0.15 gm of the BTC solution in a polypropylene beaker. Add 0.10 ml of a 0.005% TB solution and 50 ml of pH 4, Nanopure® water. Set the beaker on the titrator stirrer.

4. Insert the colorimeter probe into the beaker and shake gently to remove any bubbles from the probe void. Insert the burette tip into the beaker as far from the probe as possible and start the stirrer.

5. Start the titration without delay by pressing the "measure" paddle switch.

6. After the titration has passed the end point, press the "measure" paddle switch again to stop the titration and turn off the stirrer.

7. Remove the burette tip and the colorimeter probe from the beaker. Rinse the burette tip and the probe colorimeter with distilled water.

8. Determine the titration end point using the end point ruler (supplied by Brinkmann) according to method 1 in Figure X-1 below. Count the number of mm from the start of the titration to the end point. Multiply the mm by 0.1 ml/mm to get ml of titrant added.

Use the equation given in step 2 of the preparation section and the solution concentration of the BTC primary standard to determine the concentration of the titrant.

9. Repeat steps 4 through 9 as desired and average the results.

10. Weigh 0.1 to 10 gm of the unknown PAAm solution in a polypropylene beaker. Add 0.10 ml of a 0.005% TB solution and 50 ml of pH 4, Nanopure® water. Set the beaker on the titrator stirrer.

11. Perform steps 5 through 7 using the PAAm solution.

12. Determine the titration end point by extending the curves according to method 2 in Figure X-1 below. Count the number of mm from the start of the titration to the end point. Multiply the mm by 0.1 ml/mm to get ml of titrant added. Calculate the concentration of the PAAm sample using the equation given in step 2 of the preparation section and the titrant concentration from step 8 above.

13. Repeat steps 11 and 12 as desired and average the results.

The end point determinations used require some explanation. Method 1 is the technique recommended by Brinkmann, which is based on the assumption that the titration curves are symmetric. This method gives reproducible results for BTC titrations. However, PAAm titration curves can exhibit visually detectable asymmetry. Method 2 was developed by Matthew H. Lang at IPST to compensate for the asymmetry. When titrating PAAm, end point detection was more reproducible if Method 2 was used. The two methods are shown below in Figure X-1.

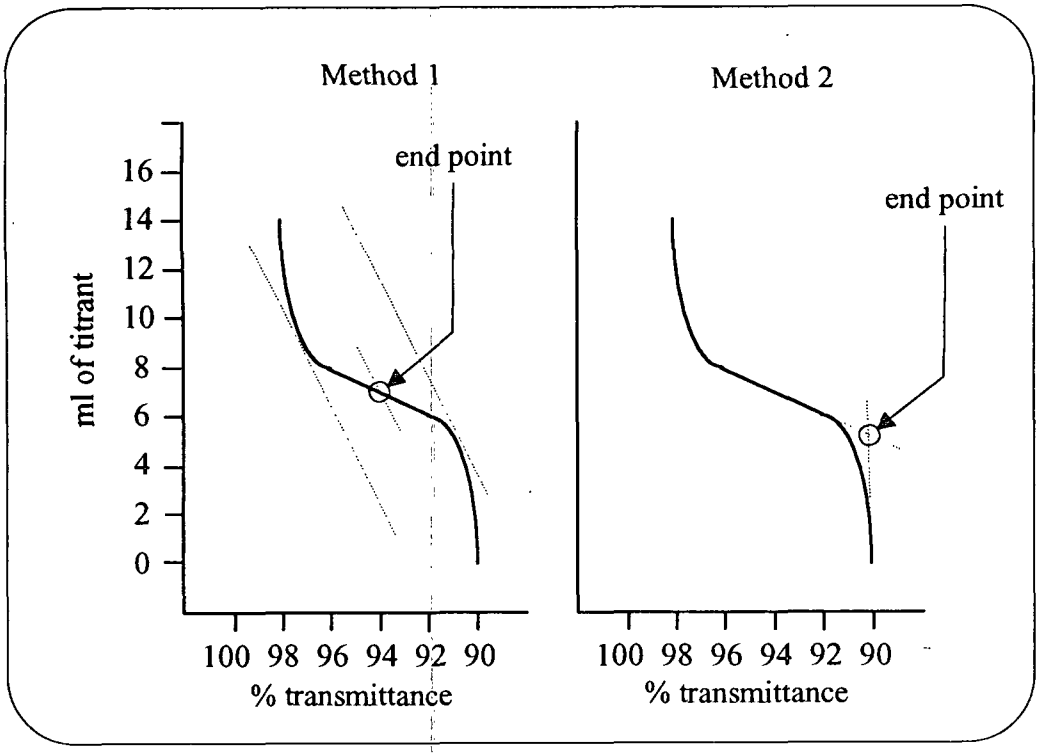

Figure X-1. Alternate methods for determining the end point of the colloid titration curve.

APPENDIX XI - ADSORPTION ISOTHERMS

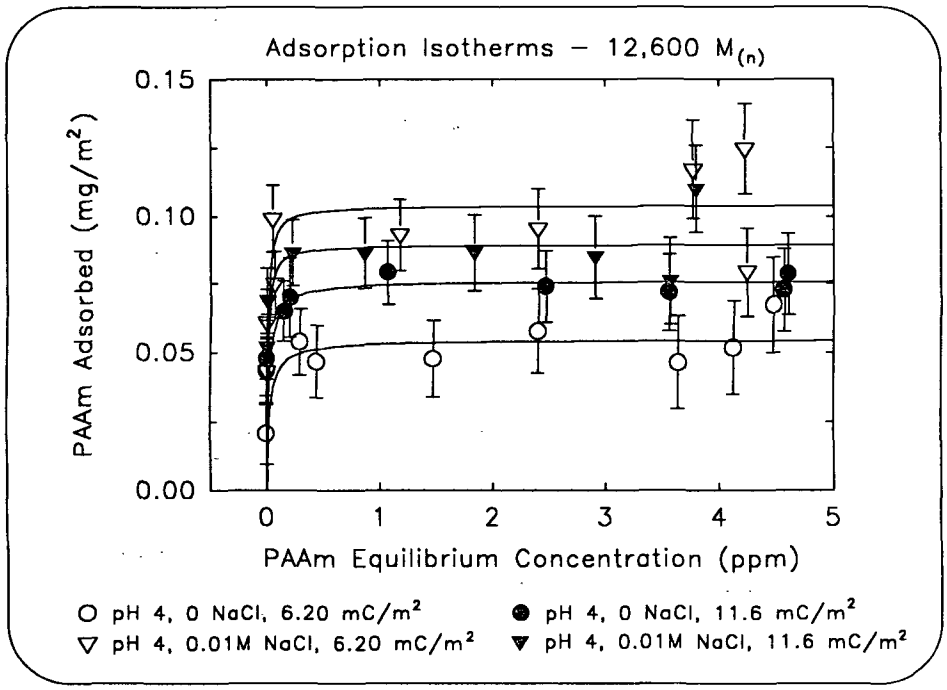

Figure XI-1. Adsorption at pH 4.0 for 12,600 $M_{(n)}$ PAAm.

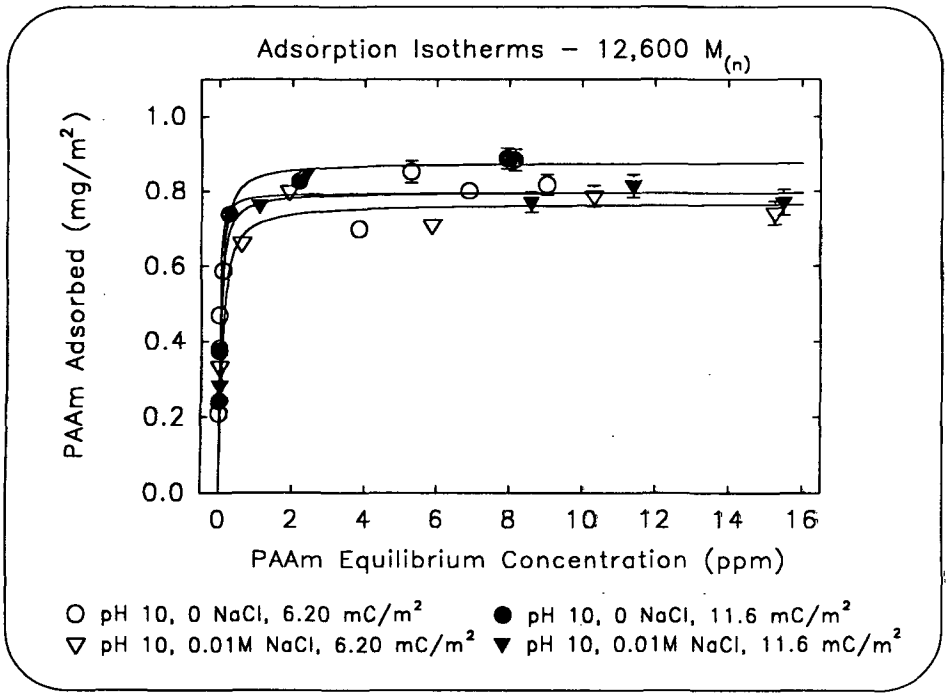

Figure XI-2. Adsorption at pH 10.0 for 12,600 $M_{(n)}$ PAAm.

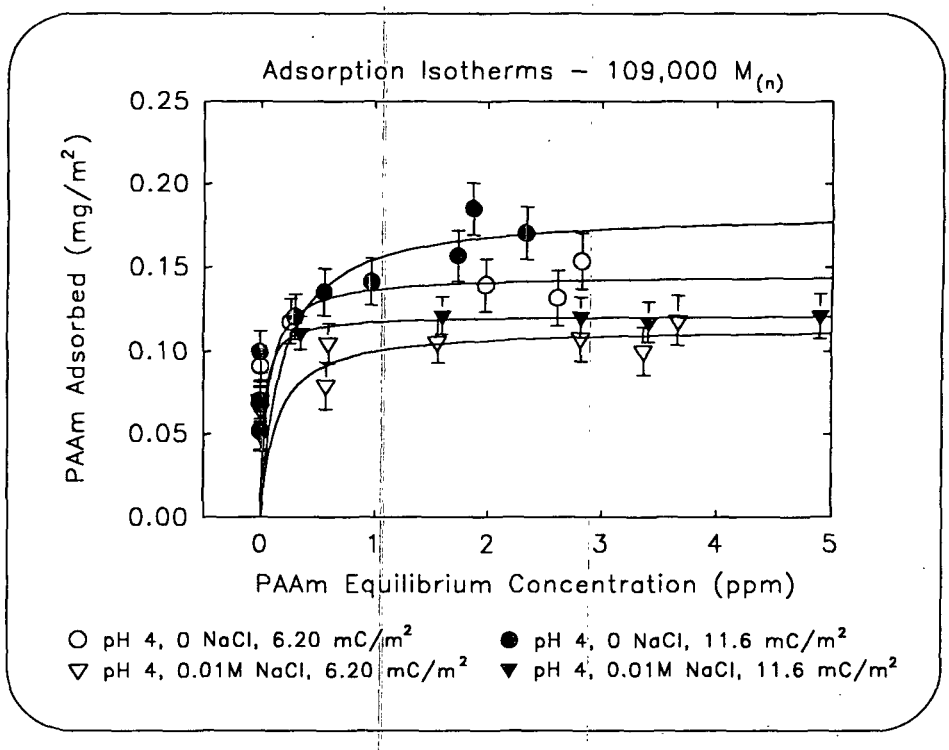

Figure XI-3. Adsorption at pH 4.0 for 109,000 $M_{(n)}$ PAAm.

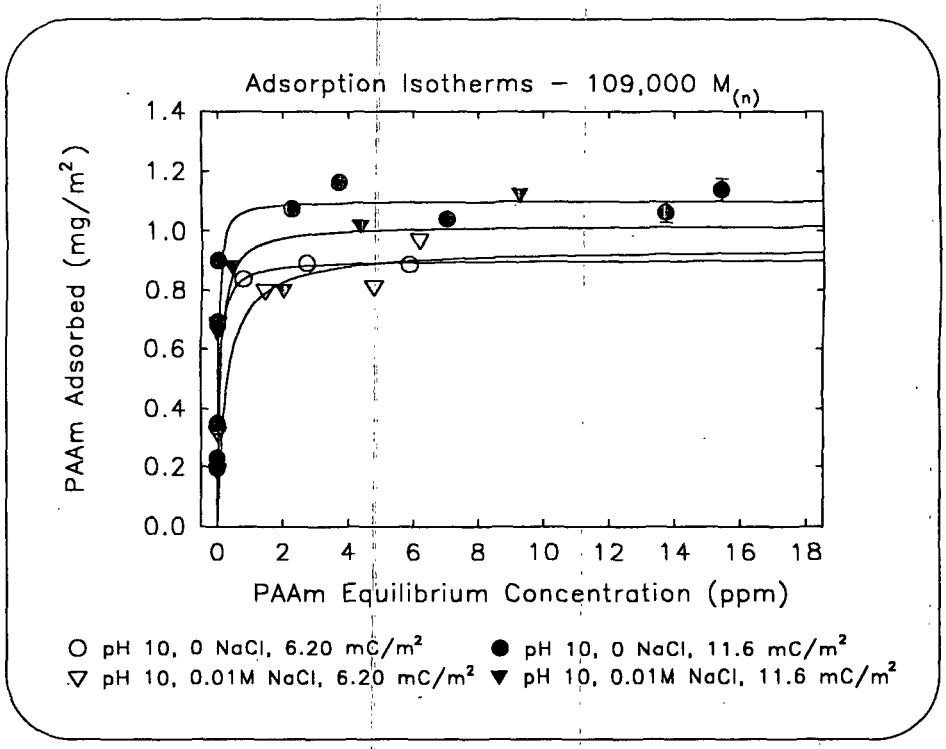

Figure XI-4. Adsorption at pH 10.0 for 109,000 $M_{(n)}$ PAAm.

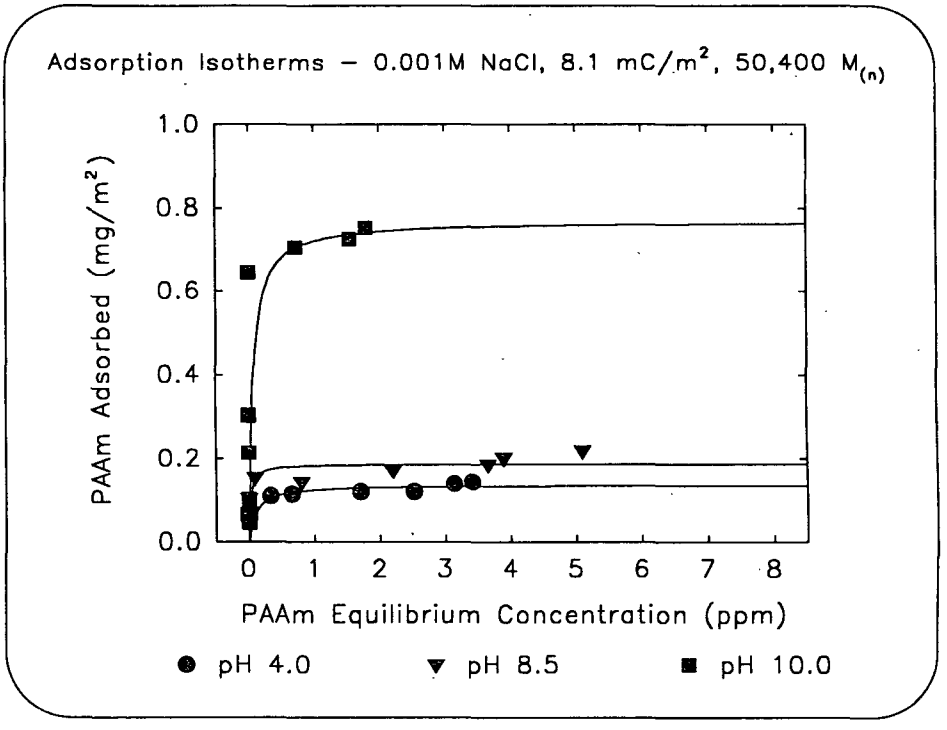

Figure XI-5. PAAm adsorption at pH 4.0, 8.5, and 10.0.

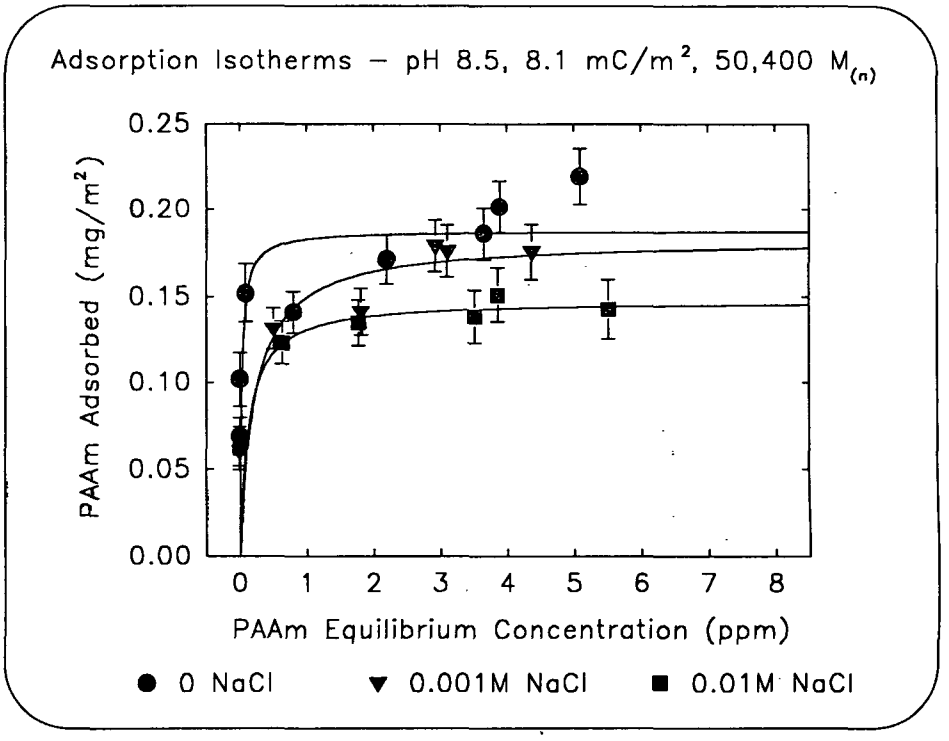

Figure XI-6. PAAm adsorption at 0, 0.001, and 0.01M NaCl.

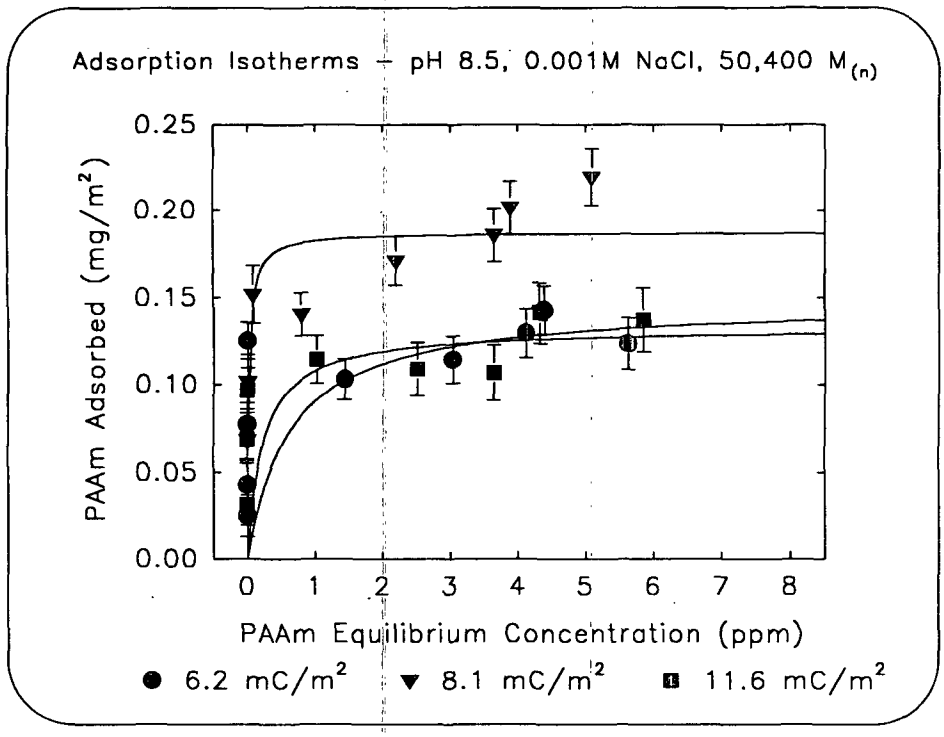

Figure XI-7. PAAm adsorption on 6.2, 8.1, and 11.6 mC/m^2 PSL.

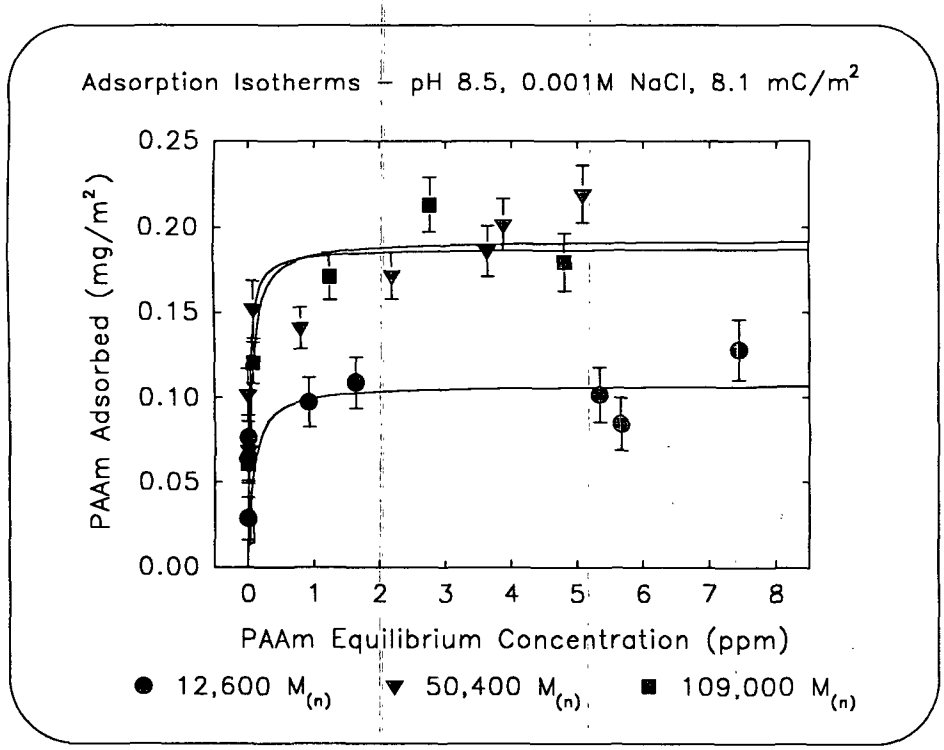

Figure XI-8. Adsorption with 12,600, 50,400, and 109,000 $M_{(n)}$ PAAm.

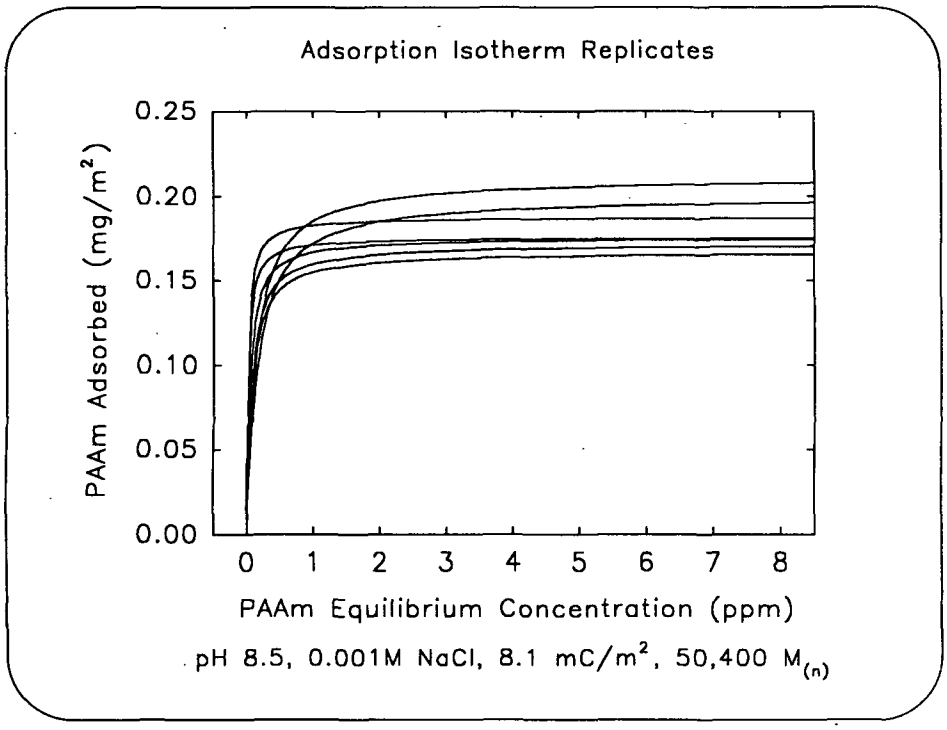

Figure XI-9. Adsorption isotherm replicates.

APPENDIX XII - ADSORPTION ISOTHERM DATA

Table XII-1 contains the data points shown in the adsorption isotherms in Appendix XI. The eq./gm values for PAAm and Filtrate are titrated values. The PAAm and PSL masses are the sample masses used in each adsorption. The remainder of the data are calculated values.

Table XII-1. Adsorption isotherm data.

Treatment	PAAm eq./gm	Filtrate eq./gm	PAAm gms	PSL gms	Surface Area m^2	Filtrate ppm	Adsorbed mg/m^2	Adsorbed error
#1A-A1	2.3035E-08	4.7143E-09	5.1357	5.0253	1.4083E-01	0.4411	0.0468	0.0132
#1A-B1	4.6324E-08	1.5777E-08	4.9200	4.9945	1.3997E-01	1.4761	0.0478	0.0140
#1A-C1	6.8917E-08	2.5686E-08	5.0795	5.1107	1.4322E-01	2.4032	0.0577	0.0151
#1A-D1	8.7711E-08	3.8945E-08	5.3526	4.9428	1.3852E-01	3.6436	0.0463	0.0169
#1A-E1	1.0298E-07	4.4105E-08	4.9879	4.9263	1.3805E-01	4.1264	0.0518	0.0170
#1A-F1	1.1677E-07	4.7847E-08	4.8362	4.9034	1.3741E-01	4.4764	0.0672	0.0173
#1A-G1	6.8541E-09	0.0000E+00	4.9998	5.1697	1.5601E-01	0.0000	0.0206	0.0113
#1A-H1	1.3264E-08	0.0000E+00	5.1141	4.8227	1.4554E-01	0.0000	0.0436	0.0120
#1A-I1	2.3825E-08	3.1072E-09	4.7868	4.8378	1.4599E-01	0.2907	0.0539	0.0120
#2B-A1	1.1769E-07	0.0000E+00	5.3113	5.2499	1.2481E-01	0.0000	0.4686	0.0189
#2B-B1	3.1201E-07	5.6342E-08	5.2152	4.8917	1.1630E-01	5.2712	0.8509	0.0292
#2B-C1	7.1229E-08	0.0000E+00	5.0930	5.0872	1.6198E-01	0.0000	0.2095	0.0127
#2B-D1	1.2494E-07	0.0000E+00	5.0086	4.8264	1.5367E-01	0.0000	0.3810	0.0145
#2B-E1	1.9590E-07	1.2594E-09	5.0614	4.9021	1.5608E-01	0.1178	0.5868	0.0165
#2B-F1	3.0937E-07	4.1153E-08	5.1434	4.9498	1.5760E-01	3.8502	0.6980	0.0210
#2B-G1	3.9958E-07	7.3453E-08	5.1324	4.8407	1.5413E-01	6.8721	0.8002	0.0248
#2B-H1	4.8573E-07	9.6353E-08	5.1865	5.3950	1.7178E-01	9.0145	0.8168	0.0266
#3A-A1	2.3689E-08	0.0000E+00	5.1144	4.9739	1.6192E-01	0.0000	0.0700	0.0112
#3A-B1	4.7808E-08	6.4014E-09	5.0672	4.8933	1.5929E-01	0.5989	0.1048	0.0122
#3A-C1	6.8859E-08	1.6654E-08	5.0823	4.9626	1.6155E-01	1.5581	0.1058	0.0130
#3A-D1	9.5889E-08	3.0118E-08	5.0932	4.9556	1.6132E-01	2.8177	0.1077	0.0141
#3A-E1	1.0438E-07	3.5991E-08	4.9961	4.8250	1.5707E-01	3.3672	0.1001	0.0146
#3A-F1	1.1909E-07	3.9195E-08	5.2043	5.1746	1.6845E-01	3.6670	0.1183	0.0149
#3A-G1	1.8362E-08	0.0000E+00	5.0235	4.9840	1.3395E-01	0.0000	0.0644	0.0133

Treatment	PAAm eq./gm	Filtrate eq./gm	PAAm gms	PSL gms	Surface Area m^2	Filtrate ppm	Adsorbed mg/m^2	Adsorbed error
#3A-H1	3.3600E-08	6.1427E-09	5.1473	4.8978	1.3163E-01	0.5747	0.0791	0.0143
#4B-A1	5.8581E-08	0.0000E+00	5.3032	5.2215	1.5232E-01	0.0000	0.1908	0.0136
#4B-B1	9.6671E-08	0.0000E+00	5.1032	4.9605	1.4471E-01	0.0000	0.3190	0.0148
#4B-C1	2.0238E-07	0.0000E+00	5.1874	4.8903	1.4266E-01	0.0000	0.6885	0.0184
#4B-D1	2.6991E-07	1.5230E-08	5.1778	4.9807	1.4530E-01	1.4249	0.8002	0.0209
#4B-E1	3.4648E-07	5.0827E-08	5.0829	4.9380	1.4405E-01	4.7552	0.8130	0.0243
#4B-F1	4.2310E-07	6.5824E-08	5.2845	5.1207	1.4938E-01	6.1583	0.9714	0.0272
#5A-A1	2.6309E-08	1.5741E-09	5.0769	5.0263	1.6950E-01	0.1473	0.0649	0.0109
#5A-B1	5.1871E-08	1.1451E-08	5.0858	5.1421	1.7340E-01	1.0713	0.0791	0.0117
#5A-C1	7.7646E-08	2.6419E-08	5.1615	4.9812	1.6798E-01	2.4717	0.0740	0.0131
#5A-D1	9.9990E-08	3.8084E-08	5.1249	4.9615	1.6731E-01	3.5630	0.0717	0.0140
#5A-E1	1.1869E-07	4.8846E-08	5.2002	4.8407	1.6324E-01	4.5699	0.0727	0.0151
#5A-F1	1.2689E-07	4.9218E-08	3.9139	3.9210	1.3222E-01	4.6047	0.0785	0.0148
#5A-G1	1.3319E-08	0.0000E+00	4.9923	5.0543	1.2966E-01	0.0000	0.0480	0.0136
#5A-H1	2.2449E-08	2.1428E-09	5.0500	4.8098	1.2339E-01	0.2005	0.0699	0.0145
#6B-A1	7.3149E-08	0.0000E+00	5.2409	5.0526	1.4898E-01	0.0000	0.2408	0.0140
#6B-B1	1.1846E-07	0.0000E+00	5.1276	5.1575	1.5207E-01	0.0000	0.3737	0.0151
#6B-C1	2.3265E-07	2.7042E-09	5.0327	4.9243	1.4519E-01	0.2530	0.7371	0.0189
#6B-D1	2.9642E-07	2.3351E-08	5.1604	4.9686	1.4650E-01	2.1847	0.8258	0.0217
#6B-E1	4.1845E-07	8.4575E-08	5.2759	4.8365	1.4261E-01	7.9126	0.8873	0.0281
#6B-F1	4.4349E-07	8.6939E-08	5.2090	5.0856	1.4995E-01	8.1337	0.8830	0.0281
#7A-A1	2.2423E-08	0.0000E+00	5.0202	5.1258	1.5318E-01	0.0000	0.0688	0.0119
#7A-B1	4.5554E-08	9.2614E-09	5.0399	4.9688	1.4848E-01	0.8665	0.0862	0.0131
#7A-C1	6.5942E-08	1.9677E-08	5.0517	4.9448	1.4777E-01	1.8409	0.0864	0.0141
#7A-D1	8.7119E-08	3.1110E-08	5.1021	4.9116	1.4678E-01	2.9106	0.0848	0.0152
#7A-E1	9.8548E-08	3.8177E-08	5.0277	4.8592	1.4521E-01	3.5718	0.0760	0.0158
#7A-F1	1.1667E-07	4.0611E-08	5.0863	5.1096	1.5269E-01	3.7994	0.1099	0.0161
#7A-G1	1.6982E-08	0.0000E+00	5.1255	5.2630	1.5652E-01	0.0000	0.0520	0.0118
#7A-H1	3.2590E-08	2.4057E-09	4.5272	4.5763	1.3610E-01	0.2251	0.0864	0.0124
#8B-A1	8.9994E-08	0.0000E+00	5.2460	5.2933	1.5725E-01	0.0000	0.2809	0.0141
#8B-B1	2.5073E-07	1.1610E-08	5.1978	4.9003	1.4558E-01	1.0862	0.7622	0.0200
#8B-C1	3.2283E-07	2.5278E-08	5.1804	5.2551	1.5612E-01	2.3649	0.8442	0.0219
#8B-D1	4.0753E-07	9.1643E-08	5.0680	4.7589	1.4138E-01	8.5739	0.7708	0.0275

Treatment	PAAm eq./gm	Filtrate eq./gm	PAAm gms	PSL gms	Surface Area m^2	Filtrate ppm	Adsorbed mg/m^2	Adsorbed error
#8B-E1	4.8381E-07	1.2166E-07	5.1690	4.9271	1.4637E-01	11.3824	0.8134	0.0306
#8B-F1	5.5398E-07	1.6555E-07	5.0748	4.8066	1.4279E-01	15.4885	0.7702	0.0342
#9A-A1	2.1173E-08	0.0000E+00	5.2399	5.2221	1.4849E-01	0.0000	0.0699	0.0126
#9A-B1	4.2201E-08	2.8441E-09	4.7923	4.8748	1.3861E-01	0.2661	0.1180	0.0133
#9A-C1	6.1633E-08	9.4381E-10	5.2860	4.9306	1.4020E-01	0.0883	0.2110	0.0144
#9A-D1	8.1833E-08	2.1143E-08	5.1457	4.9173	1.3982E-01	1.9780	0.1394	0.0156
#9A-E1	9.2488E-08	2.7905E-08	5.2435	4.9857	1.4177E-01	2.6107	0.1317	0.0162
#9A-F1	1.0034E-07	3.0132E-08	5.4079	4.9423	1.4053E-01	2.8190	0.1536	0.0168
#9A-G1	1.7030E-08	0.0000E+00	4.8493	5.0065	1.5027E-01	0.0000	0.0514	0.0116
#9A-H1	2.8612E-08	0.0000E+00	5.0046	4.9163	1.4756E-01	0.0000	0.0908	0.0123
#10B-A1	6.3559E-08	0.0000E+00	4.9360	4.9431	1.4884E-01	0.0000	0.1972	0.0132
#10B-B1	1.0025E-07	0.0000E+00	5.2973	4.8649	1.4648E-01	0.0000	0.3392	0.0149
#10B-C1	2.0804E-07	0.0000E+00	5.2819	4.9670	1.4956E-01	0.0000	0.6874	0.0181
#10B-D1	2.8101E-07	8.1912E-09	5.2408	5.1452	1.5492E-01	0.7664	0.8380	0.0201
#10B-E1	3.5211E-07	2.8979E-08	4.7842	4.8910	1.4727E-01	2.7112	0.8920	0.0225
#10B-F1	4.1223E-07	6.2594E-08	5.1850	5.2052	1.5673E-01	5.8561	0.8877	0.0255
#11A-A1	2.5789E-08	7.2590E-10	5.0778	5.0842	1.5450E-01	0.0679	0.0748	0.0120
#11A-B1	5.4709E-08	1.2593E-08	5.0857	4.9999	1.5193E-01	1.1782	0.0931	0.0133
#11A-C1	7.7466E-08	2.5705E-08	5.0324	4.5951	1.3963E-01	2.4049	0.0954	0.0149
#11A-D2	1.0239E-07	2.2213E-08	2.7340	2.8260	8.5875E-02	2.0782	0.1704	0.0146
#11A-E1	1.1438E-07	4.5392E-08	5.1433	4.9864	1.5152E-01	4.2468	0.0793	0.0162
#11A-F1	1.3225E-07	4.5194E-08	2.5431	2.5832	7.8497E-02	4.2283	0.1247	0.0163
#11A-G1	1.1359E-07	4.0327E-08	4.9705	4.9209	1.3225E-01	3.7729	0.1172	0.0179
#11A-H1	1.8245E-07	7.4314E-08	4.9246	4.9637	1.3340E-01	6.9526	0.1148	0.0212
#11A-J1	1.3587E-08	0.0000E+00	5.2502	5.1731	1.5522E-01	0.0000	0.0430	0.0118
#11A-K1	1.9675E-08	0.0000E+00	4.9918	5.0260	1.5081E-01	0.0000	0.0609	0.0119
#11A-L1	3.1813E-08	5.2220E-10	4.8344	4.6843	1.4056E-01	0.0489	0.0991	0.0125
#12B-A1	1.0845E-07	0.0000E+00	5.3663	5.2891	1.6454E-01	0.0000	0.3309	0.0142
#12B-B1	2.2295E-07	6.6133E-09	5.1783	4.9571	1.5421E-01	0.6187	0.6597	0.0180
#12B-C1	2.8975E-07	2.0292E-08	5.2369	4.9356	1.5354E-01	1.8984	0.7988	0.0205
#12B-D1	3.7417E-07	6.2600E-08	5.0350	5.2654	1.6380E-01	5.8567	0.7077	0.0231
#12B-E1	4.5440E-07	1.1015E-07	5.2260	4.8419	1.5063E-01	10.3054	0.7862	0.0284
#12B-F1	5.3755E-07	1.6305E-07	5.1575	4.7188	1.4680E-01	15.2541	0.7406	0.0327

Treatment	PAAm eq./gm	Filtrate eq./gm	PAAm gms	PSL gms	Surface Area m^2	Filtrate ppm	Adsorbed mg/m^2	Adsorbed error
#13A-D2	8.2480E-08	1.8477E-08	5.1548	4.9150	1.4274E-01	1.7286	0.1567	0.0152
#13A-E1	9.3666E-08	1.9923E-08	5.3249	5.0795	1.4752E-01	1.8639	0.1849	0.0156
#13A-F1	1.0311E-07	2.4909E-08	5.2492	5.2802	1.5334E-01	2.3304	0.1702	0.0156
#13B-A1	1.6396E-08	0.0000E+00	5.0495	5.0190	1.4784E-01	0.0000	0.0524	0.0121
#13B-B1	2.1933E-08	0.0000E+00	4.8982	4.9402	1.4552E-01	0.0000	0.0691	0.0122
#13B-C1	3.0714E-08	0.0000E+00	5.0014	4.8978	1.4427E-01	0.0000	0.0996	0.0126
#13B-D1	4.2126E-08	3.2631E-09	5.0843	4.7873	1.4102E-01	0.3053	0.1207	0.0133
#13B-E1	5.1702E-08	5.9557E-09	5.1773	4.8792	1.4373E-01	0.5572	0.1353	0.0137
#13B-F1	6.4265E-08	1.0378E-08	5.4232	5.3230	1.5680E-01	0.9709	0.1414	0.0139
#14B-A1	6.9094E-08	0.0000E+00	5.0790	5.0463	1.4306E-01	0.0000	0.2295	0.0142
#14B-B1	1.0709E-07	0.0000E+00	5.0643	5.1254	1.4530E-01	0.0000	0.3492	0.0153
#14B-C1	2.1443E-07	0.0000E+00	5.0142	5.1206	1.4516E-01	0.0000	0.6929	0.0186
#14B-D1	2.7541E-07	0.0000E+00	5.2125	5.2566	1.4902E-01	0.0000	0.9013	0.0207
#14B-E1	3.6345E-07	2.4231E-08	5.2823	5.1165	1.4505E-01	2.2670	1.0758	0.0247
#14B-F1	3.9999E-07	3.9745E-08	4.7855	4.3889	1.2442E-01	3.7184	1.1651	0.0272
#14B-G1	4.5153E-07	7.5041E-08	5.2939	4.8830	1.4612E-01	7.0206	1.0415	0.0284
#14B-H1	6.0694E-07	1.4667E-07	5.2418	4.9562	1.4831E-01	13.7216	1.0634	0.0351
#14B-I1	7.0912E-07	1.6491E-07	4.9310	5.0691	1.5169E-01	15.4289	1.1395	0.0372
#15A-A1	2.0994E-08	0.0000E+00	5.1456	5.1358	2.0737E-01	0.0000	0.0487	0.0089
#15A-B1	5.1319E-08	3.7883E-09	5.1651	4.7455	1.9161E-01	0.3544	0.1111	0.0101
#15A-C1	8.2957E-08	1.7083E-08	5.2770	5.0055	2.0211E-01	1.5982	0.1213	0.0109
#15A-D1	1.0976E-07	3.0109E-08	5.2152	5.0634	2.0445E-01	2.8169	0.1203	0.0117
#15A-E1	1.2321E-07	3.6477E-08	5.0684	5.0424	2.0360E-01	3.4127	0.1175	0.0120
#15A-F1	1.5389E-07	5.2430E-08	5.0914	4.9329	1.9918E-01	4.9052	0.1212	0.0132
#16B-A1	6.0965E-08	0.0000E+00	4.9993	5.0197	1.4949E-01	0.0000	0.1908	0.0132
#16B-B1	2.0285E-07	0.0000E+00	5.1182	4.9419	1.4717E-01	0.0000	0.6600	0.0179
#16B-C1	2.7755E-07	4.4841E-09	5.2310	4.9966	1.4880E-01	0.4195	0.8840	0.0204
#16B-D1	3.0264E-07	2.1331E-08	4.9324	5.0146	1.4934E-01	1.9956	0.8023	0.0210
#16B-E1	4.0249E-07	4.6495E-08	5.1195	4.9058	1.4610E-01	4.3499	1.0210	0.0256
#16B-F1	5.4795E-07	9.8934E-08	5.2040	5.1058	1.5205E-01	9.2560	1.1269	0.0313
#17A-A1	2.5841E-08	0.0000E+00	4.9356	5.1532	1.7356E-01	0.0000	0.0688	0.0106
#17A-B1	6.5950E-08	8.5468E-09	5.2226	5.0615	1.7047E-01	0.7996	0.1408	0.0123
#17A-C1	1.0683E-07	2.3512E-08	5.2319	5.1201	1.7244E-01	2.1997	0.1712	0.0137

Treatment	PAAm eq./gm	Filtrate eq./gm	PAAm gms	PSL gms	Surface Area m^2	Filtrate ppm	Adsorbed mg/m^2	Adsorbed error
#17A-D1	1.4597E-07	3.9089E-08	4.9974	5.0387	1.6970E-01	3.6571	0.1859	0.0150
#17A-E1	1.5603E-07	4.1627E-08	5.0460	5.0558	1.7028E-01	3.8945	0.2016	0.0154
#17A-F1	1.8694E-07	5.4503E-08	4.5256	4.4906	1.5124E-01	5.0991	0.2194	0.0166
#17A-G1	2.6070E-08	0.0000E+00	4.9432	5.2359	1.1848E-01	0.0000	0.1018	0.0156
#17A-H1	3.7525E-08	9.5261E-10	4.7499	4.6085	1.0428E-01	0.0891	0.1519	0.0168
#18A-A1	2.3320E-08	0.0000E+00	4.9324	5.2100	1.5303E-01	0.0000	0.0703	0.0120
#18A-B1	4.9736E-08	7.0634E-09	5.0562	5.1172	1.5031E-01	0.6608	0.1118	0.0132
#18A-C1	7.1446E-08	1.8214E-08	5.1480	4.9452	1.4525E-01	1.7040	0.1185	0.0146
#18A-D1	9.1012E-08	2.6985E-08	5.0168	4.9986	1.4682E-01	2.5247	0.1187	0.0152
#18A-E1	1.0862E-07	3.3545E-08	4.9322	4.8062	1.4117E-01	3.1383	0.1386	0.0161
#18A-F1	1.2173E-07	3.6502E-08	4.7015	4.9312	1.4484E-01	3.4150	0.1426	0.0160
#18A-G1	1.7826E-08	0.0000E+00	4.9330	4.9129	1.4536E-01	0.0000	0.0566	0.0120
#18A-H1	3.9474E-08	3.5911E-09	5.2351	4.9771	1.4726E-01	0.3360	0.1080	0.0131
#19A-A1	1.7604E-08	0.0000E+00	5.0366	5.1607	1.8267E-01	0.0000	0.0454	0.0099
#19A-B1	3.7344E-08	0.0000E+00	5.1834	5.0742	1.7960E-01	0.0000	0.1008	0.0107
#19A-C1	7.6012E-08	0.0000E+00	5.1838	4.8673	1.7228E-01	0.0000	0.2140	0.0119
#19A-D1	1.1574E-07	0.0000E+00	5.0228	5.0617	1.7916E-01	0.0000	0.3036	0.0125
#19A-G1	1.8722E-07	0.0000E+00	5.0387	5.2030	1.3690E-01	0.0000	0.6447	0.0190
#19A-H1	2.1806E-07	7.6959E-09	4.8166	4.9160	1.2935E-01	0.7200	0.7055	0.0204
#19A-I1	2.4249E-07	1.9286E-08	4.9308	4.7680	1.2545E-01	1.8043	0.7522	0.0223
#19A-K1	3.3199E-07	1.6581E-08	5.0445	4.8004	1.9495E-01	1.5512	0.7254	0.0165
#20A-A1	2.1457E-08	0.0000E+00	4.9999	4.9695	1.6592E-01	0.0000	0.0605	0.0108
#20A-B1	5.5658E-08	5.3400E-09	5.2676	5.0743	1.6942E-01	0.4996	0.1314	0.0120
#20A-C1	8.3000E-08	1.9394E-08	5.3651	4.8907	1.6329E-01	1.8145	0.1412	0.0136
#20A-D1	1.2045E-07	3.1304E-08	5.2117	4.8816	1.6298E-01	2.9287	0.1790	0.0148
#20A-E1	1.2669E-07	3.3196E-08	5.1030	4.9668	1.6583E-01	3.1057	0.1761	0.0147
#20A-F1	1.5916E-07	4.6700E-08	5.0639	5.2081	1.7388E-01	4.3691	0.1756	0.0155
#21A-A1	2.1515E-08	0.0000E+00	5.1375	5.1133	1.6374E-01	0.0000	0.0632	0.0112
#21A-B1	5.3869E-08	6.7336E-09	5.0472	4.8652	1.5580E-01	0.6300	0.1232	0.0125
#21A-C1	8.6085E-08	1.8986E-08	5.0220	5.1753	1.6573E-01	1.7763	0.1348	0.0134
#21A-D1	1.1654E-07	3.7656E-08	5.2870	4.9106	1.5725E-01	3.5230	0.1381	0.0155
#21A-E1	1.3420E-07	4.1331E-08	5.0065	5.0020	1.6018E-01	3.8668	0.1508	0.0156
#21A-F1	1.6198E-07	5.9026E-08	5.2713	5.0341	1.6121E-01	5.5223	0.1425	0.0172

Treatment	PAAm eq./gm	Filtrate eq./gm	PAAm gms	PSL gms	Surface Area m^2	Filtrate ppm	Adsorbed mg/m^2	Adsorbed error
#22A-A1	4.8636E-08	0.0000E+00	5.0396	5.0497	1.8287E-01	0.0000	0.1254	0.0106
#22A-B1	6.6980E-08	1.5334E-08	5.1300	4.7926	1.7356E-01	1.4346	0.1032	0.0118
#22A-C1	9.9523E-08	3.2444E-08	5.1810	4.5272	1.6395E-01	3.0354	0.1145	0.0136
#22A-D1	1.3860E-07	4.4037E-08	5.0824	5.0990	1.8466E-01	4.1200	0.1297	0.0139
#22A-E1	1.5312E-07	4.6995E-08	4.9633	5.1457	1.8635E-01	4.3967	0.1431	0.0141
#22A-F1	1.7265E-07	6.0153E-08	5.1085	5.3219	1.9273E-01	5.6277	0.1236	0.0149
#22A-G1	7.6581E-09	0.0000E+00	5.0369	4.9144	1.4356E-01	0.0000	0.0251	0.0120
#22A-H1	1.2856E-08	0.0000E+00	5.1209	4.8925	1.4292E-01	0.0000	0.0431	0.0123
#22A-I1	2.4368E-08	0.0000E+00	5.0571	5.1115	1.4932E-01	0.0000	0.0772	0.0123
#23A-A1	2.2214E-08	0.0000E+00	4.8841	4.9609	1.4721E-01	0.0000	0.0690	0.0120
#23A-B1	5.6810E-08	1.0913E-08	5.0809	4.9349	1.4644E-01	1.0210	0.1146	0.0137
#23A-C1	8.6682E-08	2.6856E-08	5.1345	4.9937	1.4819E-01	2.5125	0.1093	0.0151
#23A-D1	1.1518E-07	3.8974E-08	4.9482	5.1722	1.5349E-01	3.6463	0.1070	0.0158
#23A-E1	1.2979E-07	4.6241E-08	5.3562	4.9163	1.4589E-01	4.3262	0.1412	0.0176
#23A-F1	1.6644E-07	6.2561E-08	5.1499	5.0403	1.4957E-01	5.8530	0.1374	0.0186
#23A-G1	9.8515E-09	0.0000E+00	5.0275	5.0939	1.4570E-01	0.0000	0.0318	0.0121
#23A-H1	2.8077E-08	0.0000E+00	5.1033	4.8367	1.3834E-01	0.0000	0.0969	0.0131
#24A-A1	2.7133E-08	0.0000E+00	5.3431	5.2418	1.7858E-01	0.0000	0.0760	0.0108
#24A-D1	1.4302E-07	5.7148E-08	5.2522	4.7879	1.6311E-01	5.3466	0.1018	0.0160
#24A-E1	1.5122E-07	6.0547E-08	5.1656	5.1267	1.7466E-01	5.6646	0.0846	0.0156
#24A-F1	2.0319E-07	7.9613E-08	5.0529	4.9438	1.6842E-01	7.4484	0.1282	0.0177
#24B-A1	8.6757E-09	0.0000E+00	4.9349	5.1354	1.4161E-01	0.0000	0.0283	0.0124
#24B-B1	1.8030E-08	0.0000E+00	5.1880	4.9455	1.3637E-01	0.0000	0.0642	0.0132
#24B-C1	2.1900E-08	0.0000E+00	4.9978	4.8550	1.3387E-01	0.0000	0.0765	0.0132
#24B-E1	4.5933E-08	9.8964E-09	5.1893	4.8474	1.3366E-01	0.9259	0.0973	0.0146
#24B-F1	6.7842E-08	1.7580E-08	5.1398	5.1975	1.4332E-01	1.6448	0.1090	0.0150
#25A-A1	2.0385E-08	0.0000E+00	4.9802	4.9621	1.5644E-01	0.0000	0.0607	0.0114
#25A-B1	4.0725E-08	8.8228E-10	5.1582	4.9465	1.5595E-01	0.0825	0.1207	0.0122
#25A-C1	8.0834E-08	1.3430E-08	5.2563	4.9851	1.5716E-01	1.2565	0.1711	0.0138
#25A-D1	1.2177E-07	2.9654E-08	5.2043	4.7226	1.4889E-01	2.7743	0.2133	0.0159
#25A-E1	1.6255E-07	5.1566E-08	5.3147	5.2645	1.6597E-01	4.8243	0.1795	0.0170
#25A-F1	1.9539E-07	4.5773E-08	4.9227	5.0563	1.5941E-01	4.2824	0.2965	0.0174
#26A-A1	6.5477E-09	0.0000E+00	4.9801	5.2332	1.5617E-01	0.0000	0.0195	0.0113

Treatment	PAAm eq./gm	Filtrate eq./gm	PAAm gms	PSL gms	Surface Area m^2	Filtrate ppm	Adsorbed mg/m^2	Adsorbed error
#26A-B1	2.8565E-08	0.0000E+00	5.0241	5.0980	1.5214E-01	0.0000	0.0883	0.0122
#26A-C1	5.6824E-08	3.5206E-09	5.0702	5.1370	1.5330E-01	0.3294	0.1539	0.0131
#26A-D1	7.7909E-08	1.2193E-08	4.9408	4.8611	1.4507E-01	1.1408	0.1712	0.0142
#26A-E1	1.1750E-07	2.6010E-08	4.8750	4.9500	1.4772E-01	2.4334	0.2009	0.0156
#26A-F1	1.5212E-07	4.2552E-08	4.6922	4.6338	1.3828E-01	3.9810	0.2144	0.0174
#27A-A1	6.2637E-09	0.0000E+00	4.9000	4.9512	1.4261E-01	0.0000	0.0201	0.0119
#27A-B1	2.8355E-08	0.0000E+00	5.0227	4.8935	1.4095E-01	0.0000	0.0945	0.0128
#27A-C1	5.6818E-08	6.0493E-09	5.1823	4.9368	1.4220E-01	0.5660	0.1535	0.0141
#27A-D1	8.0881E-08	1.2989E-08	4.9977	4.9573	1.4279E-01	1.2152	0.1801	0.0148
#27A-E1	1.2190E-07	3.3080E-08	4.9604	4.7667	1.3730E-01	3.0949	0.1928	0.0170
#27A-F1	1.5589E-07	4.4290E-08	5.0882	5.5573	1.6007E-01	4.1437	0.1880	0.0173
#28A-A1	6.1529E-09	0.0000E+00	5.0604	5.0175	1.8958E-01	0.0000	0.0154	0.0092
#28A-B1	2.7686E-08	0.0000E+00	5.0875	4.9432	1.8677E-01	0.0000	0.0706	0.0098
#28A-C1	5.7264E-08	2.3259E-09	5.0885	4.7721	1.8031E-01	0.2176	0.1393	0.0108
#28A-D1	5.8893E-08	9.1825E-09	5.0268	5.0600	1.9119E-01	0.8591	0.0995	0.0106
#28A-E1	1.1322E-07	2.1892E-08	4.9923	5.0669	1.9145E-01	2.0481	0.1686	0.0121
#28A-F1	1.5134E-07	3.7233E-08	5.1070	5.0464	1.9067E-01	3.4834	0.1938	0.0136
#29A-A1	4.5606E-09	0.0000E+00	5.2038	4.9376	1.5643E-01	0.0000	0.0142	0.0111
#29A-B1	2.9650E-08	0.0000E+00	4.8012	5.1049	1.6173E-01	0.0000	0.0824	0.0112
#29A-C1	5.5953E-08	5.9530E-09	5.1251	5.0002	1.5842E-01	0.5569	0.1338	0.0126
#29A-D1	7.9786E-08	6.0815E-09	5.0094	4.9773	1.5769E-01	0.5690	0.2011	0.0132
#29A-E1	1.2282E-07	3.1274E-08	5.1267	4.9693	1.5744E-01	2.9259	0.1866	0.0154
#29A-F1	1.5115E-07	4.9539E-08	5.0732	4.9361	1.5639E-01	4.6347	0.1621	0.0167
#30A-A1	4.5184E-09	0.0000E+00	5.2142	4.9395	1.6747E-01	0.0000	0.0132	0.0104
#30A-B1	2.7410E-08	0.0000E+00	5.1273	4.7556	1.6124E-01	0.0000	0.0816	0.0112
#30A-C1	5.1075E-08	2.6918E-09	5.3781	4.9667	1.6840E-01	0.2518	0.1371	0.0119
#30A-D1	7.2491E-08	1.0768E-08	4.9936	4.8057	1.6294E-01	1.0075	0.1473	0.0125
#30A-E1	1.0732E-07	2.7683E-08	5.3091	4.9632	1.6828E-01	2.5900	0.1587	0.0141
#30A-F1	1.4059E-07	3.9161E-08	5.2575	5.0192	1.7018E-01	3.6638	0.1851	0.0152
#31A-A1	5.7491E-09	0.0000E+00	5.0373	5.0908	1.8213E-01	0.0000	0.0149	0.0096
#31A-B1	2.6043E-08	0.0000E+00	5.3241	4.9623	1.7753E-01	0.0000	0.0731	0.0105
#31A-C1	4.9681E-08	1.2960E-09	5.1942	5.0771	1.8164E-01	0.1213	0.1261	0.0109
#31A-D1	7.2631E-08	8.8800E-09	5.2595	5.0149	1.7942E-01	0.8308	0.1516	0.0118

Treatment	PAAm eq./gm	Filtrate eq./gm	PAAm gms	PSL gms	Surface Area m^2	Filtrate ppm	Adsorbed mg/m^2	Adsorbed error
#31A-E1	1.1249E-07	2.4274E-08	5.0786	5.0024	1.7897E-01	2.2710	0.1707	0.0130
#31A-F1	1.4953E-07	4.0484E-08	5.0907	5.0031	1.7899E-01	3.7875	0.1843	0.0144

APPENDIX XIII - STATISTICAL ANALYSIS OF THE ADSORPTION DATA

The following is the output generated by SAS statistical software (SAS Institute Inc.). The data was analyzed using the RSREG procedure for regression analysis of response surfaces. The data was analyzed without coding.

SAS 10:26 Friday, April 2, 1993

Response Surface for Variable GAMMA: Gamma

Response Mean	0.363729
Root MSE	0.053874
R-Square	0.9875
Coef. of Variation	14.8115

Regression	Degrees of Freedom	Sum of Squares	R-Square	F-Ratio	Prob > F
Linear	4	2.513686	0.6773	216.5	0.0000
Quadratic	4	1.101515	0.2968	94.9	0.0000
Crossproduct	6	0.049945	0.0135	2.868	0.0430
Total Regress	14	3.665146	0.9875	90.201	0.0000

Residual	Degrees of Freedom	Sum of Squares	Mean Square	F-Ratio	Prob > F
Lack of Fit	11	0.045181	0.004107	16.340	0.0032
Pure Error	5	0.001257	0.000251		
Total Error	16	0.046438	0.002902		

Parameter	Degrees of Freedom	Parameter Estimate	Standard Error	T for H0: Parameter=0	Prob > |T|
INTERCEPT	1	0.588061	0.377648	1.557	0.1390
ALPHA	1	-3.097315	0.258932	-11.962	0.0000
SALT	1	-57.714252	41.483899	-1.391	0.1832
CHARGE	1	66.452315	91.471285	0.726	0.4780
M	1	-0.000000142	0.000002141	-0.0663	0.9480
ALPHA*ALPHA	1	2.978033	0.257089	11.584	0.0000
SALT*ALPHA	1	-0.349172	7.207093	-0.0484	0.9620
SALT*SALT	1	5950.864237	3888.944374	1.530	0.1455
CHARGE*ALPHA	1	-32.666948	13.584493	-2.405	0.0286

CHARGE*SALT	1	-182.416811	959.340333	-0.190	0.8516
CHARGE*CHARGE	1	-2905.429142	5052.733572	-0.575	0.5733
M*ALPHA	1	-0.000002160	0.000000763	-2.832	0.0120
M*SALT	1	0.000021337	0.000053875	0.396	0.6973
M*CHARGE	1	0.000184	0.000103	1.795	0.0916
M*M	1	4.833792E-12	1.511528E-11	0.320	0.7533

Factor	Degrees of Freedom	Sum of Squares	Mean Square	F-Ratio	Prob > F	
ALPHA	5	2.979723	0.595945	205.3	0.0000	Alpha
SALT	5	0.010675	0.002135	0.736	0.6075	Salt
CHARGE	5	0.044605	0.008921	3.074	0.0393	Charge
M	5	0.105370	0.021074	7.261	0.0010	M

Canonical Analysis of Response Surface

Factor	Critical Value	
ALPHA	0.556129	Alpha
SALT	0.005012	Salt
CHARGE	0.007626	Charge
M	-16587	M

Predicted value at stationary point -0.163371

Canonical Analysis of Response Surface

	Eigenvectors			
Eigenvalues	ALPHA	SALT	CHARGE	M
5951.803467	-0.000001074	0.999947	-0.010297	1.6328244E-9
3.069739	0.999984	-0.000056736	-0.005614	-0.000000521
7.231419E-12	0.000000521	-1.335131E-9	2.8863033E-8	1.000000
-2906.460078	0.005614	0.010297	0.999931	-3.17714E-8

Stationary point is a saddle point.

Estimated Ridge of Maximum Response for Variable GAMMA: Gamma

Radius	Estimated Response	Standard Error
0.0	-0.028422	0.068838
0.1	59.613950	38.739959
0.2	238.288555	155.304423
0.3	535.999229	349.626390
0.4	952.745972	621.705841
0.5	1488.528785	971.542773
0.6	2143.347666	1399.137185
0.7	2917.202617	1904.489076
0.8	3810.093637	2487.598447
0.9	4822.020727	3148.465296
1.0	5952.983886	3887.089625

	Factor Values			
Radius	ALPHA	SALT	CHARGE	M
0.0	0.412200	0.005000	0.008900	60800
0.1	0.412109	0.104999	0.008524	60800
0.2	0.412108	0.204995	0.007495	60800
0.3	0.412108	0.304990	0.006465	60800
0.4	0.412108	0.404985	0.005435	60800
0.5	0.412108	0.504980	0.004406	60800
0.6	0.412108	0.604975	0.003376	60800
0.7	0.412108	0.704969	0.002346	60800
0.8	0.412108	0.804964	0.001317	60800
0.9	0.412108	0.904959	0.000287	60800
1.0	0.412108	1.004954	-0.000743	60800